SEISMIC PERFORMANCE AND

DESIGN CONSIDERATIONS OF

LONG SPAN SUSPENSION BRIDGES

by

Wen David Liu, Allaoua Kartoum, Kevin Chang and Roy Imbsen

Imbsen and Associations
Sacramento, California

CALIFORNIA DEPARTMENT OF CONSERVATION
DIVISION OF MINES AND GEOLOGY
OFFICE OF STRONG MOTION STUDIES

DIVISION OF MINES AND GEOLOGY
JAMES F. DAVIS
STATE GEOLOGIST

DISCLAIMER

The content of this report was developed under Contract No. 1091-534 from the Strong Motion Instrumentation Program in the Division of Mines and Geology of the California Department of Conservation. This report has not been edited to the standards of a formal publication. Any opinions, findings, conclusions or recommendations contained in this report are those of the authors, and should not be interpreted as representing the official policies, either expressed or implied, of the State of California.

SEISMIC PERFORMANCE AND

DESIGN CONSIDERATIONS OF

LONG SPAN SUSPENSION BRIDGES

by

Wen David Liu, Allaoua Kartoum, Kevin Chang and Roy Imbsen

Imbsen and Associations
Sacramento, California

PREFACE

The California Strong Motion Instrumentation Program (CSMIP) in the Division of Mines and Geology of the California Department of Conservation promotes and facilitates the improvement of seismic codes through the Data Interpretation Project. The objective of the this project is to increase the understanding of earthquake strong ground shaking and its effects on structures through interpretation and analysis studies of CSMIP and other applicable strong motion data. The ultimate goal is to accelerate the process by which lessons learned from earthquake data are incorporated into seismic code provisions and seismic design practices.

The specific objectives of the CSMIP Data Interpretation Project are to:

1. Understand the spatial variation and magnitude dependence of earthquake strong ground motion.

2. Understand the effects of earthquake motions on the response of geologic formations, buildings and lifeline structures.

3. Expedite the incorporation of knowledge of earthquake shaking into revision of seismic codes and practices.

4. Increase awareness within the seismological and earthquake engineering community about the effective usage of strong motion data.

5. Improve instrumentation methods and data processing techniques to maximize the usefulness of SMIP data. Develop data representations to increase the usefulness and the applicability to design engineers.

This report is part of CSMIP data utilization reports designed to transfer recent research findings on strong-motion data to practicing seismic design professionals and earth scientists. CSMIP extends its appreciation to the members of the Strong Motion Instrumentation Advisory Committee and its subcommittees for their recommendations regarding the Data Interpretation Research Project.

Anthony F. Shakal
CSMIP Program Manager

Moh J. Huang
CSMIP Data Interpretation
Project Manager

Contents

Acknowledgement

1. Introduction

1.1 Background

The most significant impact of recent earthquakes in California is the damages incurred in the transportation structures. The 1989 Loma Prieta earthquake in Northern California was probably the first instance that a major long span bridge, i.e., the East Bay Crossing of the San Francisco–Oakland Bay Bridge, was damaged by an earthquake. Recognizing the significant economical and social impact of such major structures, Governor Deukmejian's Board of Inquiry recommended that "all transportation structures be seismically safe and important transportation structures maintain their function after earthquake." In other words, for important structures, not only collapse failure must be prevented, but also that the extent of damage due to an earthquake must be limited and the function of the bridge must be restored quickly.

Neither current AASHTO nor Caltrans Specifications for seismic bridge design cover bridges with spans exceeding 500 feet. Specifically, suspension, cable-stayed, arch and movable bridges are not covered by the Specifications.

The new requirement for functionality in addition to collapse prevention poses a greater demand on the state-of-the-art seismic evaluation technology. To predict the seismic response (demand) of these long span bridges, several structural modeling aspects and dynamic response characteristics should be considered:

1. Three dimensionality of the structure-foundation system must be properly considered in the model. In the case of cable-supported bridges (suspension or cable-stayed), torsional vibration of the deck is typically coupled with lateral vibration. A sufficiently detailed analytical model (not necessarily large) is required for reliable response prediction. This aspect is especially important to satisfy the functionality criteria of major structures.

2. For flexible long span structures such as suspension and cable-stayed bridges, it is important to consider the large displacement and large rotational effects as well as the sequence of erection during construction.

1

Since the earthquake-induced loads are applied to the dead-load deformed configuration, a nonlinear static (incremental) analysis is required to establish the current bridge geometry under loads and the accurate stiffness characteristics of the bridge.

3. The analytical model should capture the coupling of various tower and deck vibration modes with closely spaced natural periods.

4. Two aspects of the ground motion input may contribute significantly to the seismic response (demand):

    a. Differential support displacement input resulting in quasi-static response.

    b. Dynamic response caused by ground acceleration input. The spatially varying ground acceleration input could be decomposed into a uniform (average) support acceleration component and an out-of-phase component. Long span structures with closely coupled vibration modes are particularly sensitive to the out-of-phase component of the ground acceleration input. Primary structural responses in the towers or piers could be underestimated by 30 ~ 40% if the out-of-phase acceleration input were to be ignored. This was demonstrated in our recent seismic evaluation of the Golden Gate Suspension Bridge using both the response spectrum method with uniform support motion input and the direct time history analysis with spatially varying ground motion input. (Liu & Imbsen, 1990; Imbsen & Liu, 1991)

    It is our belief that a reasonably conservative response spectrum analysis method can be implemented to handle both the differential support displacement input and the spatially varying acceleration input at multiple supports.

5. When the response spectrum method or the modal superposition method is used in the seismic analysis, it is important that a sufficient number of modes be included to capture the magnitude of earthquake-induced inertia loading. For long structures, either long-spans or multiple spans, it is equally

important that the distribution of inertia loading throughout the length of the structure be represented well. In other words, "local" effective mass participation factors should be developed for different segments of the structure which will account for both the distribution and magnitude of inertia loading.

These aspects need to be verified with measured responses. The recorded responses of the Vincent Thomas Suspension Bridge during the 1987 Whittier earthquake provide the best set of data available for calibrating the analytical methods. Once a better understanding of the structural responses under the given earthquake input is established, analysis methodology for seismic design can be developed. For design applications, it is extremely important that a multiple-support-excitation response spectrum method be developed which incorporates spatial variations of ground acceleration as well as ground displacements.

1.2 Objectives

The seismic response (demand) evaluation of long span bridges and long bridges (i.e., viaduct structures), which are sensitive to spatially-varying ground motion input, remains a challenge to the profession. The main issues are (1) our ability to describe the spatially-varying input for design applications, and (2) our ability to assess the effect of spatially-varying ground motion input. The recorded motions of the Vincent Thomas Bridge during the Whittier Earthquake provided a unique opportunity to critically scrutinize our analytical technology. When supplemented by other recording in the Los Angeles area during the same earthquake, the spatial variation of ground motion input can be characterized by a coherency function. This latter aspect may allow us to verify simplified analytical methods, i.e. multiple input response spectrum method.

More specifically, the project objectives are:

1. Calibrate the analytical model for the structural system of the Vincent-Thomas suspension bridge based on measured structural responses. Special attention will be placed on the 3D nature and closely-coupled modes of the structure.

2. Assess the spatial variations of ground motion during the 1987 Whittier earthquake based on measurements taken at several CSMIP stations and Caltech recordings (digitized by CDMG). A coherence function will be developed to characterize the spatial variation of input ground motion at the bridge.

3. Quantify the structural response characteristics based on measured strong motion records, and identify the closely-coupled modes with the aid of analytical modeling/prediction.

4. Identify those response measurements that are sensitive to multiple-support-excitation, and compare a multiple input response spectrum method with the measured responses. For responses not measured, time history analysis results will be used to compare with the multiple input response spectrum analysis results to assess the validity of the simplified method.

1.3 Past Studies

The vibrational characteristics of suspension bridges have been the subjects of study by several researchers over the past 30 years. Studies in Japan in the early 1960's of 3-span suspension bridges adopted an approximation that vibration of the tower-piers may be analyzed separately from the suspended structures provided the elastic restrain effect of the cables at the top of the tower is accounted for. They emphasized the effect of rocking motion on stresses and bending moments in the tower and the significant contribution from higher modes.

The work of Abdel-Ghaffar in the late 1970's utilizing the finite element method and linearized deflection theory provided major advances in the knowledge of suspension bridges and how they perform under vibration loading. His theoretical results were compared with the results of ambient vibration tests on the Vincent Thomas Bridge. Abdel-Ghaffar continued his studies in the 1980's with other researchers, applying their analytical approach to the Golden Gate Bridge. Their comparisons showed good agreement with previously determined two- and three-dimensional analytical models.

After the 1989 Loma Prieta earthquake, a study was commissioned by the Golden Gate Bridge District to evaluate the seismic performance of the Golden Gate Bridge and propose alternative retrofit schemes. The structural responses under multiple-support-excitations was examined very closely using the direct-integration time history analysis method. Several important conclusions are:

1. the main tower responses are very sensitive to the out-of-phase ground acceleration input;

2. the side-span stiffening truss system is strongly coupled with the longitudinal vibration of the main towers; and,

3. the ground displacement in the order of 15 to 20 inches could result in the closure of movement gap and impacting between the main tower and the suspended deck system.

Very recently, a comprehensive evaluation of the Vincent Thomas Bridge has been completed (Niazy, 1991). Using the Whittier earthquake records, the study reveals strong evidence of spatial variation of the ground motion and the potential structural effects. Deficiencies in the existing instrumentation were identified. However, to correlate with measured responses in the time-domain, the study used "modal" time history analysis method using only 50 modes. A better approach would be to conduct direct-integration time history analysis.

Multiple Input Response Spectrum Method – For design applications using the response spectrum method with multiple-support-excitations, we need to consider not only the cross-modal correlation of the responses, but also the cross-support correlation of the input. Yamamura and Tanaka (1990) reported similar behavior of tower vibration modes as obtained in the Golden Gate Bridge study and suggested an extension of the CQC method for multiple-support-excitations. In their approach, ground motions are non-uniform and non-correlated among different support groups. A more general approach has been suggested by Der Kiureghian and Neuenhofer (1991) which will also account for correlated multiple support inputs and local site soil effect (Der Kiureghian, 1994).

1.4 Scope of the Study

The development of an analytical model for the bridge structure will be summarized. Results of measurements during the 1987 Whittier earthquake was used to verify the analytical model.

Two sets of spatially varying ground motions will be used. One set is the records obtained at Caltech stations and was digitized by CSMIP. This set has the proper separation distances between stations; however, the local site condition is different from the bridge site. The second set is derived from records collected at Long Beach areas which has the Los Angeles basin effect with a pronounced period of about 1 second. This is very significant because the structure's natural periods are in that period range. The analysis results based on these two sets will be presented and compared.

These time history analysis results are compared with the multiple-support response spectrum analysis results to establish some benchmark comparisons.

2. The Vincent Thomas Bridge

The Vincent Thomas Bridge spans the main channel of the Los Angeles Harbor between San Pedro in the west and Terminal Island in the east, as shown in Figure 2.1. Its total 6,060 feet length is made up of the three span suspension bridge and 19 steel plate-girder approach spans (ranging from 150 feet to 230 feet in length). The roadway width is 52 feet from curb to curb to accommodate four lanes of traffic. The suspension bridge has a 1,500 foot center span, two 507 foot side spans, and two 151.5 foot backstay spans to the anchorages, see Figure 2.2.

The suspended span consisted of two stiffening trusses spaced at 59 feet apart, transverse floor trusses spaced at 31 feet apart; and the bottom lateral bracing system of the K truss type. The lightweight concrete roadway deck is supported on stringers (seven feet center to center spacing) which are simply supported on the transverse floor truss. The stiffening truss is 15 feet deep and the floor truss is ten feet deep. The superstructure is a closed box system with relatively high torsional rigidity.

The suspended spans are hung from the main cables through vertical suspenders at each floor truss location. The main cable has a vertical sag of 150 feet in the center span. The elevations at key locations of the bridge and cable profiles are shown in Figure 2.3.

The main towers are 335 feet high and extend about 360 feet above the mean high water level as shown in Figure 2.4. The towers are made of two steel box section legs. The tower legs have cruciform cross section made of four welded sections ($^3/_4$ inch plates), field bolted with one inch diameter high strength bolts. At the base, the tower legs rest on the 3-inch thick base plate and are anchored to the concrete footings by prestressing rods (2-$^1/_2$ inch in diameter). There are 39 rods for each tower leg and they were stressed to 360 kip to anchor the tower legs to the concrete piers. The cross section of each leg tapers toward the top as shown in Figure 2.4.

The tower legs were shop assembled in its entirety, and the strut sections linking the two legs were matched and drilled. Then the towers were erected in seven tiers.

At the connection of the tower and stiffening truss, the trusses are hung from the tower at the truss hangers.

The main cable consists of 4,028 cold drawn, galvanized 6 gage steel wires providing 121.5 in^2 of steel area. The ultimate strength of the cable was specified to be at least 225 ksi thus providing a theoretical cable strength of 27,337 kips. The maximum cable tension at the tower location is 9,620 kips for both gravity load and live loads. The horizontal component of cable tension is 6,750 kips.

The cable bents are hollow concrete constructions. Main cables are connected to the main towers and cable bents through cable saddles (as shown in Figure 2.5) which are bolted to the towers and bents.

At the cable bents, the stiffening truss is supported vertically on truss brackets, and is restrained longitudinally and transversely through the wind shoe bracket which is embedded in the concrete bent as shown in Figures 2.6 and 2.7.

At the main towers, four bearing guides go through the gusset plates of the strut C, and form a longitudinal slot. As shown in Figure 2.8, the total slot lengths are seven feet in the main span side and 5 feet in the side span. The stiffening trusses are supported by truss hangers (19 feet long) from the tower as shown in Figure 2.9.

All foundations of the bridge are supported on steel piles. The 14B117 steel H piles were driven to elevation -75 feet at the Terminal Island tower and -135 feet at the San Pedro tower. At the time of construction (1961 ~ 1963), it was the only suspension bridge in the world supported entirely on piles.

Figure 2.1: Vincent Thomas Bridge, Approach Spans and the Los Angeles Harbor
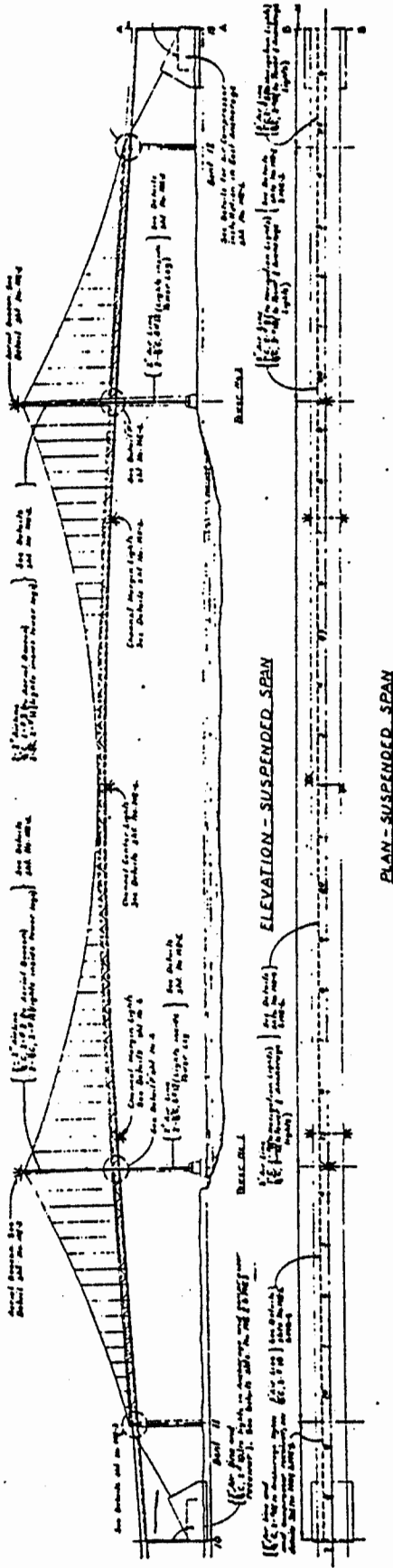
ELEVATION – SUSPENDED SPAN

PLAN – SUSPENDED SPAN

Figure 2.2: Vincent Thomas Bridge – Suspended Spans

10

ELEVATION
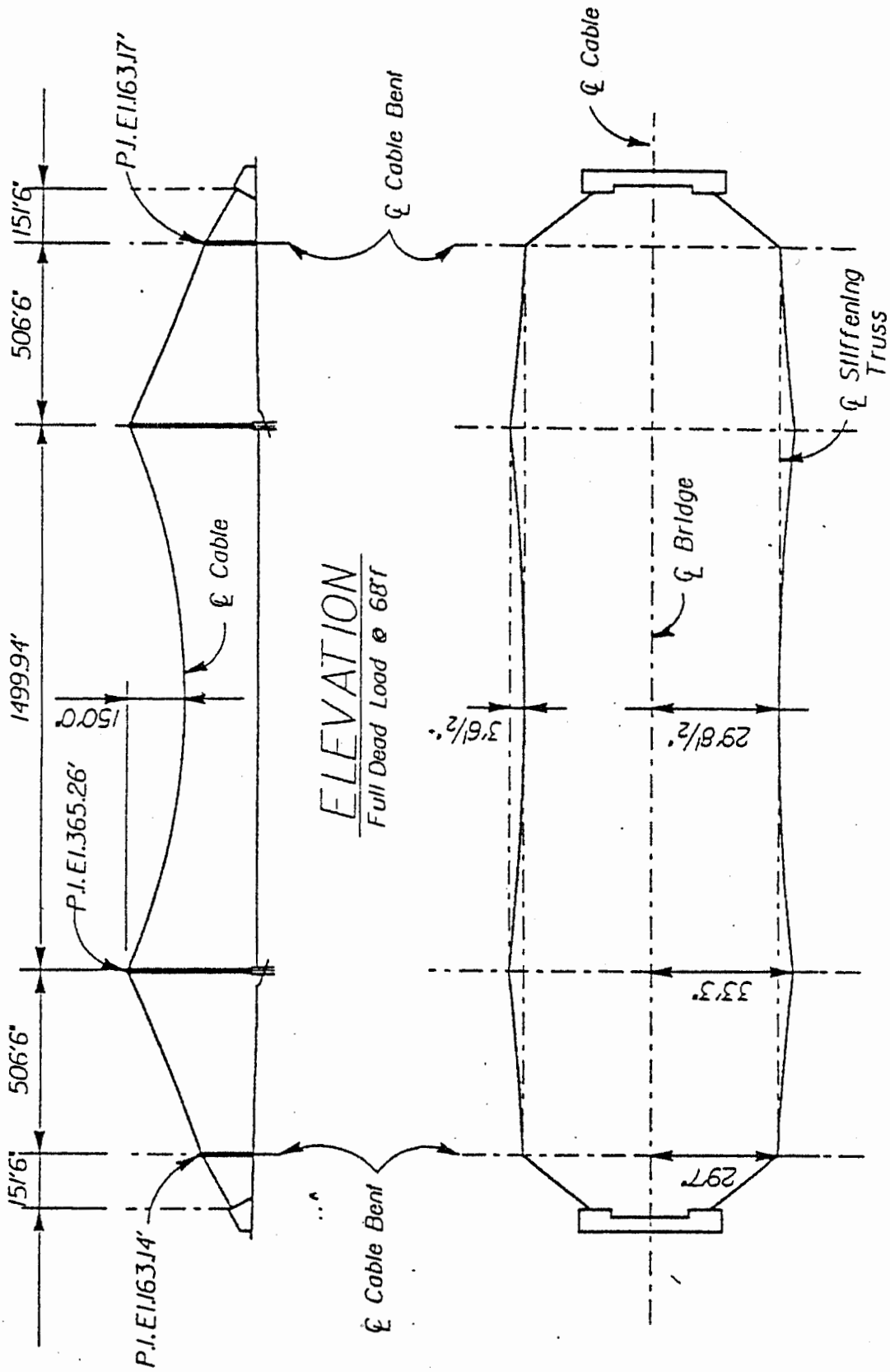*Full Dead Load @ 68°F*

Figure 2.3: Cable Profiles — Vincent Thomas Bridge

11
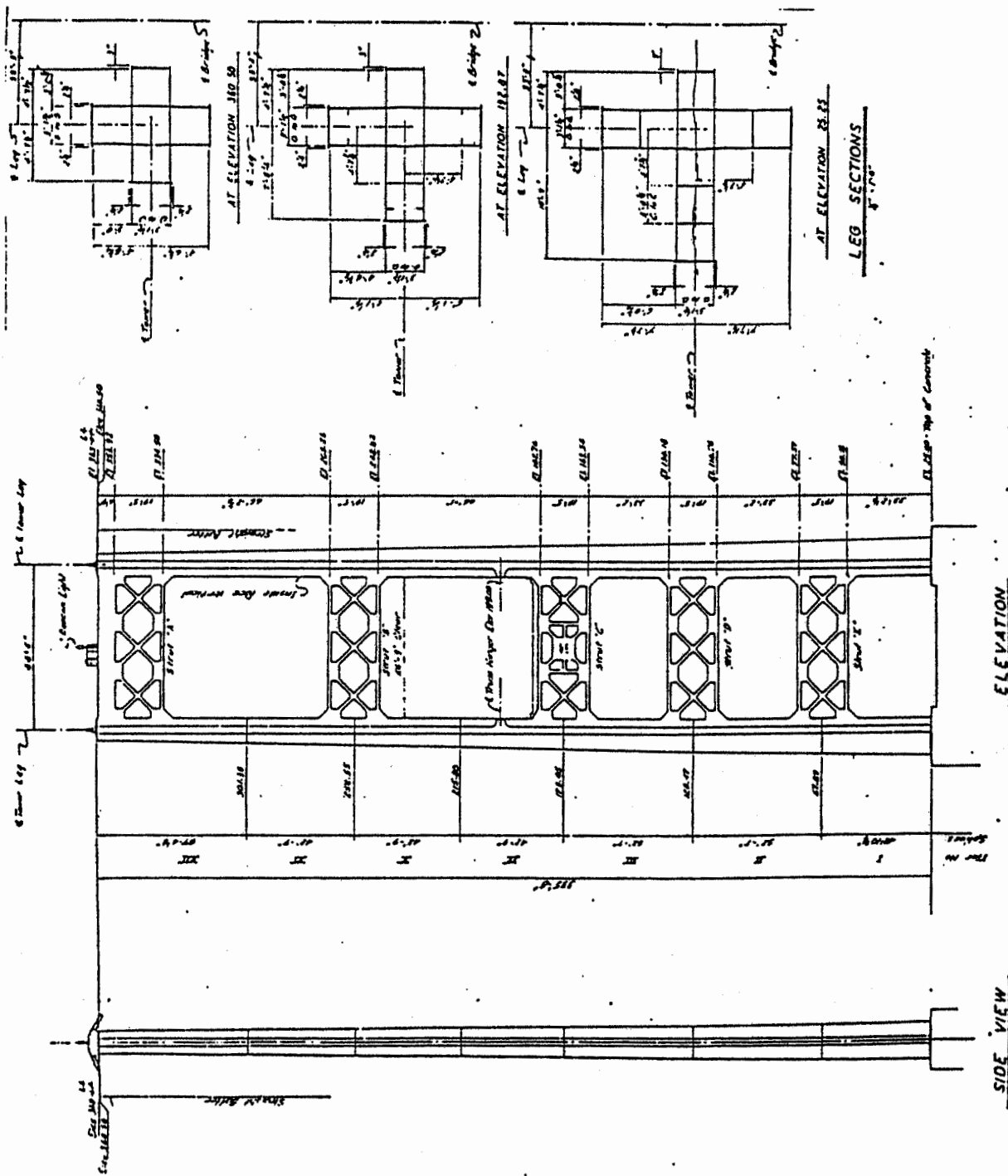
Figure 2.4: Vincent Thomas Bridge Towers – Elevation and Cross Sections
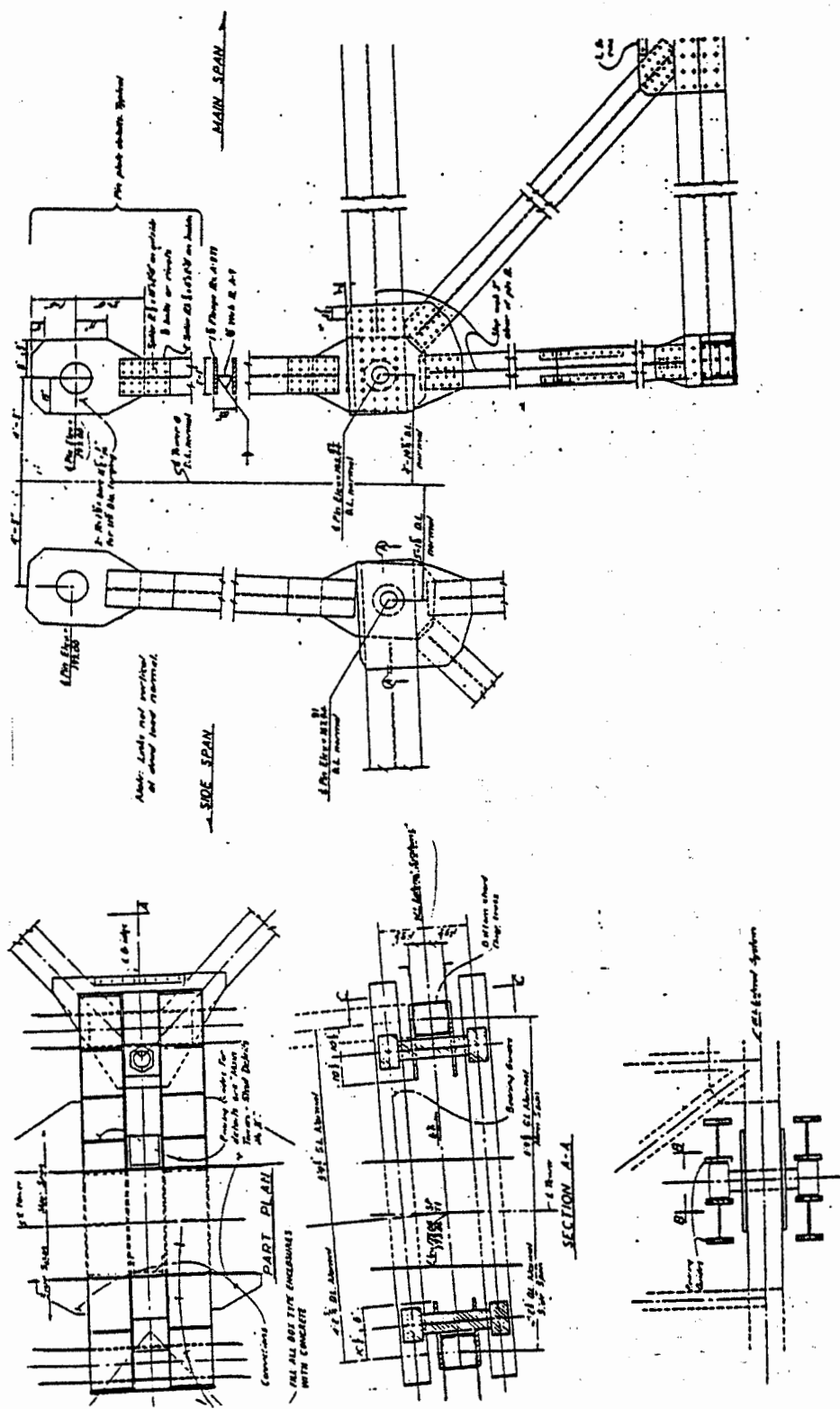
12

Cable Bent

Main Tower

Figure 2.5 : Cable Saddles at Main Tower and Cable Bent

13

Figure 2.6: Cable Bent and Wind Shoe Bracket

14
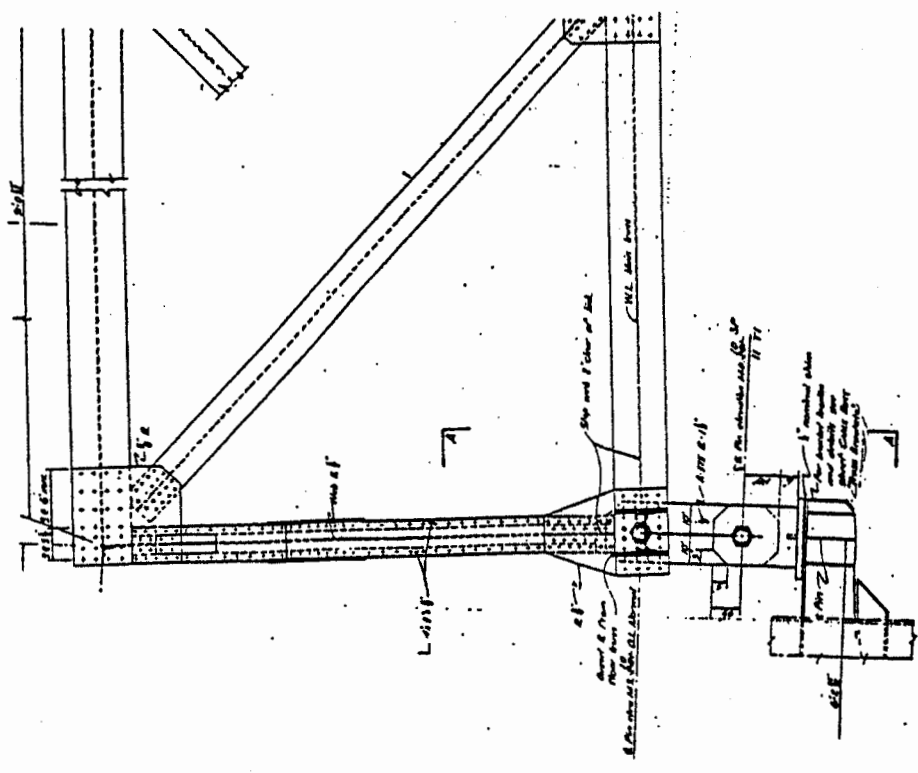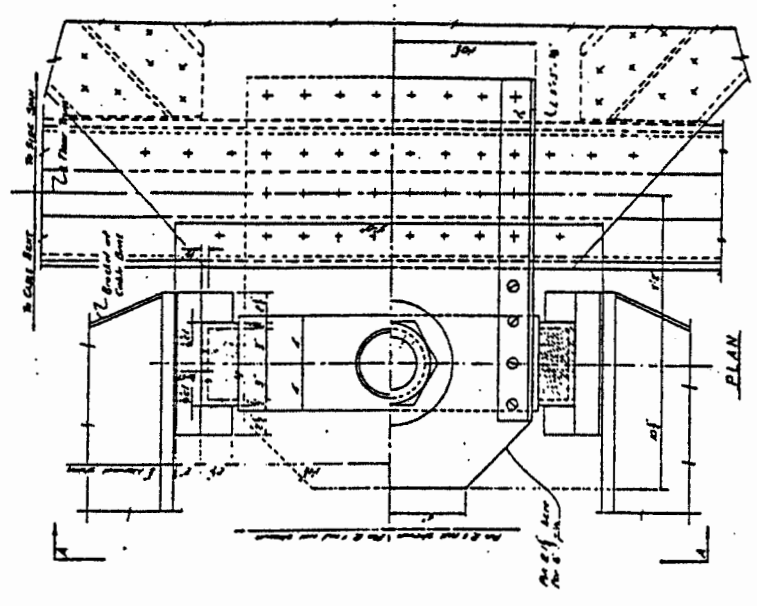
Wind Shoe

Truss Bracket

Figure 2.7 : Truss Bracket and Wind Shoe at Cable Bent

15

Figure 2.8: Connection of Stiffening Truss to Main Towers at Strut C

Truss Hangers

Wind Shoe

Figure 2.9 : Wind Shoe and Truss Hangers at Main Tower

3. Description of Instrumentation and Data Collected During the 1987 Whittier Earthquake

3.1 Description of Instrumentation and Data Analysis

The CSMIP instrumentation at the Vincent Thomas Bridge (Station No. 14406) includes a total of 26 sensors:

- 13 sensors on the stiffening truss deck;
- three sensors on top of East Tower; and
- ten sensors at the foundation of East Anchorage, East Tower and West tower.

These locations are shown in Figure 3.1. These sensors could be grouped in four sets:

1. Foundation Motions

Location	Longitudinal	Transverse	Vertical	Distance from Reference*
East Anchorage*	Ch. 25	Ch. 24	Ch. 26	0 feet
East Tower	Ch. 13	Ch. 9	Ch. 19/20	658 feet
West Tower	Ch. 23	Ch. 1	Ch. 14	2158 feet

*East Anchorage is the reference point.

These motions include both the spatial variation of ground motions as well as the soil-structure interaction effect.

2. Vibration of the East Side Span

Location	Transverse	Vertical
Midspan	Ch. 7	Ch. 21 (N)
		Ch. 22 (S)

18

3. Vibration of the Main Span

Location	Transverse	Vertical
West Tower	Ch. 2	–
Midspan 　Top of Deck	Ch. 4	Ch. 15 (N) Ch. 16 (S)
Bottom Lateral	Ch. 3	–
$1/3$ Span	Ch. 5	Ch. 17 (N) Ch. 18 (S)
East Tower	Ch. 6	–

4. Vibration of the East Tower

Location	Longitudinal	Transverse	Vertical
Top	Ch. 10 (S) Ch. 11 (N)	Ch. 8	–
Roadway Level	Ch. 12 (S)	Ch. 6	–
Base	Ch. 13 (S)	Ch. 9	Ch. 19 Ch. 20

The maximum values recorded at these sensor locations during the 1987 Whittier Narrows earthquake are summarized in Table 3.1.

Data Analysis – To identify the important modes from the measured responses, the Fourier amplitude spectra of the acceleration, velocity and displacement time histories were used. A three-point frequency-smoothing technique was used to reduce the random noise.

To enhance the responses, two parallel measurements were added together to emphasize the translation responses, and were subtracted to emphasize the rotational (rocking or torsional) responses. Based on the Fourier amplitude spectra of velocity responses, all significant frequencies and peak responses were summarized in Table 3.2, 3.3 and 3.4.

3.2 Foundation Motions

The displacement time histories of these foundation motions are shown in Figures 3.2, 3.3 and 3.4 for longitudinal, transverse and vertical components, respectively. The motions at East Anchorage and East Towers exhibited very similar waveform. The motions at the base of the West Tower are somewhat different in both the amplitude and frequency content. The power spectral density functions of the acceleration are shown in Figures 3.5 and 3.6. The acceleration motions at West Tower has a much higher amplitude at 1.2 Hz frequency. This is probably due to the soil structure interaction effect and the softer soil under the West Tower. In the ground displacement motions, there are long period motions in the period range from 4 to 6 seconds as shown in Figure 3.7.

Relative displacement time histories between East Tower and East Anchor, between West Tower and East Anchor and between West Tower and East Tower are shown in Figure 3.8. The maximum relative displacements are:

Separation Distance		Relative Displacement (inch)	
		Longitudinal	Transverse
658.5 ft.	(EA-ET)	0.25	0.30
1500 ft.	(ET-WT)	0.45	0.55
2158.5 ft.	(EA-WT)	0.50	0.60

As shown in Figure 3.8, there is a frequency component of 1 Hz in the relative displacement between the two sides of the channel.

Foundation Rocking Rotation

The rocking motion of East Tower foundation about the longitudinal axis is shown in Figure 3.9. The dominant frequency of rocking motion is 0.2 Hz which has an amplitude of 5.9×10^{-5} rad.

The rocking motion is caused primarily by the vertical component of horizontally propagating ground motion. For the low frequency range, an approximation can be

obtained based on the kinematic soil-structure interaction study (Wolf, 1985, pg. 74). The maximum rocking rotation is

$$\beta_{0,max} = \lambda \frac{2\pi f}{Ca} \bullet u^f_{z\,max}$$

where f =   frequency of interest (Hz)

              Ca =   apparent wave velocity

              $u^f_{z\,max}$ =   maximum free-field vertical displacement

              λ =   a constant depending on the foundation geometry, type and embedment

The measured foundation rocking measurement provided an important benchmark to correlate with the theoretical kinematic soil-structure interaction study.

3.3   Response Measurements at the East Side Span

The three sensors at the midspan allows the determination of transverse, vertical and torsional modes. The frequencies and amplitudes of the velocity Fourier amplitude spectra (as shown in Figure 3.10) are summarized below:

Response	Component	Period (sec)	Amplitude
Transverse	Ch. 7	1.47	0.464
		1.28	0.344
		1.0	0.704
Torsional	Ch. 21 - Ch. 22	1.0	4.093
Vertical	Ch. 21 + Ch. 22	4.10	0.633
		2.65	0.614
		2.22	0.625
		0.48	0.286

The torsional response of the deck is clearly shown in the two vertical channels. The acceleration time histories are shown in Figure 3.11. This torsional mode with one second period is coupled with the transverse vibration. At least three vertical

21

modes were identified using the enhanced time history (Ch. 21 + Ch. 22) as shown in Figure 3.10. These periods are 4.10 sec., 2.65 sec. and 2.22 sec.

The Fourier amplitude spectra for transverse vibration is shown in Figure 3.12. In addition to the 1 second mode, two other modes were identified also with smaller amplitude.

3.4 Response Measurements at the Main Span

There are four sensors at the midspan, and three sensors at the one-third span.

Vertical Mode – Enhanced signals were obtained by summing Ch. 15 and 16, Ch. 17 and 18. The Fourier amplitude spectra are shown in Figure 3.13. A clear vertical mode is identified with period of 4.17 sec. from the enhanced signal (Ch. 15 + Ch. 16).

Torsional Mode – Enhanced signals were obtained by taking the difference of the following three pairs to identify the torsional modes:

(Ch. 15 – Ch. 16) at midspan
(Ch. 4 – Ch. 3) at midspan
(Ch. 17 – Ch. 18) at $1/3$ span

All frequencies and the amplitudes of the Fourier amplitude spectra of these enhanced signals were summarized in the table below:

Location	Channel	1.89 sec.	1.47 sec.	1.0 sec.	0.91 sec.
Midspan	15-16 (V)	–	0.467	–	1.435
Midspan	3-4 (T)	–	0.077	–	0.241
$1/3$ Span	17-18 (V)	0.313	0.486	0.407	–

Two modes can be identified associated with the midspan with periods 1.47 second and 0.91 second. Two additional mode are associated with those higher order modes which have a node at the midspan.

22

Vertical acceleration time histories at edges of deck at midspan and $1/3$ span are shown in Figure 3.13c and 3.13d which show clearly the torsional modes.

Transverse Modes – Five transverse modes can be identified from the Fourier amplitude spectra as shown in Figure 3.14. The amplitudes at the corresponding periods are summarized in the table below:

Location	Channel	Period (sec)				
		6.67	1.61	1.16	1.0	0.91
West Tower	2	0.1	–	0.235	0.293	0.308
Midspan	4	0.439	0.176	0.351	0.205	0.200
	3	0.423	0.164	0.286	0.249	0.423
	4+3	0.886	0.355	0.638	0.456	0.606
$1/3$ Span	5	0.371	0.077	–	0.130	0.12
East Tower	6	0.07	–	0.205	0.266	0.245

3.5 Response Measurements of the East Tower

Longitudinal and Torsional Modes – Fourier amplitude spectra are shown in Figures 3.15a and 3.15b. Based on Channels 10, 11, 12 and 13, two longitudinal modes were identified at periods of 1.16 and 1.0 seconds with essentially the same mode shape. A longer period mode at 4.17 second is associated with the vertical mode of the suspended span.

The only torsional mode can be identified is that the twisting at the top of the two tower legs with a period of about 1.0 second.

Transverse Vibration Modes – Fourier amplitude spectra are shown in Figure 3.16. Two modes can be identified based on measurements at the South leg with periods of 1.0 second and 0.91 second. These are of the same general mode shape, but coupled differently with the vibration of the suspended spans and main cables.

23

Table 3.1: Location of Strong Motion Sensors on the Bridge and Their Peak Response Values During the 1987 Whittier Narrows Earthquake

Sensor	Type of Motion	Location on the Bridge and its Foundation	A_{max} (g)	V_{max} cm/sec	D_{max} cm
1.	Lateral	West Tower, at Base of South Column	0.05	5.77	1.49
2.	Lateral	West Tower, at Top of Deck Truss	0.30	15.60	2.25
3.	Lateral	Main Span Center, Deck Truss Bottom	0.11	13.90	4.57
4.	Lateral	Main Span, Center, Top of Deck Truss	0.09	9.60	4.19
5.	Lateral	Main Span, 1/3 pt., Deck Truss Top	0.09	7.49	3.48
6.	Lateral	East Tower, at Top of Deck Truss	0.35	10.60	1.88
7.	Lateral	Side Span, Center, Top of Deck Truss	0.21	20.00	3.32
8.	Lateral	East Tower, at Top of South Column	0.22	19.80	3.07
9.	Lateral	East Tower, at Base of South Column	0.05	5.71	1.57
10.	Longitudinal	East Tower, at Top of South Column	0.13	11.70	1.76
11.	Longitudinal	East Tower, at Top of North Column	0.13	12.10	2.79
12.	Longitudinal	East Tower, at Top of Deck Truss	0.20	17.8	3.46
13.	Longitudinal	East Tower, at Base of South Column	0.06	7.91	1.61
14.	Vertical	West Tower, at Base of South Column	0.02	1.63	0.71
15.	Vertical	Main Span. Center, North edge of Deck	0.12	16.90	5.40
16.	Vertical	Main Span, Center, South edge of Deck	0.14	18.20	5.81
17.	Vertical	Main Span, 1/3 pt, North edge of Deck	0.07	11.10	3.24
18.	Vertical	Main Span, 1/3 pt, South edge of Deck	0.09	10.20	3.54
19.	Vertical	East Tower, at Base of South Column	0.02	2.21	0.73
20.	Vertical	East Tower, at Base of North Column	0.02	1.84	0.56
21.	Vertical	Side Span, Center, North edge of Deck	0.27	38.80	7.53
22.	Vertical	Side Span, Center, South edge of Deck	0.27	34.20	8.71
23.	Longitudinal	West Tower at Base of South Column	0.07	10.10	1.82
24.	Lateral	East Anchor, at Base	0.06	6.00	1.65
25.	Longitudinal	East Anchor, at Base	0.05	7.65	1.64
26.	Vertical	East Anchor, at Base	0.03	1.92	1.05

A_{max}, V_{max} and D_{max} are the maximum recorded acceleration, velocity and displacement, respectively.

Table 3.2: Dominant Frequencies and the Corresponding Fourier Amplitude of Velocity Responses at the Main Span

Freq (Hz)	0.15	0.24	0.45	0.53	0.62	.66-.69	.73-.78	.84-.88	.96-1.03	1.08-1.12	1.18	1.25-1.38	1.46-1.58
Period (sec)	6.67	4.17	2.22	1.89	1.61	1.45-1.51	1.28-1.37	1.13-1.19	.97-1.04	.89-.92	.85	.72-.80	.63-.68
Chan #													
Main Span Trans.													
1	0.095	-					0.077			0.190		0.131	
2	0.100							0.235	0.293	0.308	0.399	0.255	
3	0.423				0.164			0.286	0.249	0.423	0.084		
4	0.439		0.020		0.176			0.351	0.205	0.200	0.182		
5	0.371		0.126		0.077				0.130	0.12	0.060		
4+3	0.864				0.355			0.638	0.456	0.606			
4-3						0.077		0.071		0.241			
4+5	0.810				0.270			0.850		0.293			
4-5			0.110					0.371	0.249		0.173		
6								0.205	0.266	0.245			
9	0.071						0.066	0.062	0.081	0.045			0.055
Main Span Vert.													
15		0.671				0.219				0.719			
16		0.685				0.247				0.716			
17		0.454		0.152		0.245			0.200				
18		0.464		0.167		0.241			0.205				
15+16		1.357								1.435			
15-16						0.467							
17+18		0.918				0.486							
17-18				0.313					0.407				

25

Table 3.3: Dominant Frequencies and the Corresponding Fourier Amplitude of Velocity Responses at the Side Span

Freq	0.24	0.38	0.45	.66-.69	.73-.78	.96-1.03	2.08
Period	4.17	2.63	2.22	1.45-1.51	1.28-1.37	.97-1.04	0.48
Chan #							
Side Span Vert.							
21	0.300	0.310	0.310			2.074	0.143
22	0.330	0.300	0.318			2.017	0.143
21+22	0.633	0.614	0.625				0.286
21-22						4.093	
Side Span Trans.							
7				0.464	0.344	0.390	

Table 3.4: Dominant Frequencies and the Corresponding Fourier Amplitude of Velocity Responses at the East Tower

Freq	0.15	0.24	.66-.69	.73-.78	.84-.88	.96-1.03	1.08-1.12	1.18	1.25-1.38	1.46-1.58	2.29	3.19	4.35
Period	6.67	4.17	1.45-1.51	1.28-1.37	1.13-1.19	.97-1.04	.89-.92	0.85	.72-.80	.63-.68	0.44	0.31	0.23
Chan #													
East Tower Long.													
10		0.118	0.084		0.202	0.226	0.122				0.105	0.054	0.056
11		0.105			0.217	0.288	0.173				0.110	0.030	0.045
12					0.354	0.400		0.272					
13					0.134		0.145		0.100				
10+11		0.221			0.410	0.259	0.290				0.212	0.084	0.126
10-11						0.447							
East Tower Trans.													
8						0.654	0.405		0.390				
6					0.205	0.266	0.245						
9	0.071			0.066	0.062	0.081	0.045			0.055			

27

Los Angeles – Vincent Thomas Bridge

(CSMIP Station No. 14406)
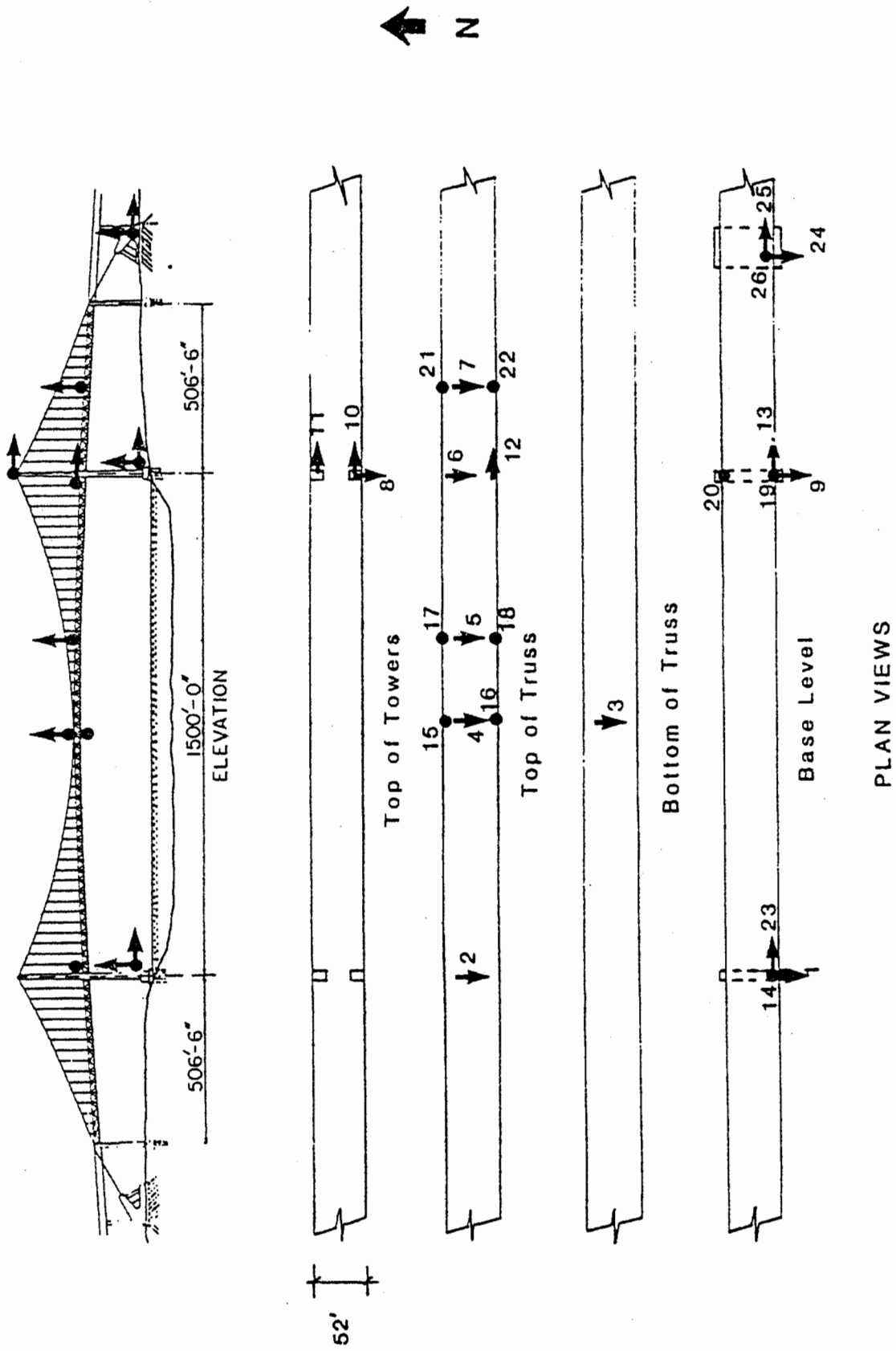
Figure 3.1: Location of Instrumentation Layout
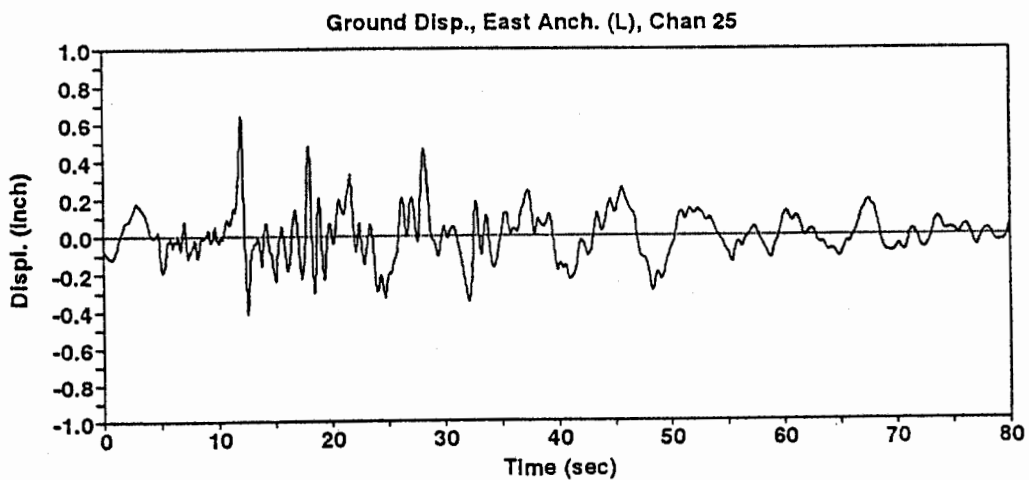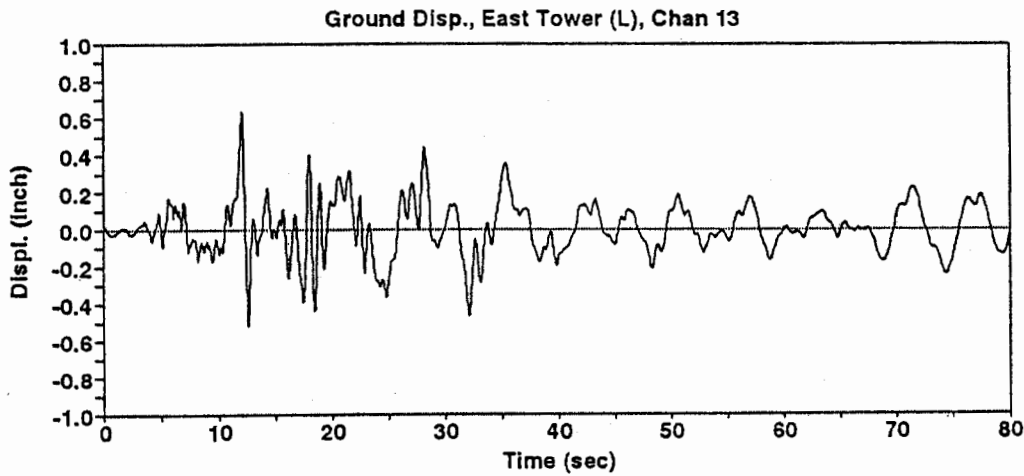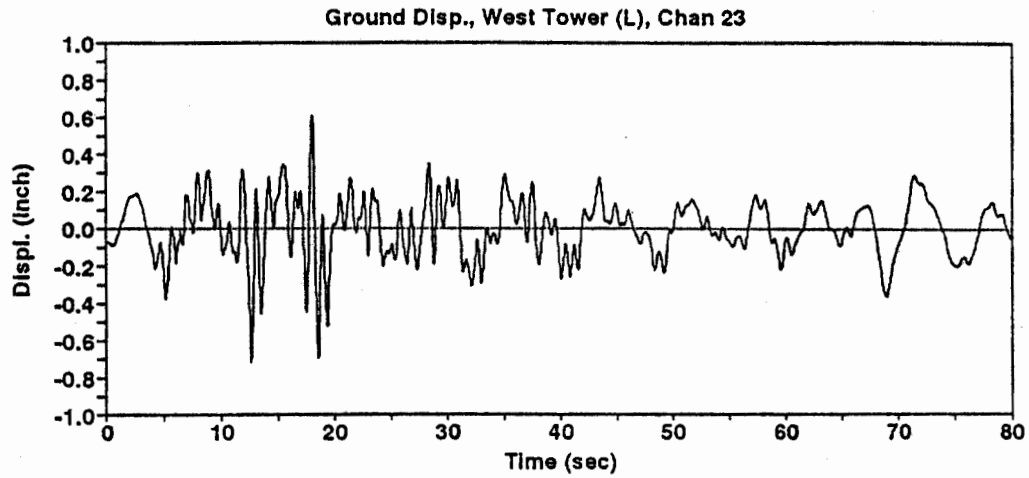
Figure 3.2: Foundation Displacement Time Histories in the Longitudinal Direction During the 1987 Whittier Narrows Earthquake

29
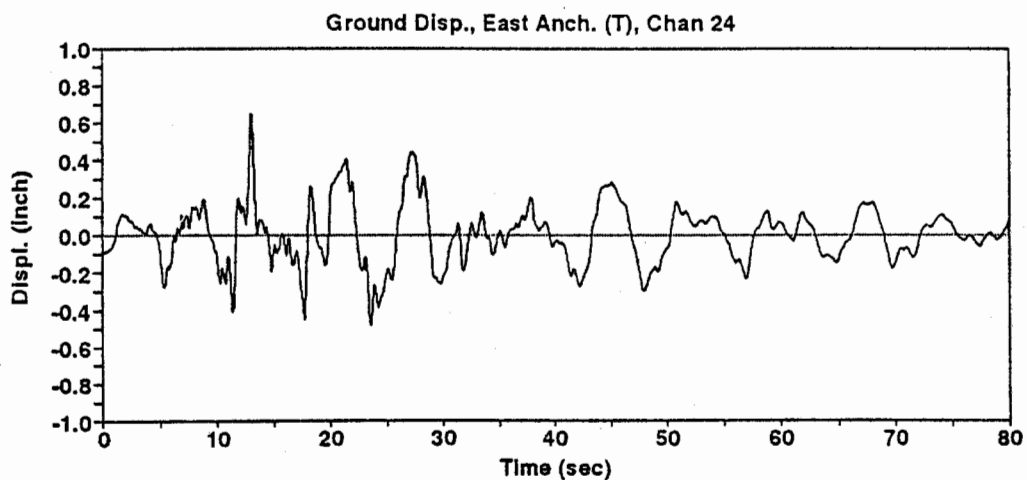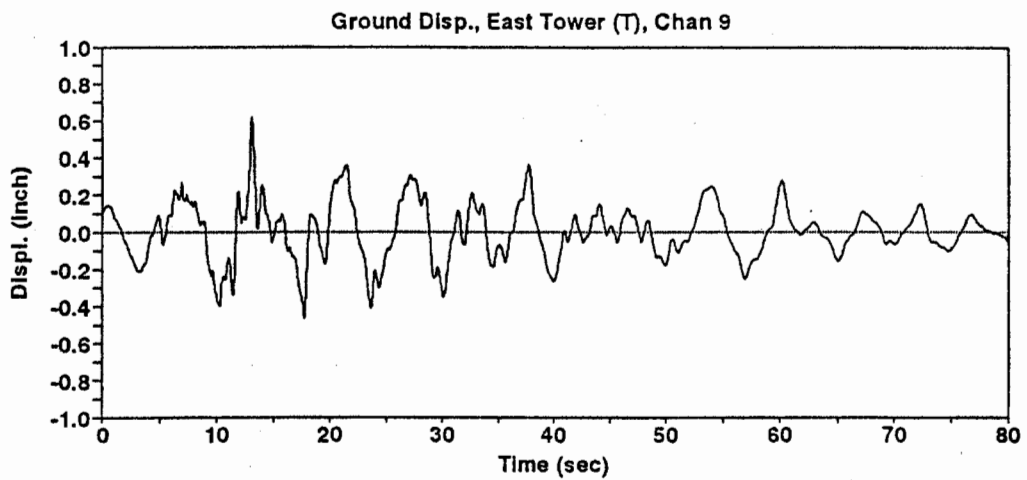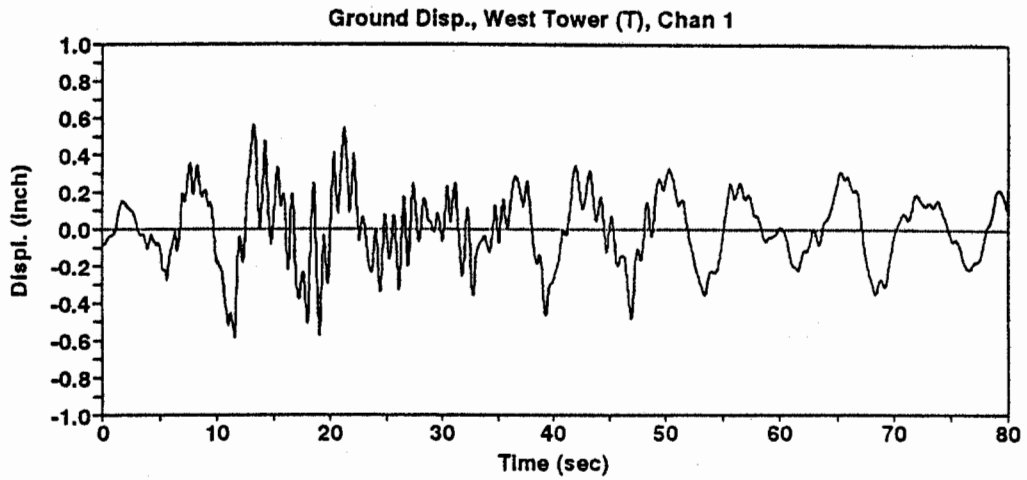
Figure 3.3: Foundation Displacement Time Histories in the Transverse Direction During the 1987 Whittier Narrows Earthquake

30
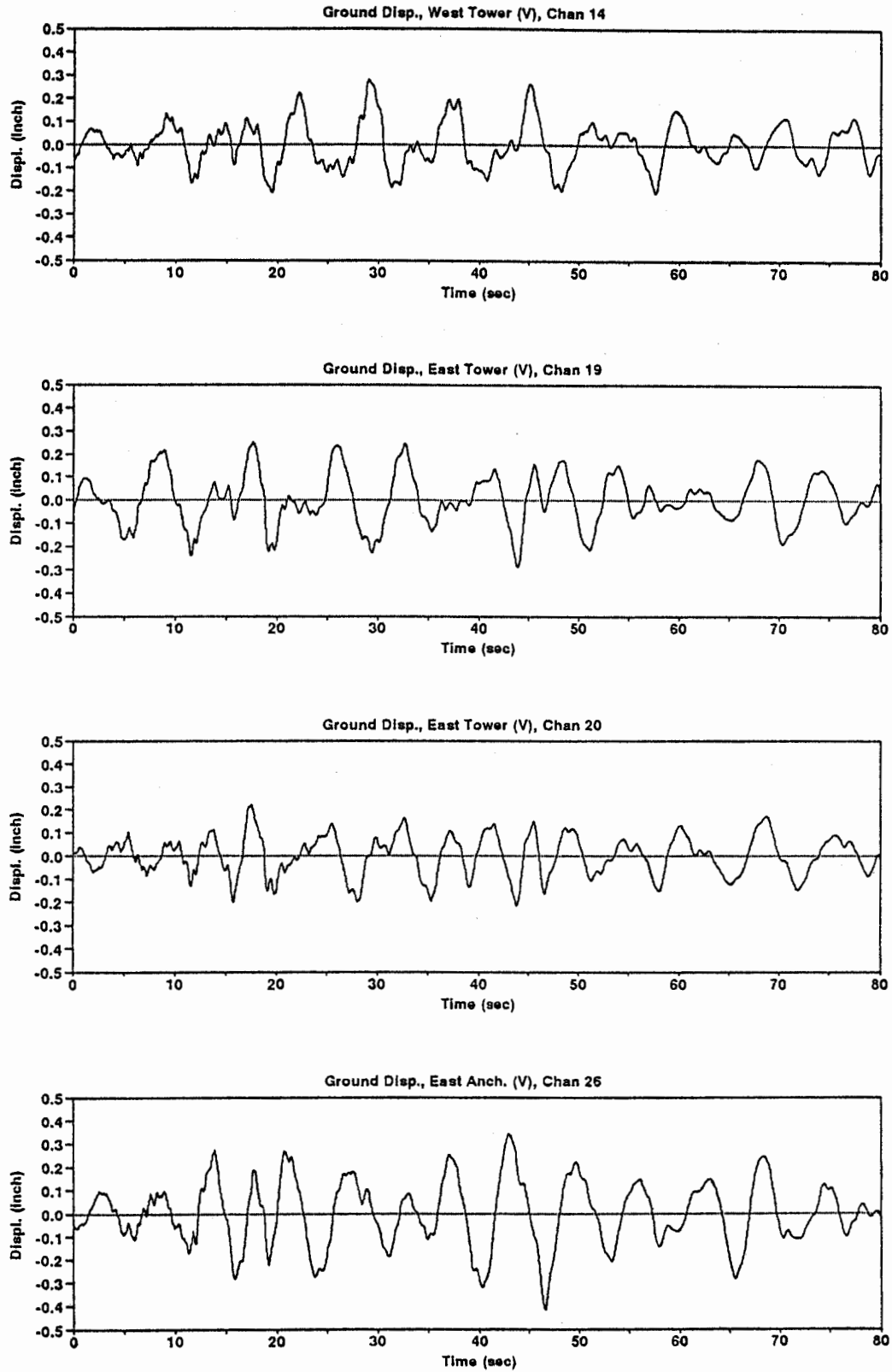
Figure 3.4: Foundation Displacement Time Histories in the Vertical Direction During the 1987 Whittier Narrows Earthquake

31

Ground Accel., West Tower (L), Chan 23

Ground Accel., East Tower (L), Chan 13

Ground Accel., East Anch. (L), Chan 25
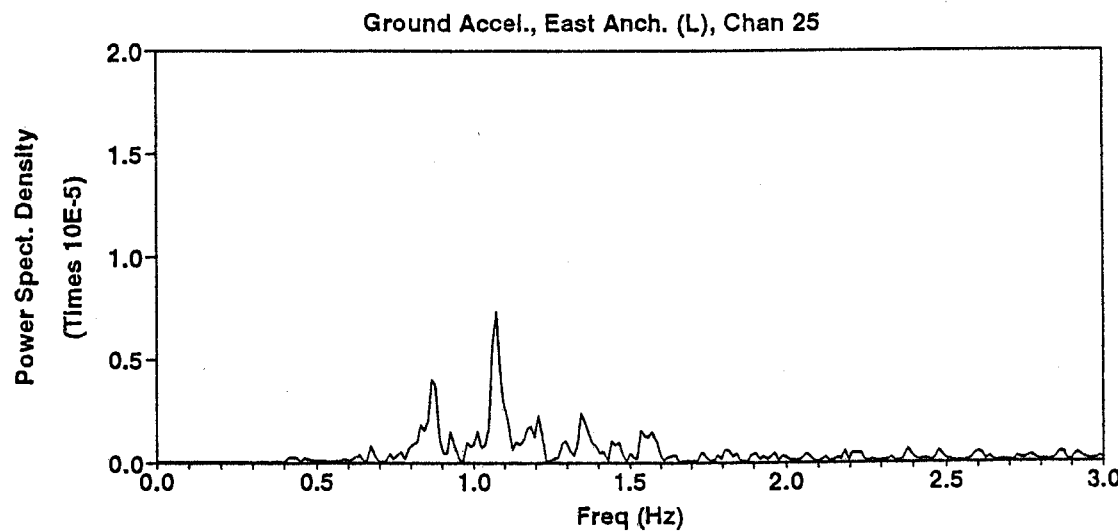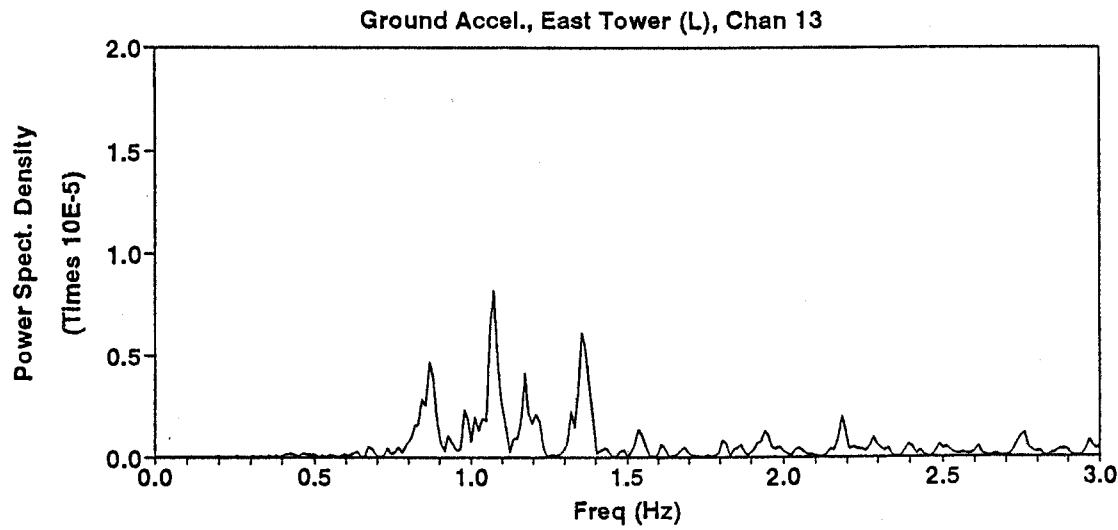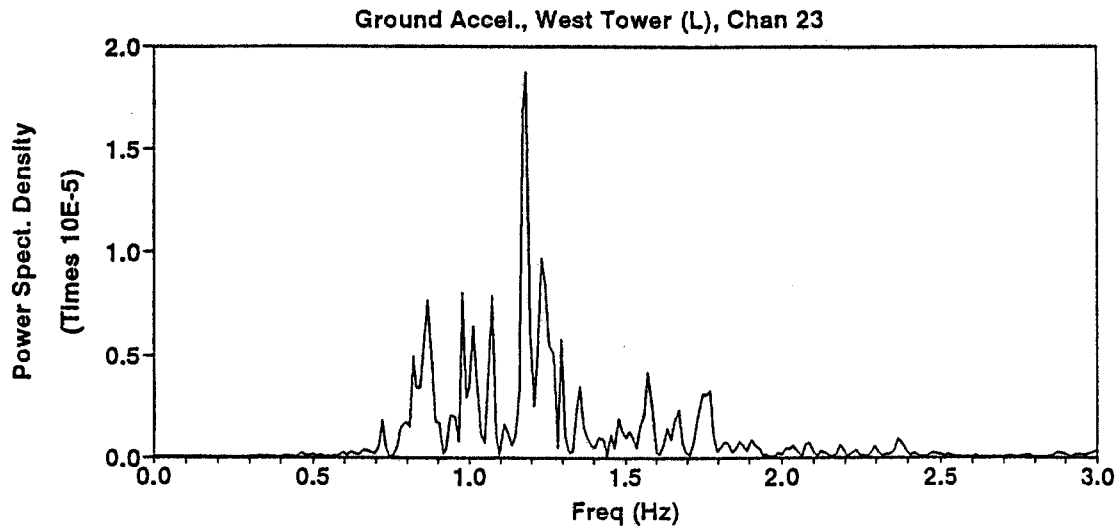
Figure 3.5: **Acceleration Power Spectral Density Functions of Longitudinal Foundation Motion**
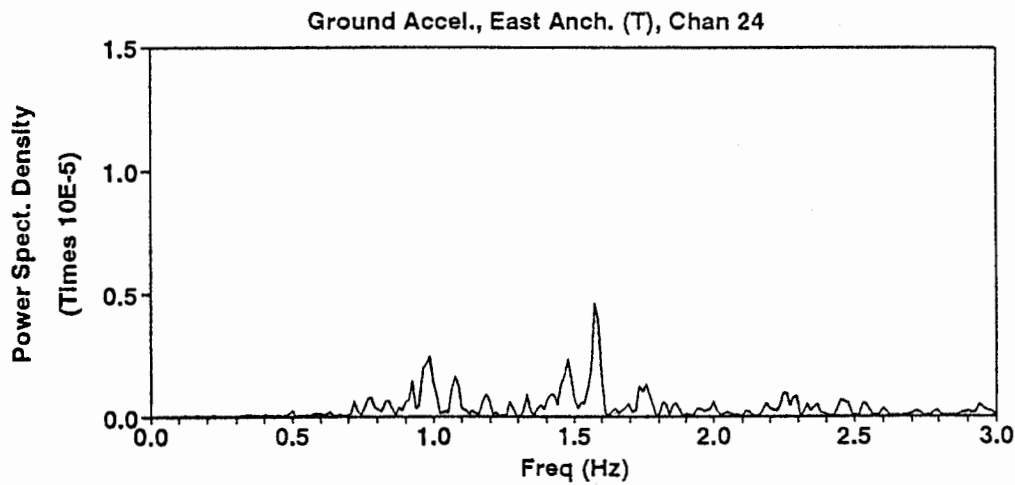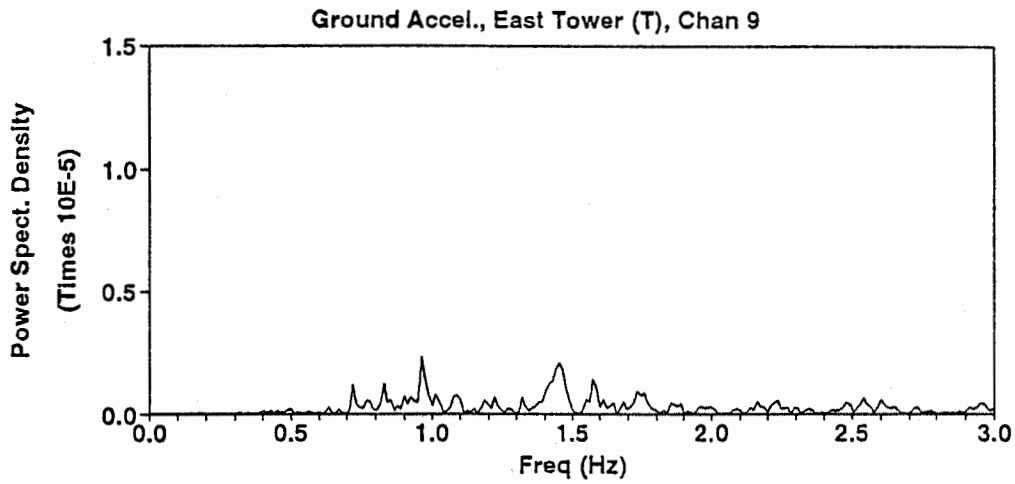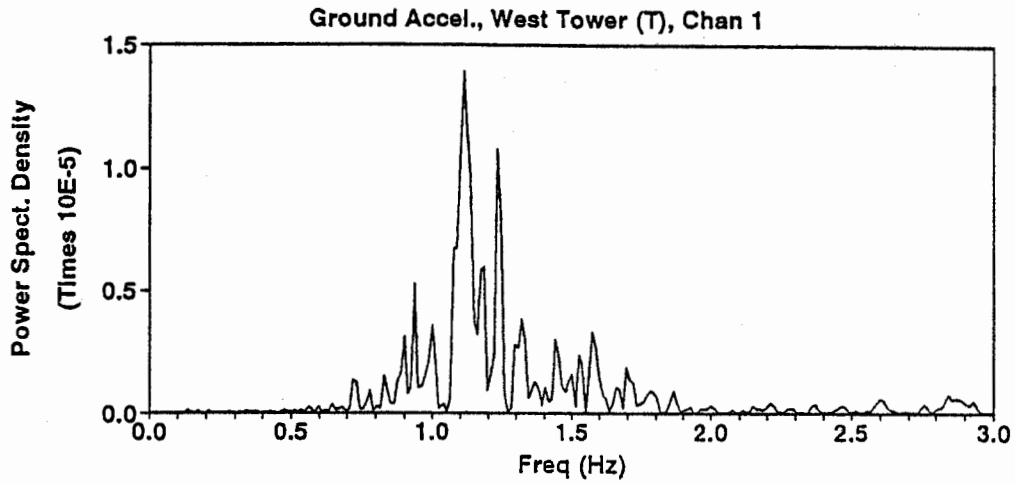
Figure 3.6: Acceleration Power Spectral Density Functions of Transverse Foundation Motion

Ground Disp.,West Tower (L), Chan 23

Ground Disp.,East Tower (L), Chan 13

Ground Disp.,East Anch. (L), Chan 25
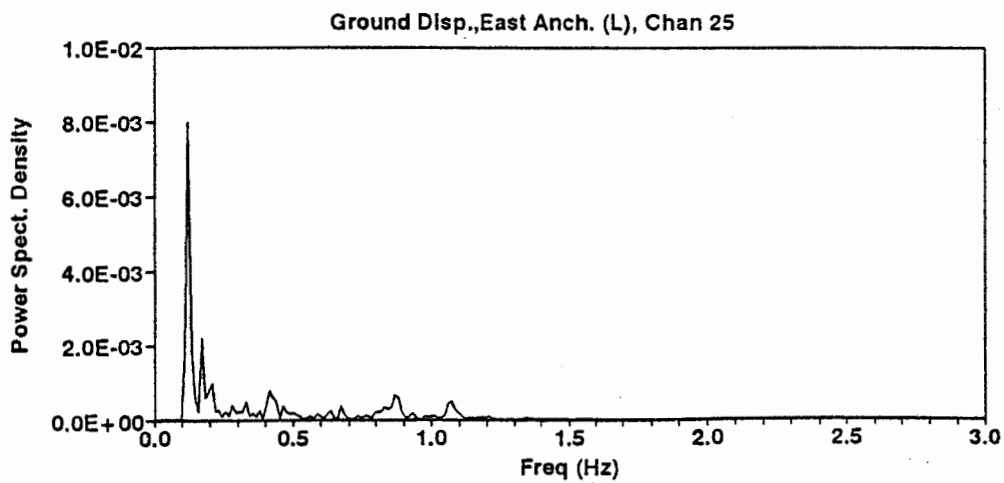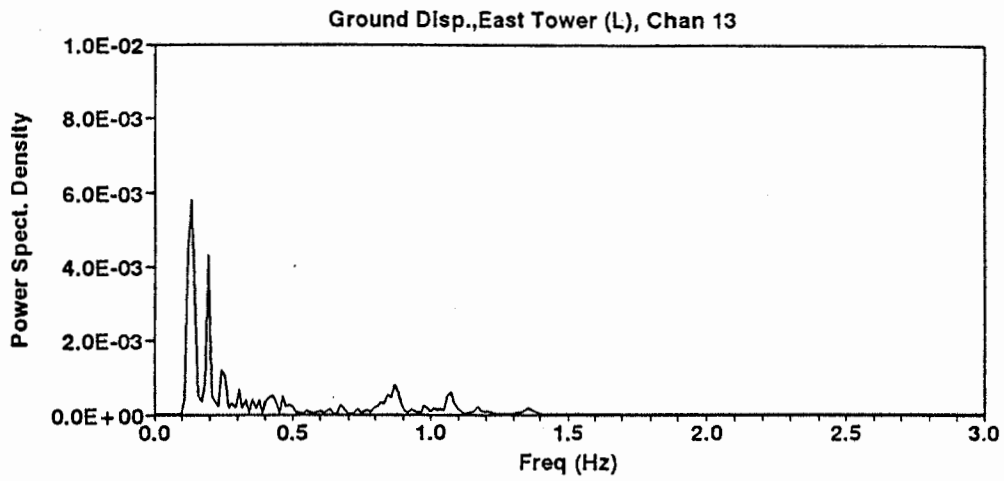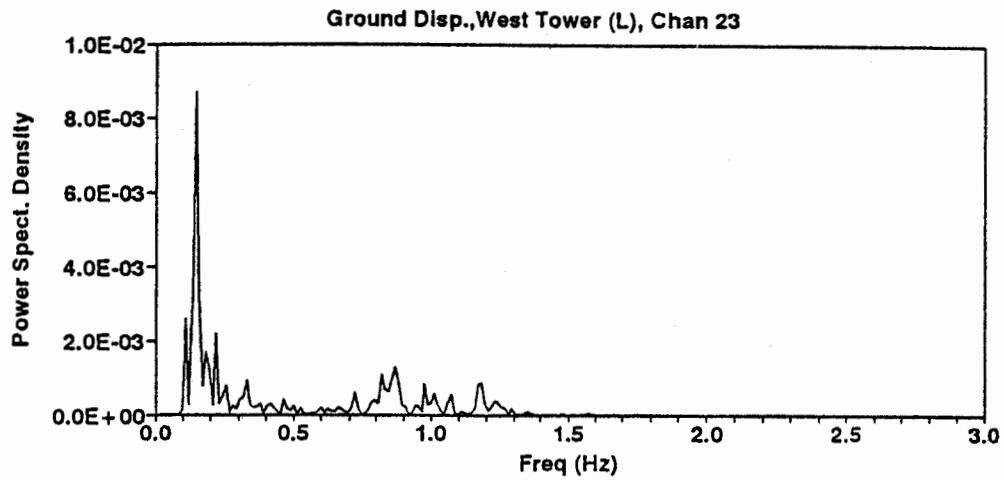
Figure 3.7a: Displacement Power Spectral Density Functions of Longitudinal Foundation Motion
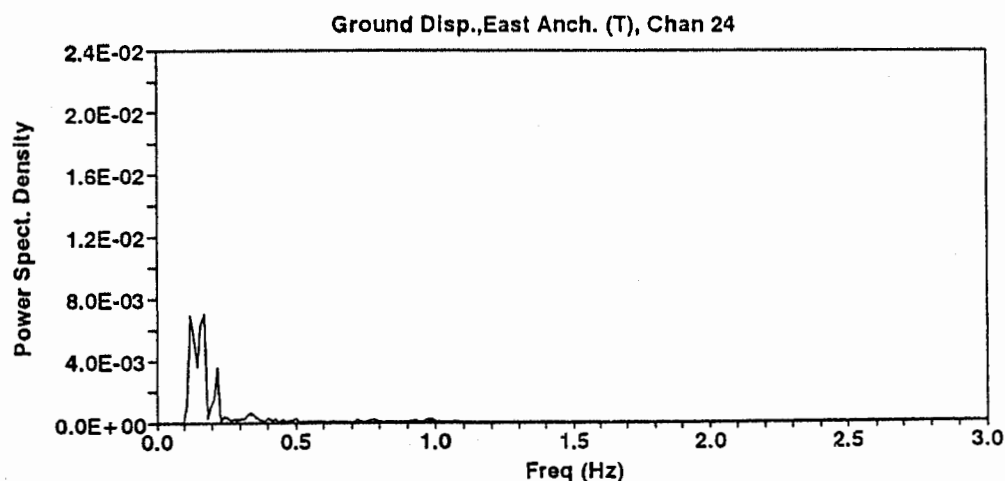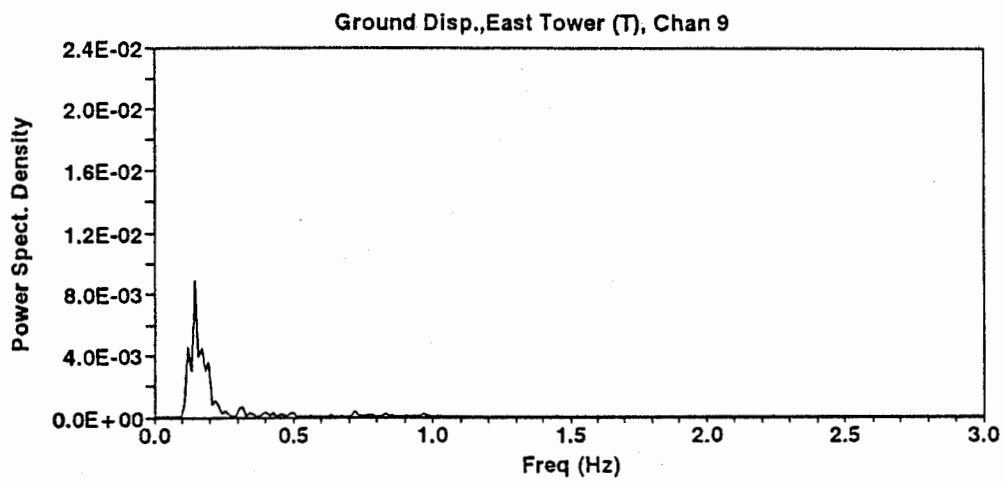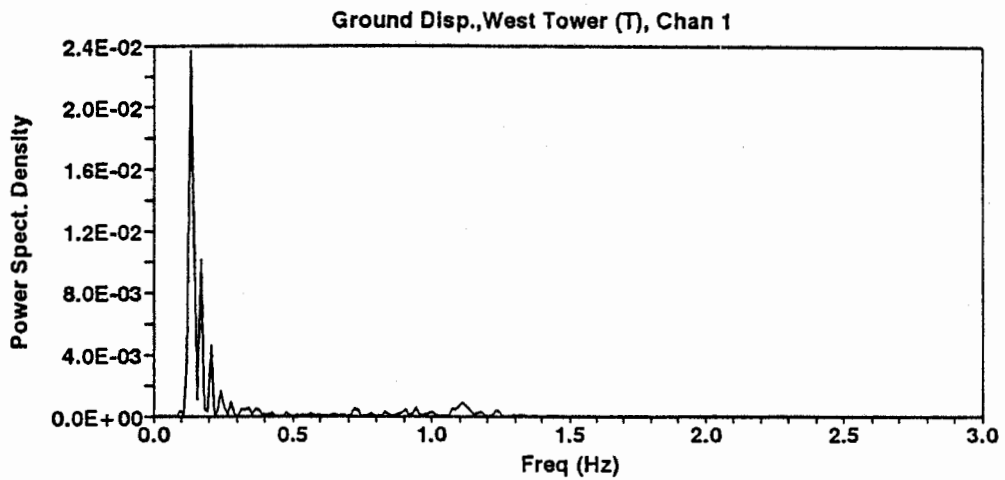
Figure 3.7b: Displacement Power Spectral Density Functions of Transverse Foundation Motion
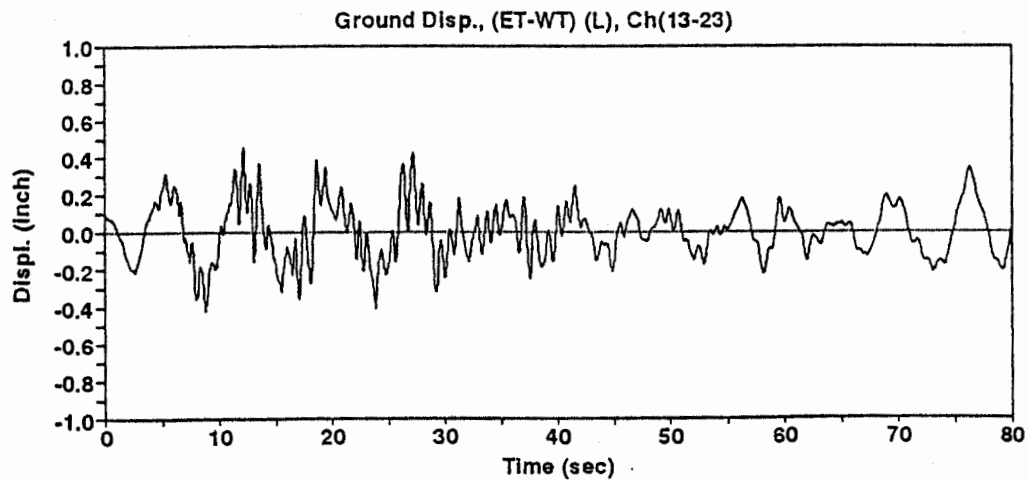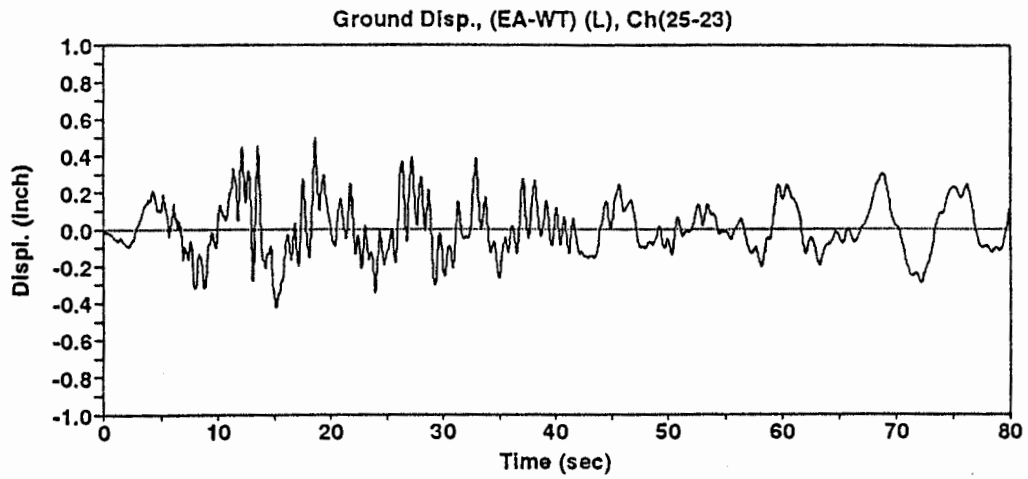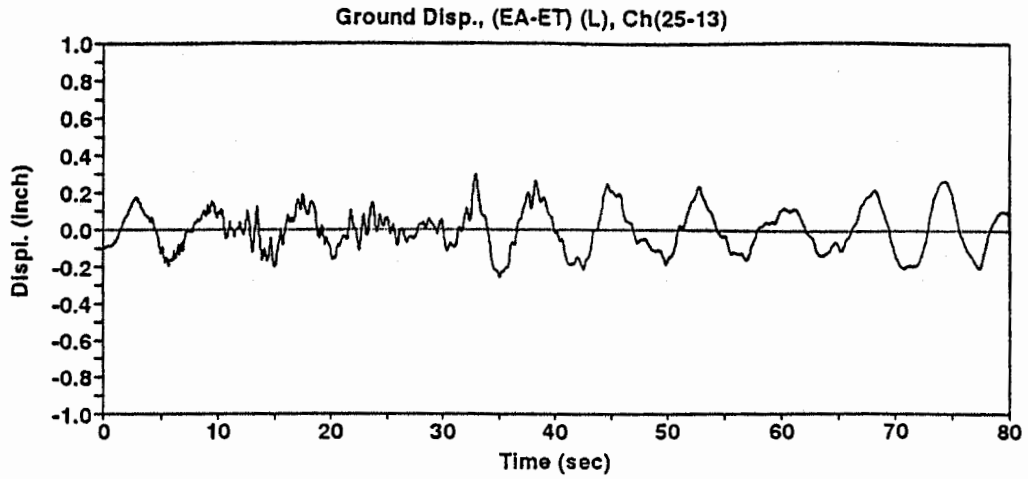
Figure 3.8a: Relative Foundation Displacement – Longitudinal Component

36
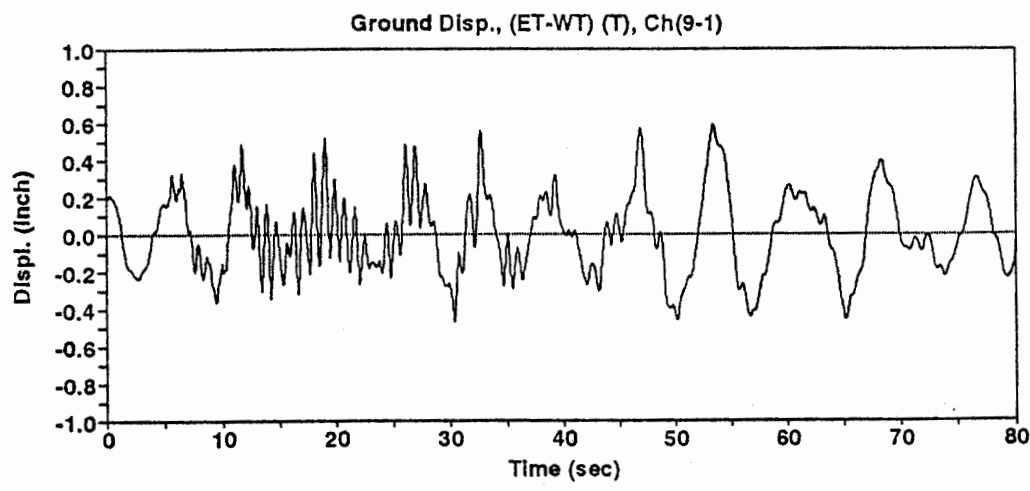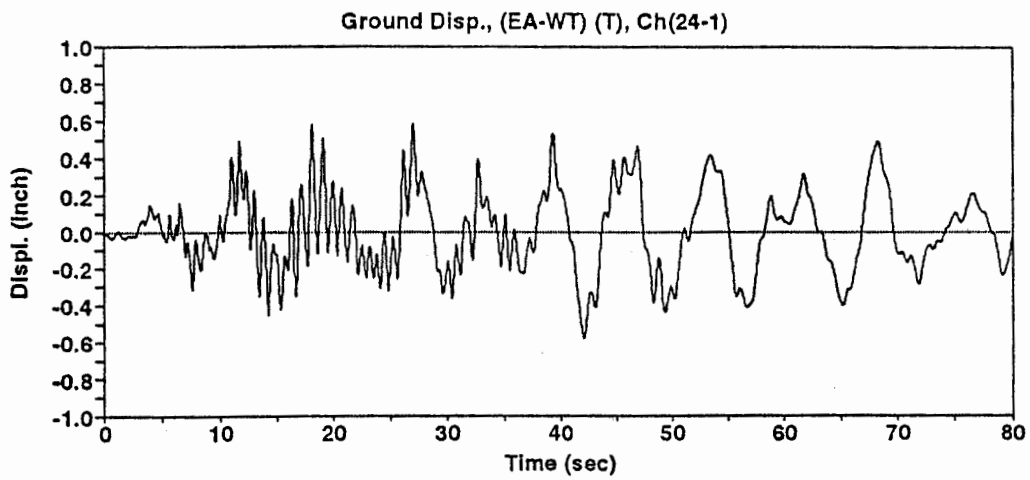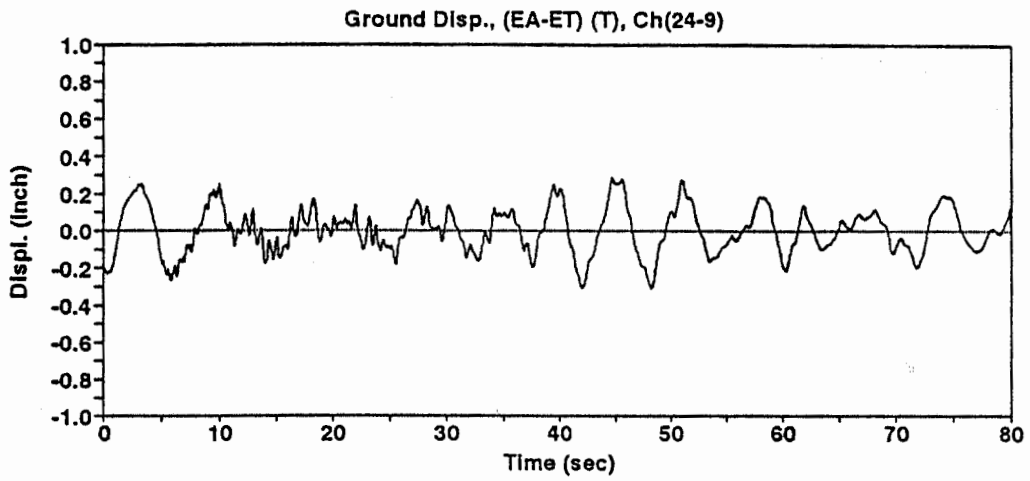
Figure 3.8b: Relative Foundation Displacement – Transverse Component

37
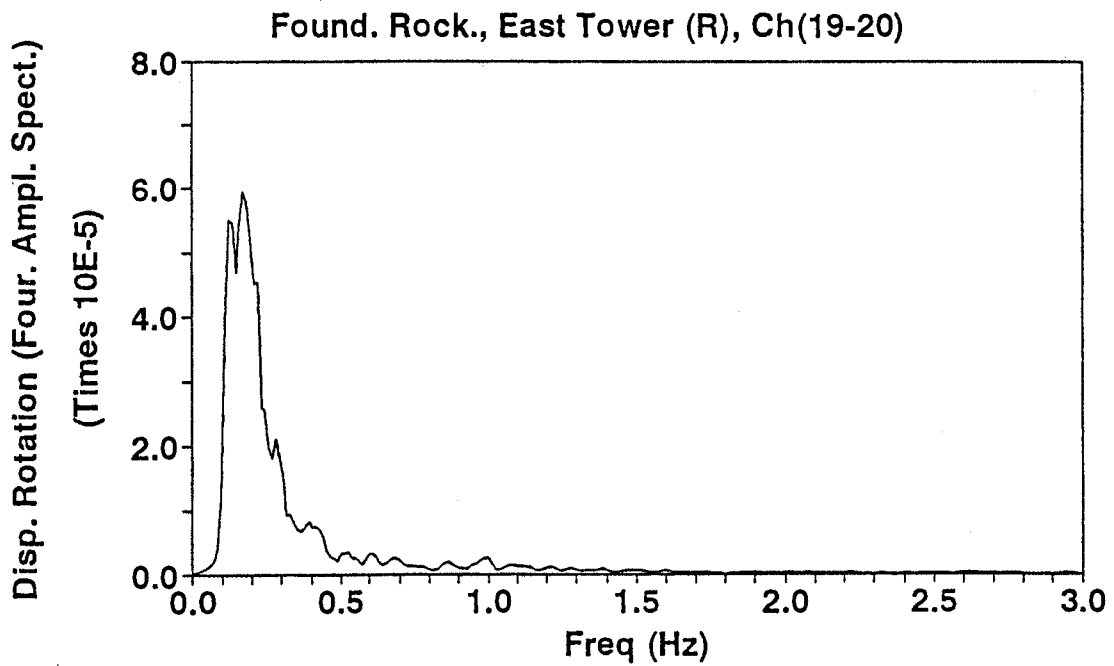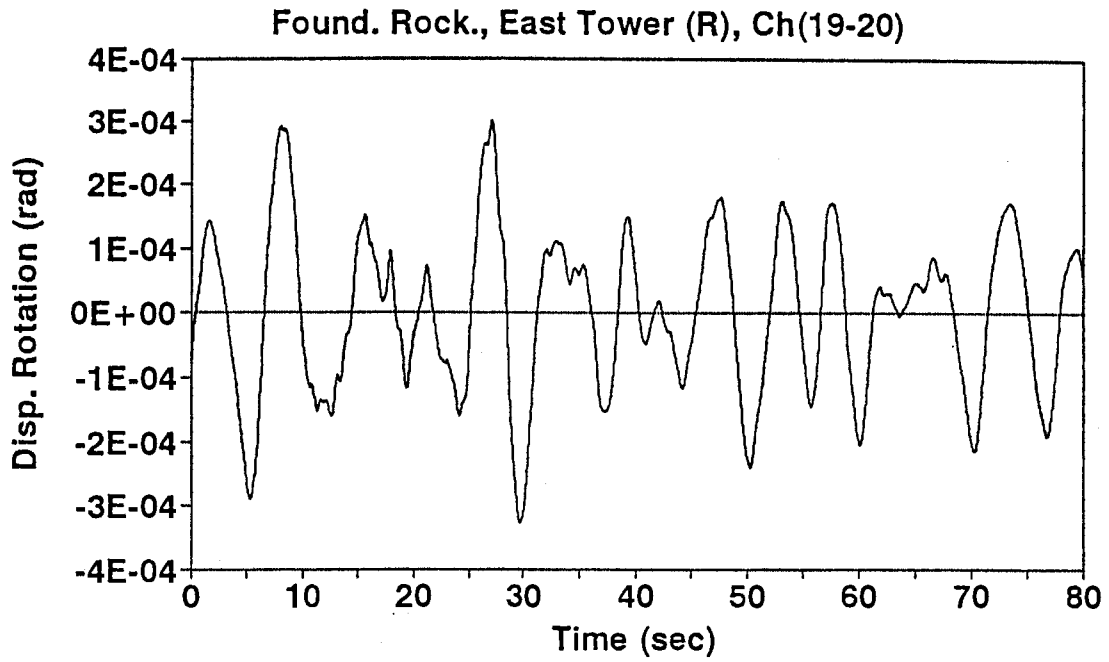
Figure 3.9: Foundation Rocking at East Tower
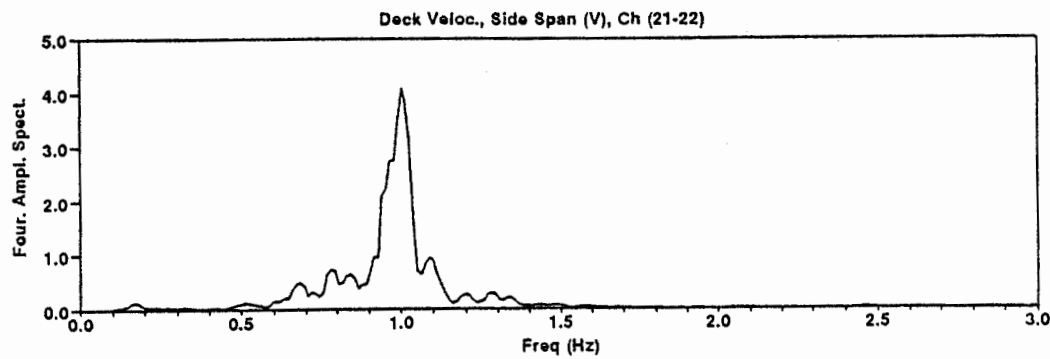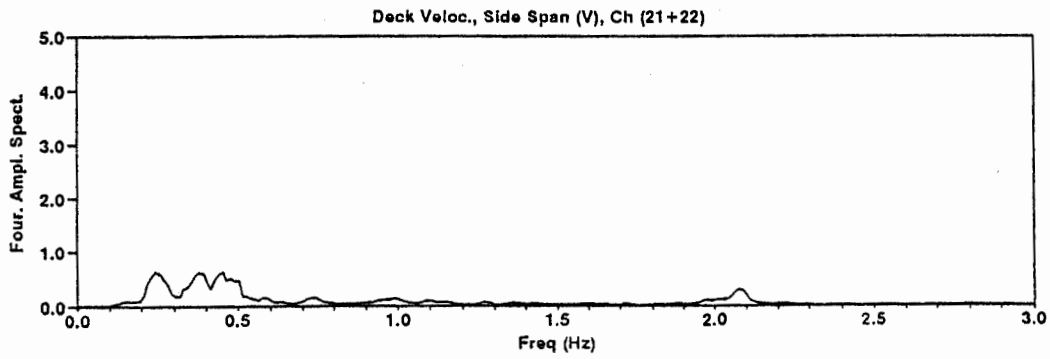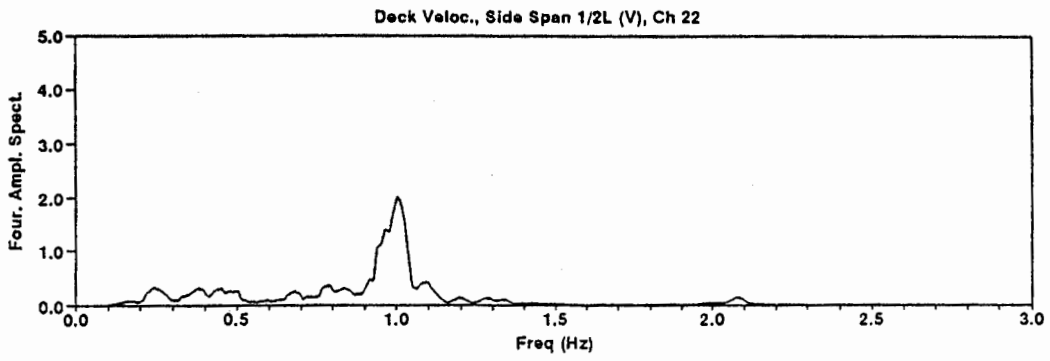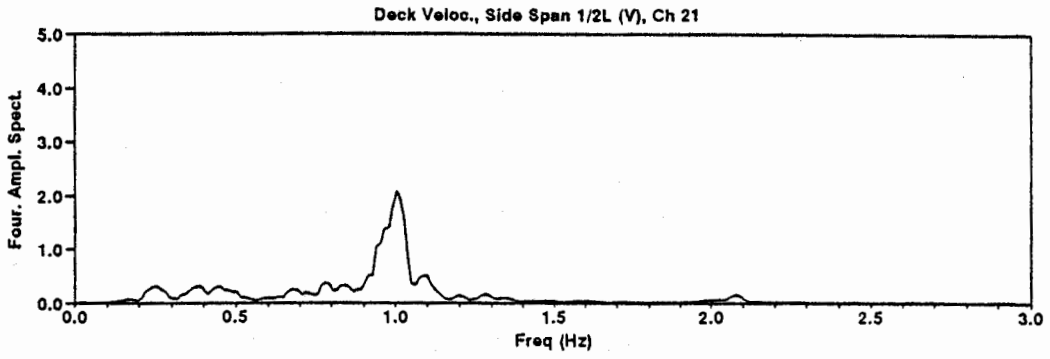
Figure 3.10: Fourier Amplitude Spectra of Vertical Motions at Midspan of the East Side Span
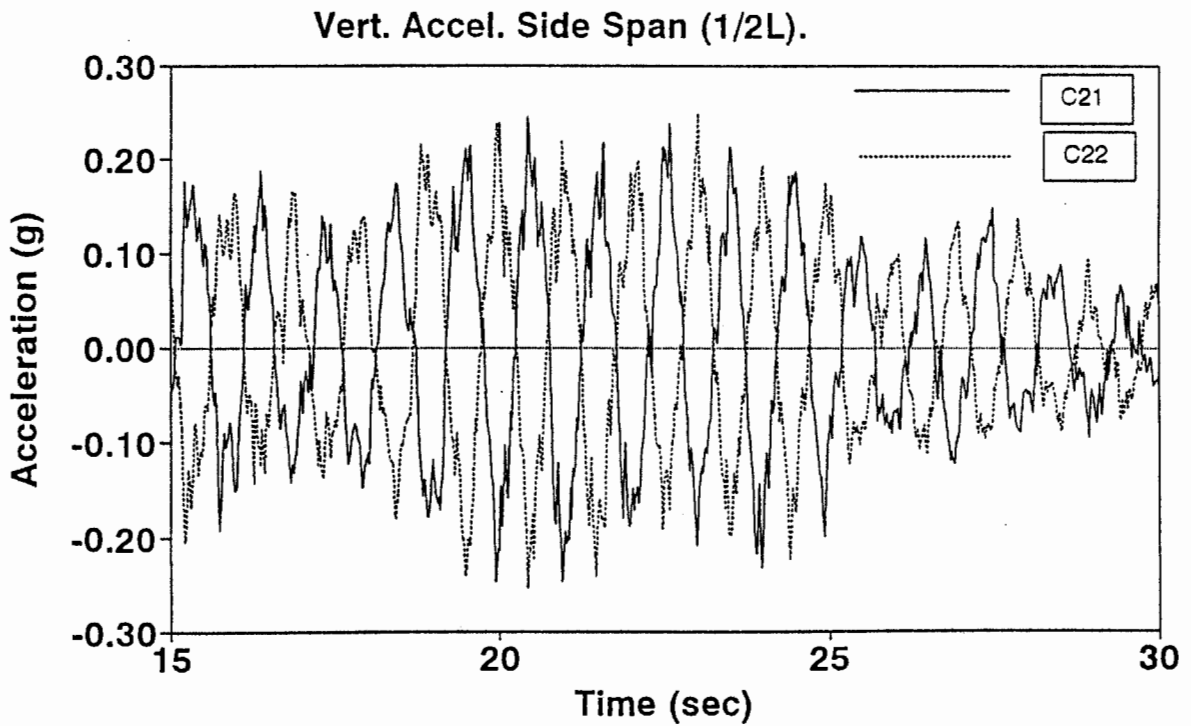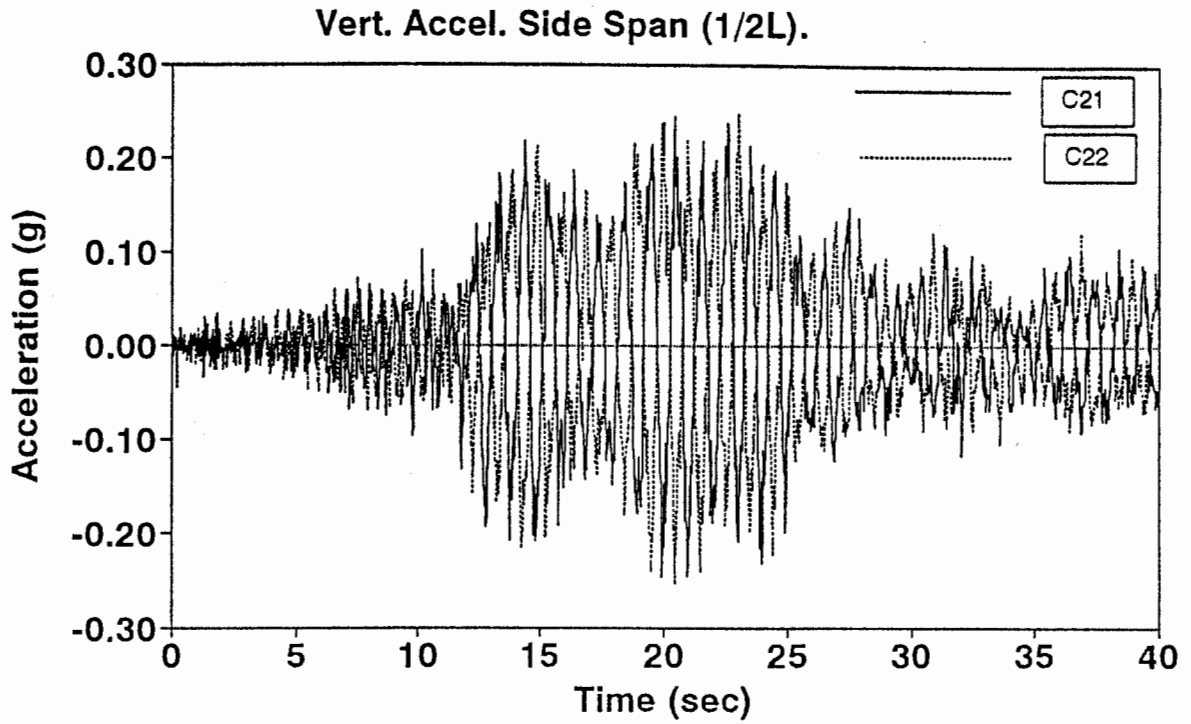
Figure 3.11: Vertical Acceleration Time Histories at Edge of Deck – Midspan of the East Side Span
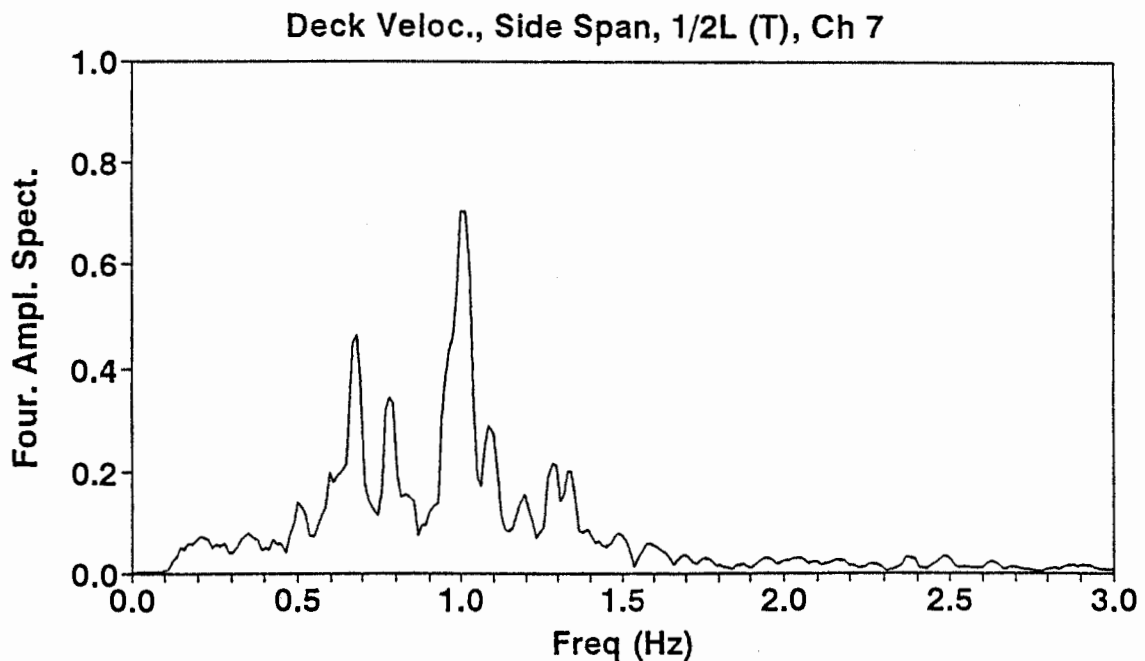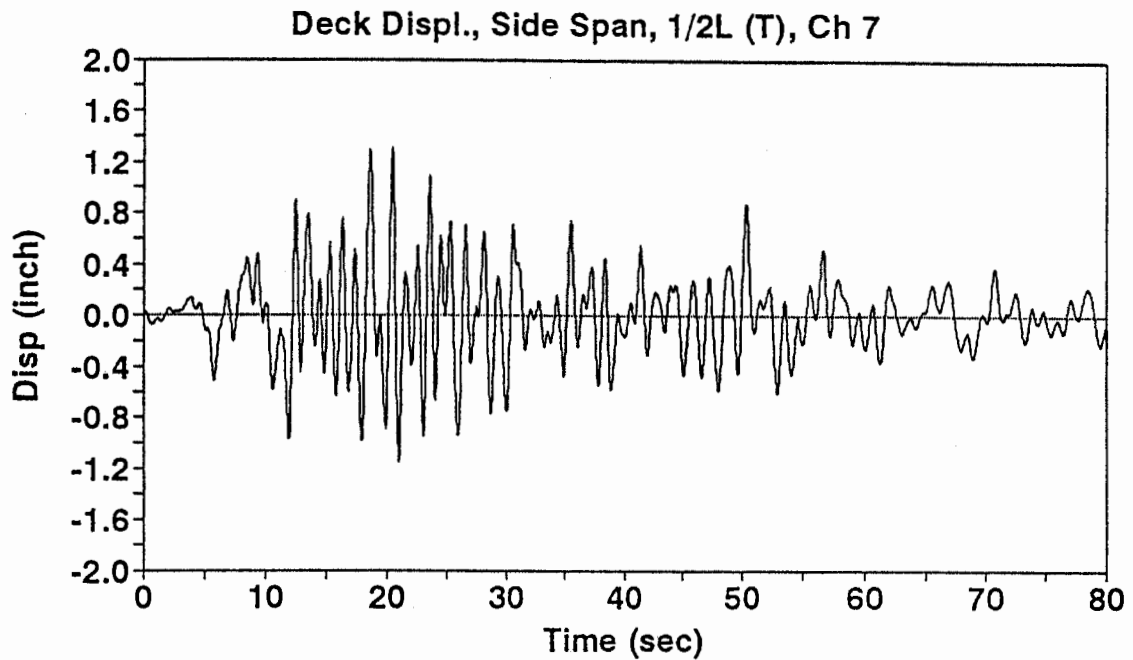
Figure 3.12: Transverse Displacement Time Histories of the Midspan of the East Side Span and the Fourier Amplitude of the Velocity
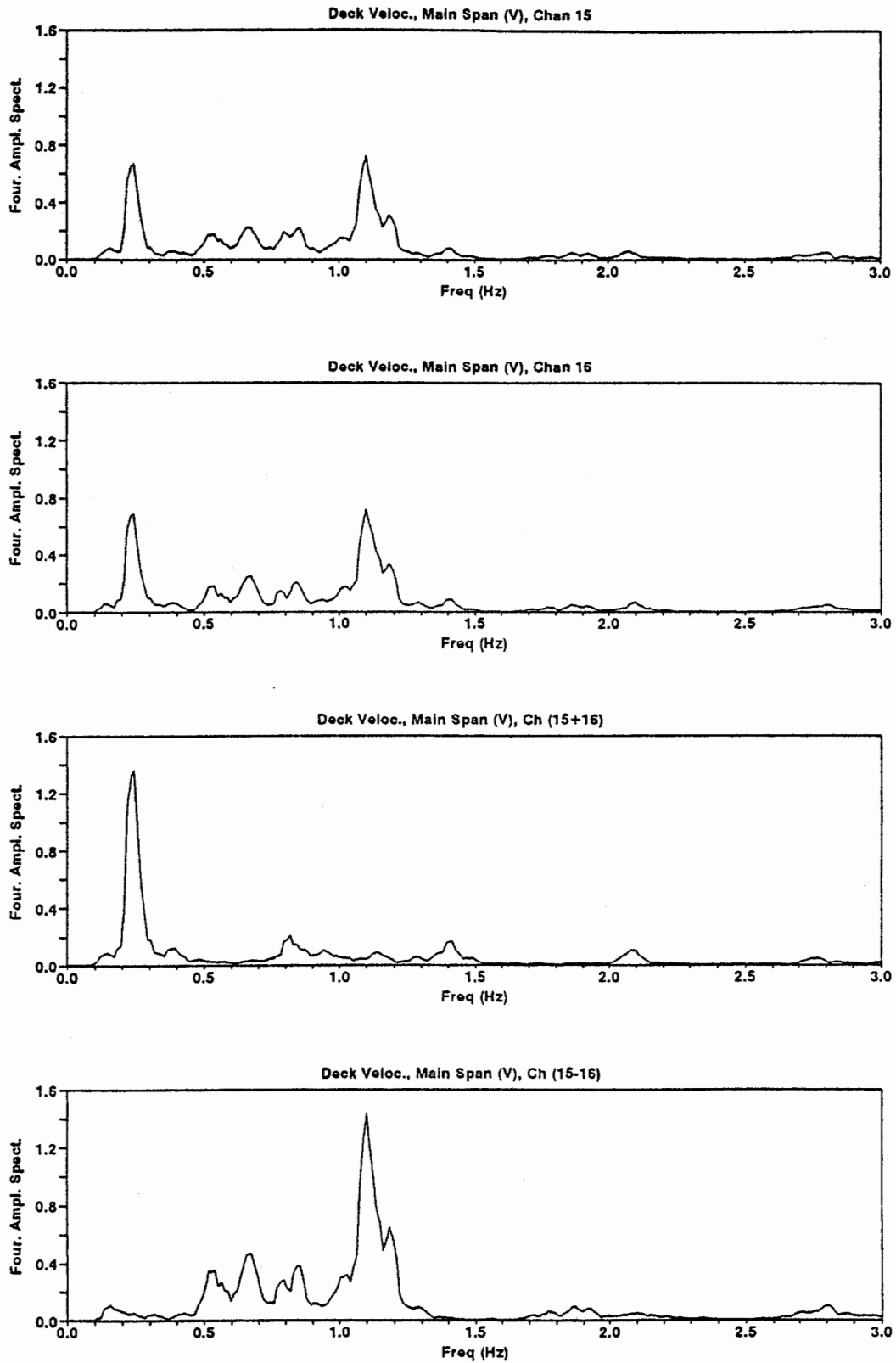
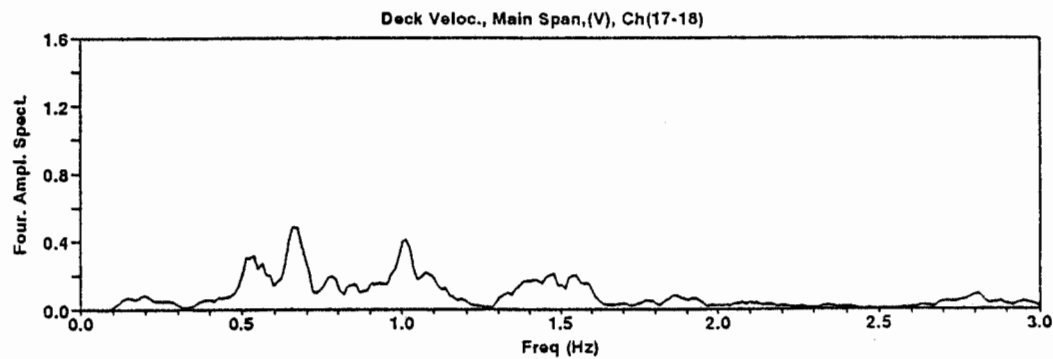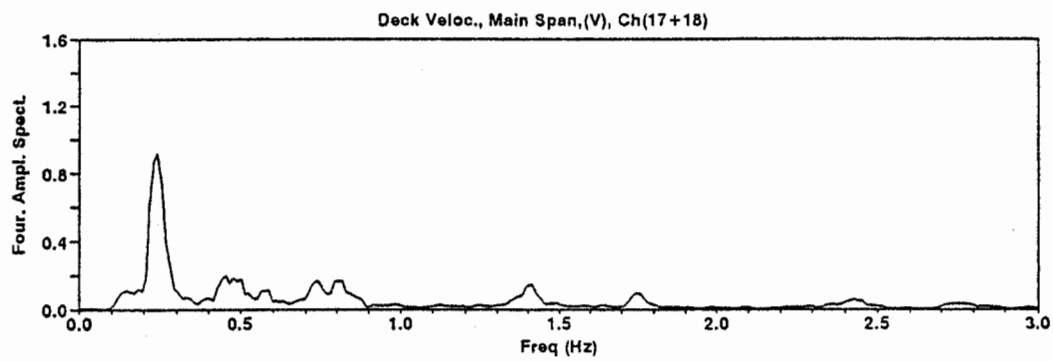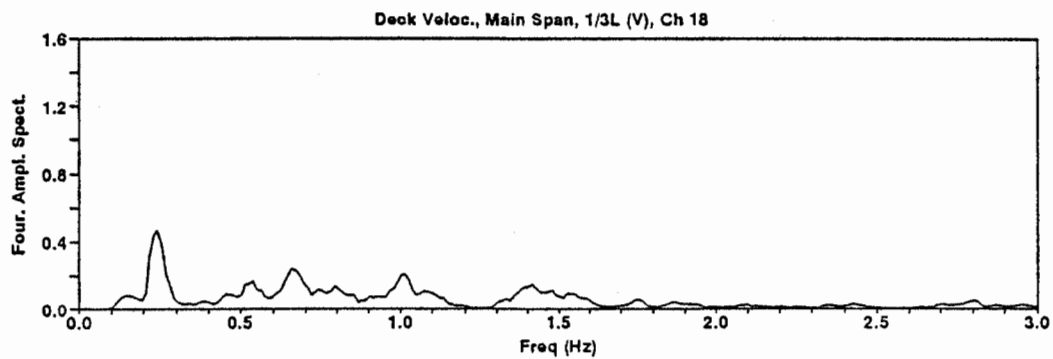**Figure 3.13a:** Fourier Amplitude Spectra of Vertical Velocity Motions at Midspan of the Main Span
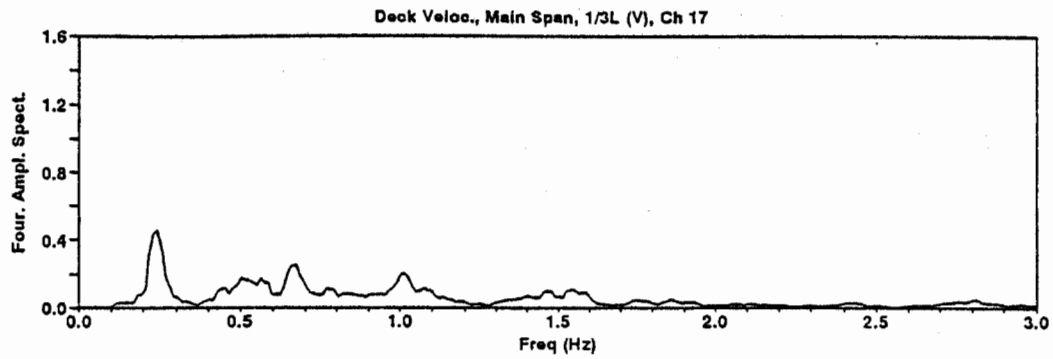
42

Figure 3.13b: Fourier Amplitude Spectra of Vertical Velocity Motions at $1/3$ L of the Main Span

43

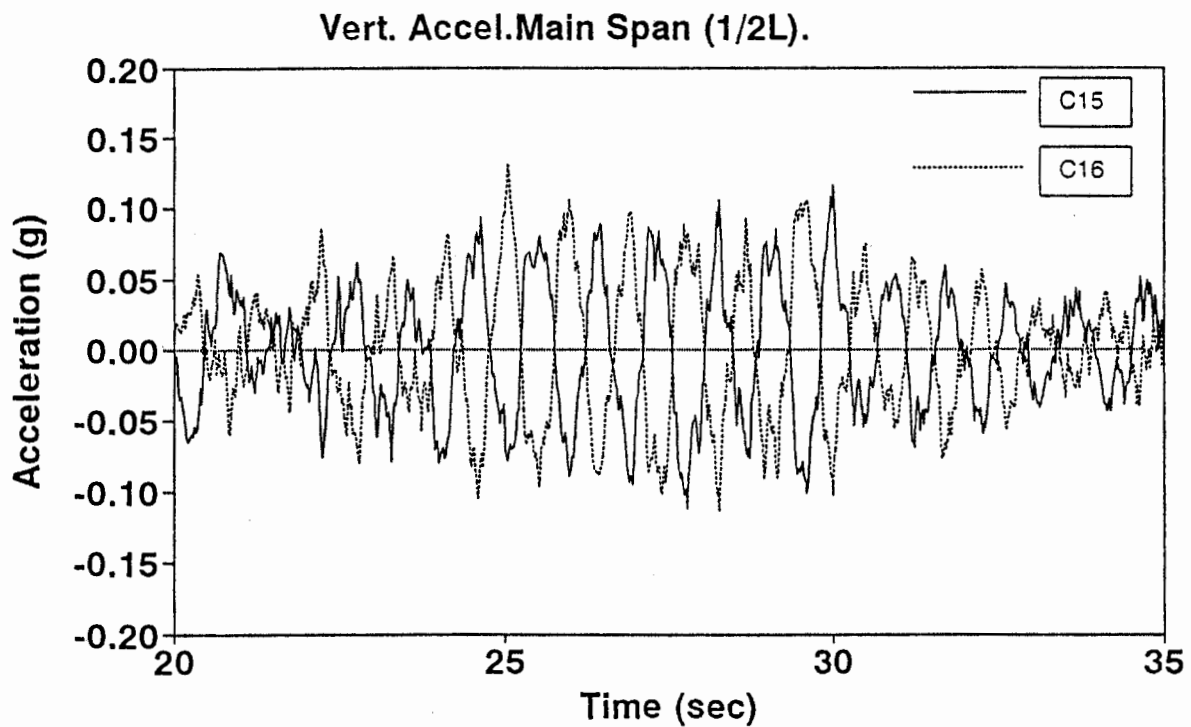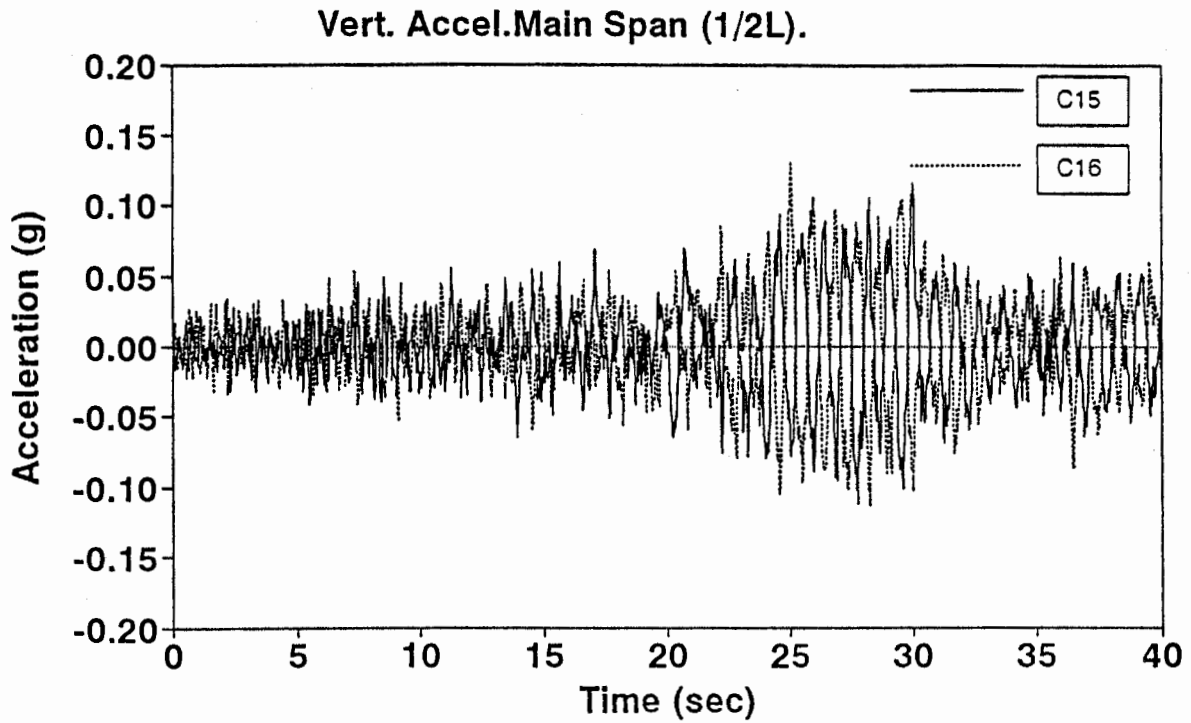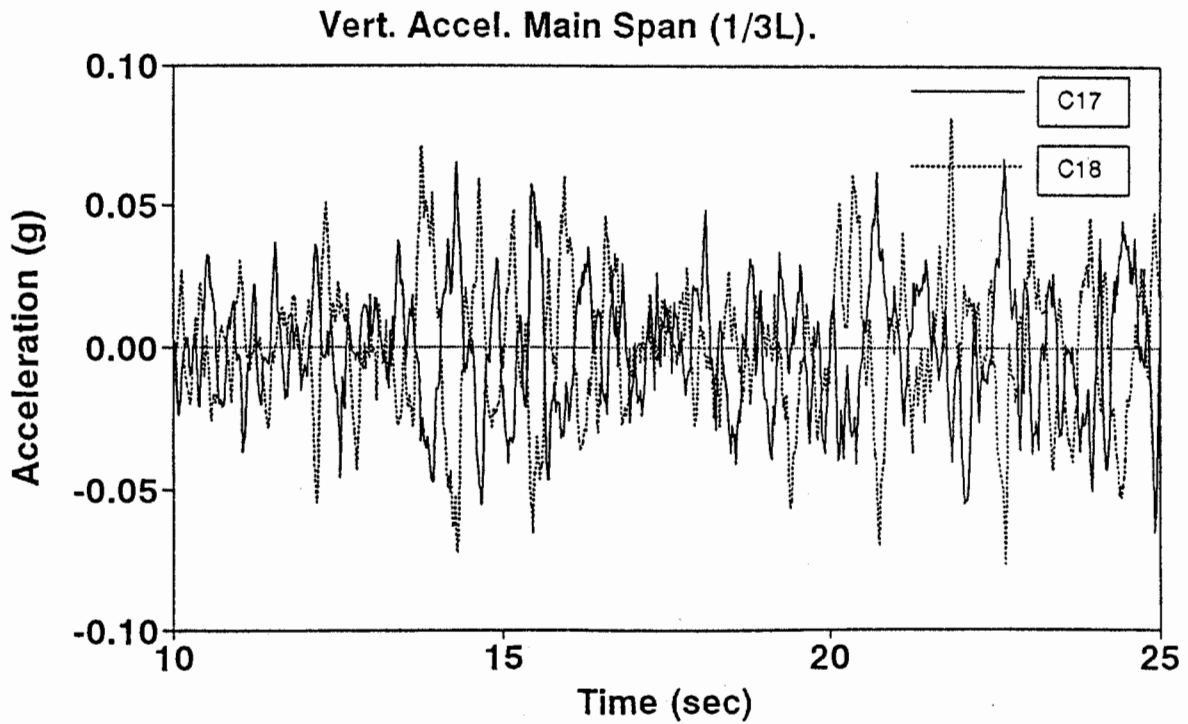**Figure 3.13c:** Vertical Acceleration Time Histories at Edge of Deck — Midspan of the Main Span

44

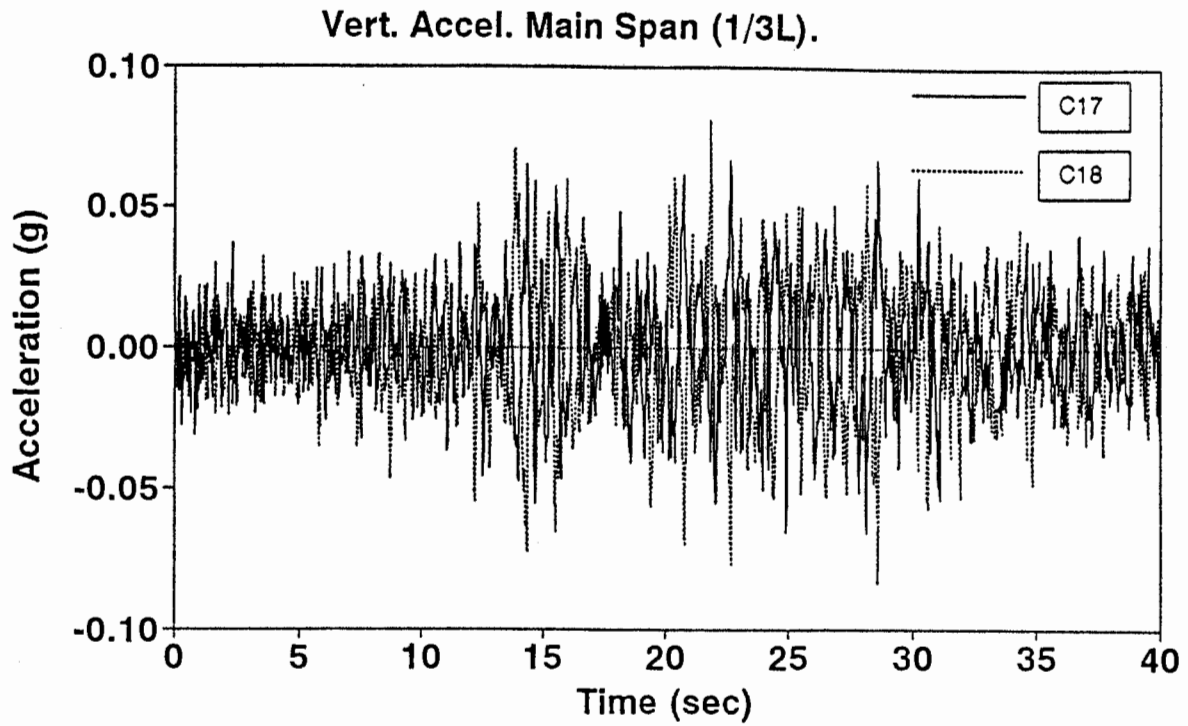**Figure 3.13d:** Vertical Acceleration Time Histories at Edge of Deck – $1/3$ L of the Main Span

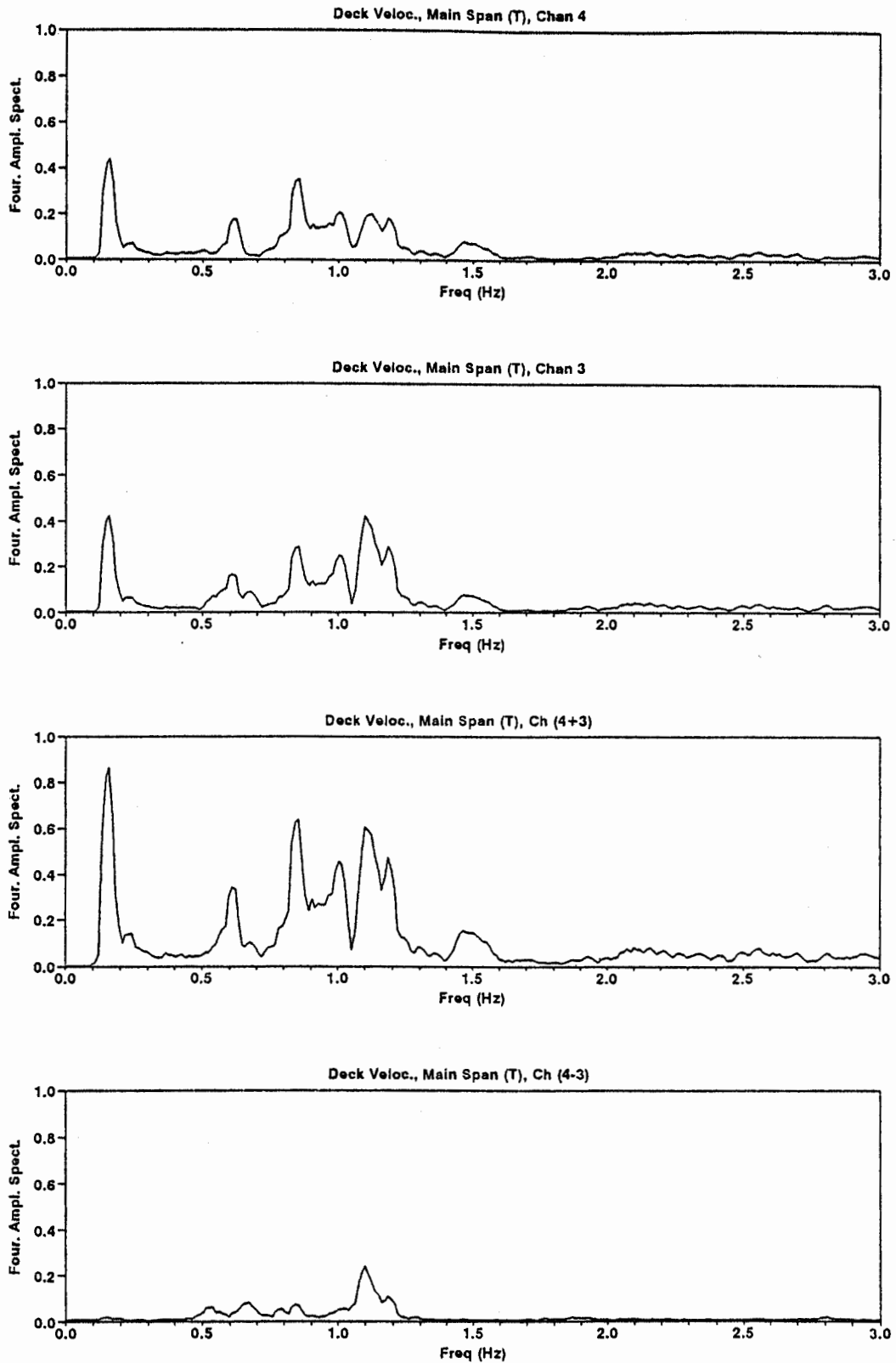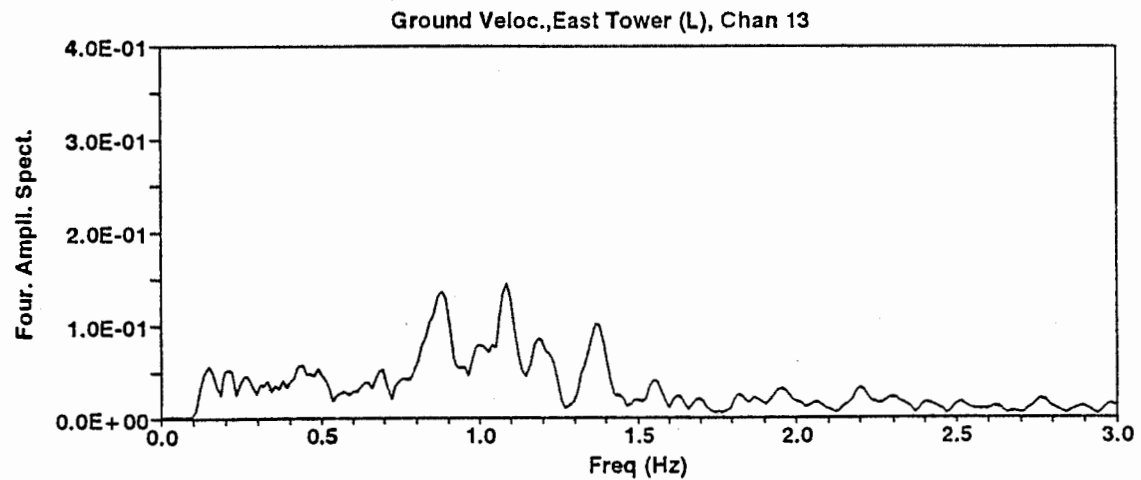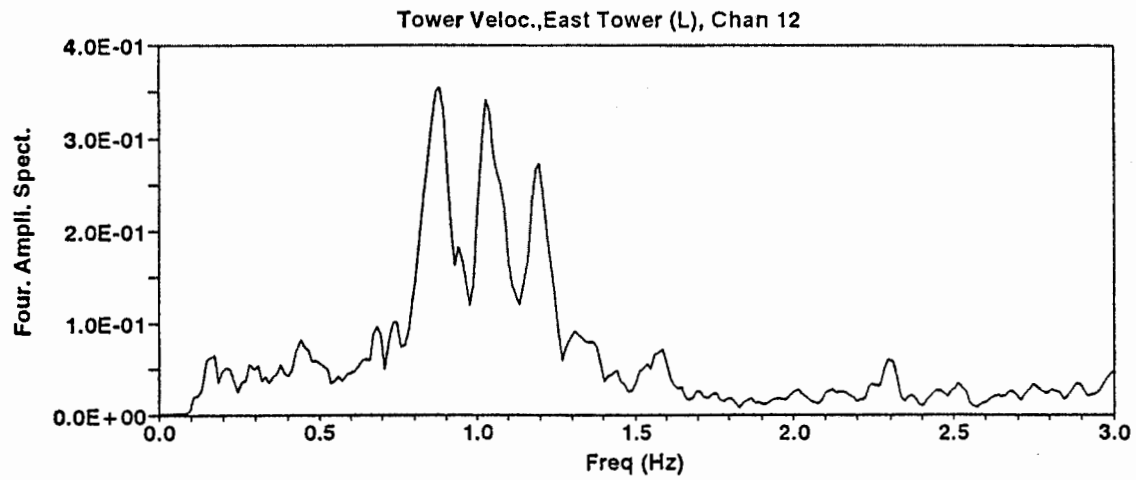**Figure 3.14: Fourier Amplitude Spectra of Transverse Velocity Motions at Midspan of the Main Span**

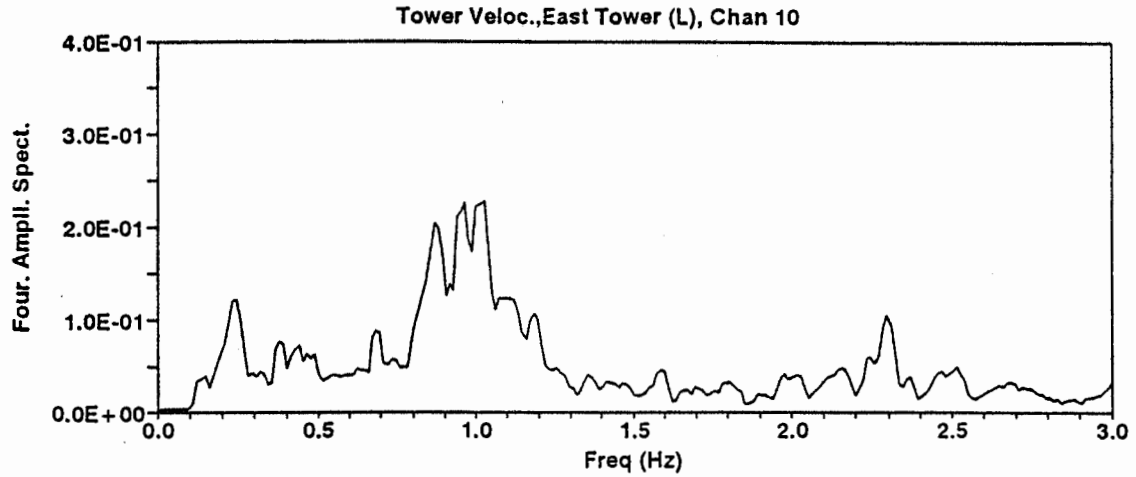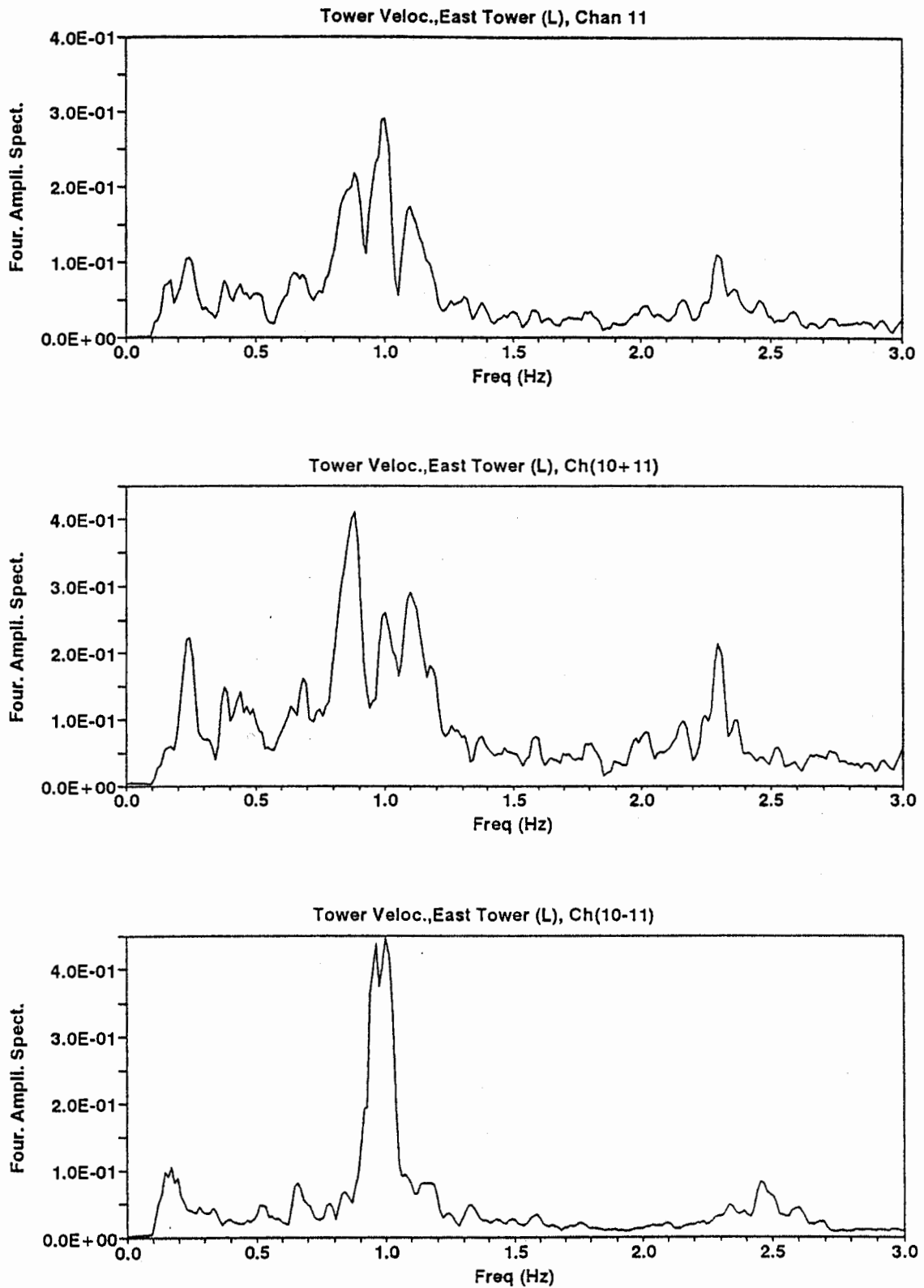**Figure 3.15a: Fourier Amplitude Spectra of Longitudinal Velocity Motions at East Tower**

47

Figure 3.15b: **Fourier Amplitude Spectra of Longitudinal Velocity Motions at East Tower**
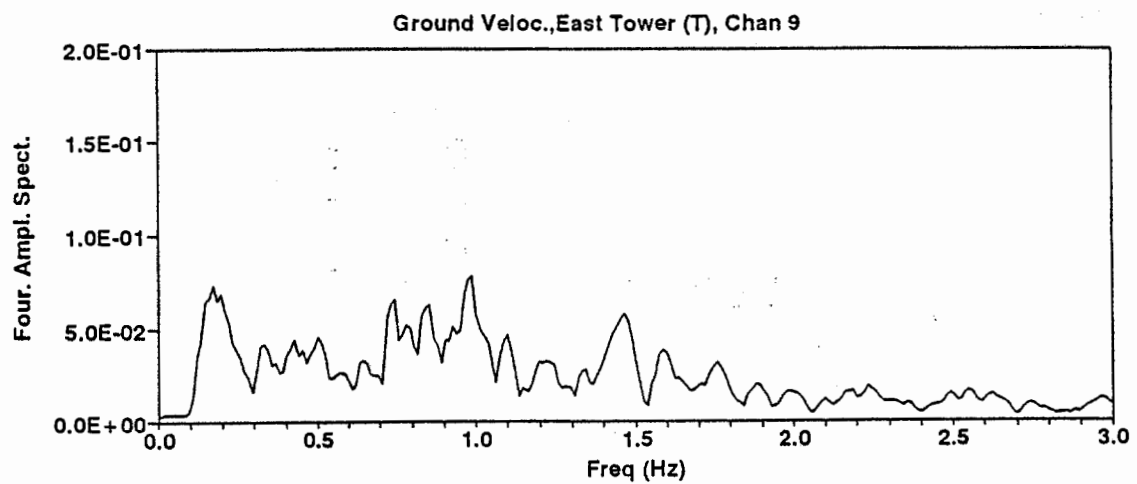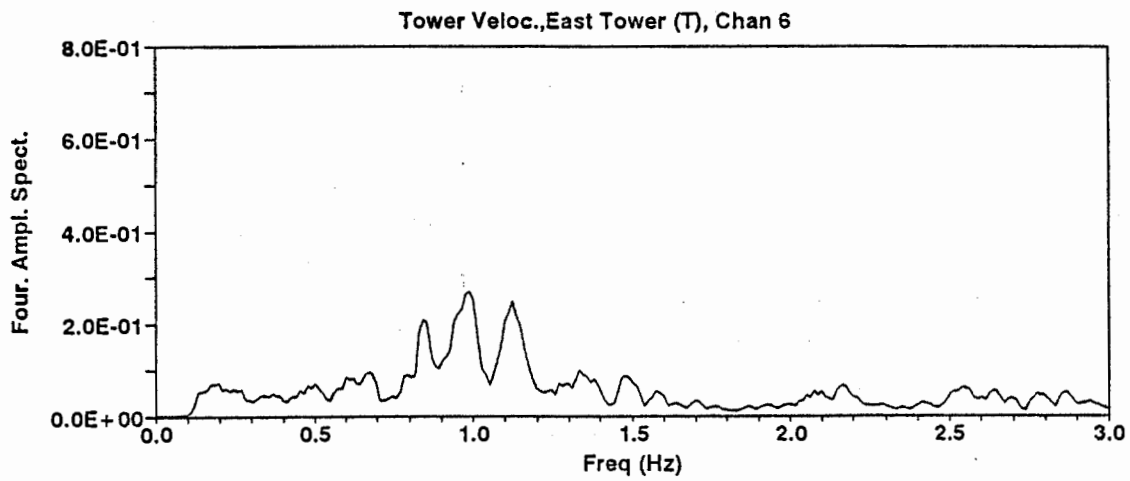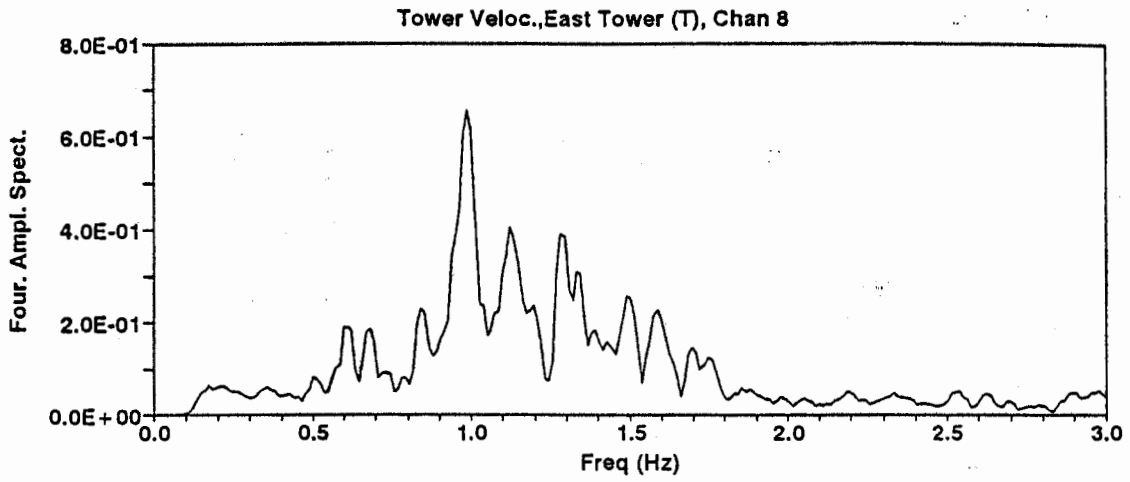
48

Figure 3.16: Fourier Amplitude Spectra of Transverse Velocity Motions at East Tower

4. Analytical Model of the Bridge

4.1 Method of Analysis

The primary characteristics of a suspension bridge is the nonlinear geometric effect even under the normal service load. Due to the high tension in the cable structure, the primary nonlinearity is the nonlinear stiffening effect. A generalized force-displacement relationship for typical cable structures is shown in Figure 4.1 (Abdel Ghaffar and Rubin, 1982). To accurately predict displacement and stress responses, it is crucial that a geometrically nonlinear analysis must be performed to establish the dead load deformed configuration of the structure which is consistent of the structural geometry. This is done using an updated Lagrangian formulation for the nonlinear large geometry problem (Bathe and Bolouschi, 1979) which accounts for both large displacement and large rotation.

Once the correct dead-load state (geometry, tangent stiffness, and member internal forces) is established, the response to seismic response can be performed using either linear or nonlinear dynamic analysis method. Typically, the earthquake-induced additional cable force is less than 25% of the dead load cable tension. Under this condition, the geometric nonlinear effect caused by the additional dynamic load is not large as shown schematically in Figure 4.1. This suggests that the dynamic response analysis can be carried out based on the linearized tangent stiffness at the dead load state and the geometric stiffness effect. However, if the seismic excitation is extremely high or inelastic component behavior is expected, the nonlinear dynamic analysis should be used to account for the material and geometric nonlinearities.

For the purpose of this study, a rigorous nonlinear static analysis was carried out first to establish the correct dead load state. For the subsequent dynamic analysis, the linearized tangent stiffness corresponding to the dead-load state was used.

Multiple-Support-Excitation Time History Analysis – The analysis is carried out by direct integration of the coupled equations of motion of the structure model. Ground displacement time histories are used to obtain the total displacement

response which includes both the quasi-static effect and the vibrational effect (Clough and Penzien, 1992).

4.2 Development of Analytical Model

To capture the essential behavior characteristics of the bridge, a three-dimensional global model of the structure was developed. The cross sectional properties of various members are tabulated in Table 4.1.

The structure is idealized as an assemblage of finite elements to represent the complicated geometry, inertia and stiffness effects.

Tower Structure and Cable Bents – All elements are included in the model using 3D two-node beam elements. At the bases of each tower legs, the tower nodes are rigidly connected to a node representing the top of concrete pier. The stiffness effects of the supporting pile groups and the soil medium are represented as a set of six lumped springs. The variation of cross section along the tower height was taken into account. The concrete cable bents and foundations were idealized in a similar manner. The cross sectional properties of different elevations are tabulated in Table 4.2.

Main Cables and Hanger Ropes – Cable elements are used to idealize the main cable as well as the hanger ropes. Main cables are discretized into short straight segments (between adjacent suspender nodes). The forces in the cables and hangers were included as initial fixed-end-forces to ensure the correct geometry (cable profile) under dead load condition and a temperature of 68°F.

Cable Anchorage – This is modeled as a rigid block. The pile-supported foundation is represented by a set of lumped springs.

Stiffening Truss System – A typical panel of the stiffening truss, transverse floor truss, bottom lateral bracing, and stringers are shown in Figure 4.2. To establish a simplified representation of the 3D truss system, equivalent 3D beam properties were derived for each of the two stiffening trusses and the floor truss. The stiffness contribution of the stringers and the concrete deck were taken into account. The

51

equivalent cross section properties are summarized in Table 4.1. The analytical model of the truss system (as shown in Figure 4.3) is now made up of these equivalent beam elements and the bottom lateral K bracing elements. The offset between nodal points are modeled as short rigid links. In this way, the typical assumption for plane section (of the truss system) to remain plane is avoided which will prevent any torsion-induced warping distortion of the cross section of the truss system. There are about 3,500 members in the stiffening truss system, which are represented by 486 equivalent elements in the analytical model.

Structural Connection Details – Zero-length hinge elements with a set of six diagonal stiffness coefficients are used to model the following connections:

- Cable saddles at top of towers and cable bents.
- Truss hangers at main towers and truss brackets at cable bents.
- Truss wind shoes at main towers and cable bents.

A cross section view and a side view of the main tower are shown in Figure 4.4. Note that the inclined hanger rope geometry is taken into account. The analytical model of the bridge is shown in Figure 4.5.

4.3 Vibration Characteristics of the Bridge

A frequency analysis was conducted to extract the lowest 100 vibration modes of the bridge. Because of the flexibility of the cable, there are many cable lateral sway modes.

Transverse and Torsional Vibration Modes – Typically the lateral vibration of the truss is coupled with the torsional motion of the truss box. The first mode is primarily the transverse vibration of the center span with a period of 7.01 seconds (Figure 4.6). As shown in the figure, there are slight torsional twist of the truss and both towers. Mode No. 4 is the second transverse mode of the center span with a period of 3.69 seconds as shown in Figure 4.7. At the quarter point, the cross section view is shown indicating strong torsional motion. Mode 6 with a period of 2.90 seconds involves the vibration of both side spans and the center spans (Figure 4.8). Torsional response of both towers are also included. Mode 10 (T_{10} =

2.10 seconds) is primarily the center span torsional response (Figure 4.9). Mode 11 (T_{11} = 2.07 seconds) is primarily response of the side spans (Figure 4.10). Mode 20 (T_{12} = 1.60 seconds) is the transverse mode of the center span (similar to Mode 4) with significant lateral sway motion of cables as shown in **Figure 4.11**. In some of these modes, torsional response of the towers are also included whenever, there is lateral sway motion of the main cables such as Modes 1, 6, 10, 11 and 20.

Longitudinal and Vertical Modes – These vibration modes are summarized in Table 4.4 which gives the period of each mode and the direction of vibration for the seven parts of the structure. Figure 4.12 shows the ten lowest vibration modes involving primarily the response of the suspended spans. Additional vibrational modes involving both the suspended structures, towers and cable bents are shown in Figure 4.13. In the period range of about 1 second , there are several modes involving significant longitudinal vibration of the towers and cable bents. The longitudinal vibration modes of towers are typically in pairs with essentially the same frequencies, but with the two towers moving either in-phase or out-of-phase.

Transverse Modes of the Tower – Transverse vibrations of the towers are affected by the interaction with

- Main cables at top.
- Stiffening truss.
- Foundation compliance effect.

The basic mode shape is of the cantilever bending type in Figure 4.14 with a period of 1.0 to 1.2 second. Depending on the interaction with lateral swaying of cables on top of tower and the transverse vibration of the stiffening truss systems, various higher order modes are exited as shown in Figure 4.15. Also shown in Figure 4.15 is a mode with some foundation translation.

53

Table 4.1: Properties of Structural Elements

Typical Tower Strut Section Property

	A(ft^2)	J(ft^4)	Iyy(ft^4)	Izz(ft^4)
Upper Two Panels	0.435	0.001	0.440	0.047
Lower Three Panels	0.615	0.003	0.653	0.082

Typical Cable Area

	A(ft^2)
Main Cable	0.844
Hanger Rope	0.035

Cable Bent

	A(ft^2)	J(ft^4)	Iyy(ft^4)	Izz(ft^4)
Vertical Elem	71	424	562	1816
Horizonal Elem	80	906	426	666

Typical Truss Sections

	A(ft^2)	J(ft^4)	Iyy(ft^4)	Izz(ft^4)
Equivalent Stiffening Truss Girder	0.85	0.51	0.26	42.67
Equivalent Floor Beam	0.45	0.00	0.09	16.94
Bottom Lateral	0.12	0.00	0.02	0.01

Mass Distribution of Truss

	A(ft^2)	Length	Unit Weig	(31' length cell) Weight(k)	Mass Moment of Inertia
Top Cord	0.34	62.00	0.49	10.33	8987
Bottom Cord	0.34	62.00	0.49	10.33	8987
Diagonal	0.11	87.00	0.49	4.69	271
Vertical	0.11	30.00	0.49	1.62	93
Floor Truss	0.44	59.00	0.49	12.72	669
Concrete Deck	29.52	31.00	0.13	118.97	28374
Curb	1.05	62.00	0.15	9.44	8212
Stringers	1.11	31.00	0.49	16.89	4029
Lateral bracing	0.11	84.00	0.49	4.53	1080
Summation				189.51	60701

Table 4.2: Cross Section Properties of the Tower

Vincent Thomas Tower Leg Section Property Table

Elevation(ft)	A(ft^2)	J(ft^4)	Iyy(ft^4)	Izz(ft^4)
360				
	3.79	20.02	28.62	28.38
335				
	3.93	21.28	32.47	32.05
301				
	4.08	22.7	37.27	36.47
268				
	4.2	23.82	41.45	40.21
249				
	4.4	24.6	46.77	43.58
224				
	4.6	25.55	52.83	47.57
199				
	4.7	26.5	56.84	51.04
183				
	4.92	28.04	63.66	57.3
163				
	5.37	30.3	73.41	69.66
130				
	5.82	32.64	84.28	82.89
111				
	6.17	33.72	99.51	92.88
78				
	6.52	34.2	115.85	103.82
58				
	6.78	35.53	129.49	115.36
25				

E=4,320,000 KSF
W=640(lb/ft^3)

Table 4.3:   Foundation Stiffness Coefficients (Units: Kip, Ft. Rad)

		Anchorage	Cable Bent	West Tower	East Tower	Cable Bent	Anchorage
a.	*Pile Group*						
	Longitudinal	82,640	25,700	104,400	95,670	34,620	1,134,000
	Transverse	58,780	13,880	35,530	123,800	17,700	75,000
	Vertical	2,104,000	749,200	2,456,000	3,672,000	1,055,000	2,895,000
	Rotation @ L	6.51×10^8	3.98×10^8	2.54×10^9	3.76×10^9	5.60×10^8	2.00×10^9
	Rotation @ T	2.64×10^9	2.43×10^7	4.12×10^8	6.42×10^8	3.41×10^7	3.63×10^9
	Rotation @ V	1.46×10^9	1.42×10^7	1.10×10^8	1.02×10^8	1.90×10^7	8.88×10^8
b.	*Pile Cap*						
	Longitudinal	165,000	144,000	122,000	738,000	305,000	349,000
	Transverse	290,000	51,800	65,750	405,200	109,200	612,000

Table 4.4: Longitudinal and Vertical Vibration Modes

Mode	T (sec)	East Cable Bent	West Side Span	West Tower	Main Span	East Tower	East Side Span	East Cable Bent
2	5.02	–	–	–	V	–	–	–
3	4.48	–	V	L	V	L	V	–
5	3.42	–	V	L	L/V	L	V	–
7	2.86	–	V	–	V	–	V	–
8	2.79	–	V	–	L	–	V	–
9	2.23	–	V	–	V	–	V	–
16	1.85	–	–	–	V	–	–	–
24	1.29	–	–	L	V	L	–	–
31	1.02	L	L/V	L	L	L	L/V	L
32	1.00	L	L/V	L	–	L	L/V	L
33	0.97	L	V	L	V	L	V	L
35	0.96	L	L/V	L	V	–	V	L
36	0.96	L	L/V	L	–	L	V	L
39	0.88	L	L	L	–	L	L	L
41	0.88	L	L	L	–	L	L	L
50	0.75	–	–	L	V	L	–	–
60	0.60	–	–	–	V	–	–	–
65	0.56	–	–	–	L	–	–	–
75	0.51	L	V	L	L	L	V	L
76	0.50	–	V	–	–	–	V	–
77	0.50	–	–	–	V	–	–	–
78	0.49	L	L/V	L	–	L	L/V	L
89	0.43	–	–	–	L	–	–	–
90	0.43		–	–	–	L	–	L
91	0.43		–	L	V	L	–	
92	0.42		–	L	–	–	L	L
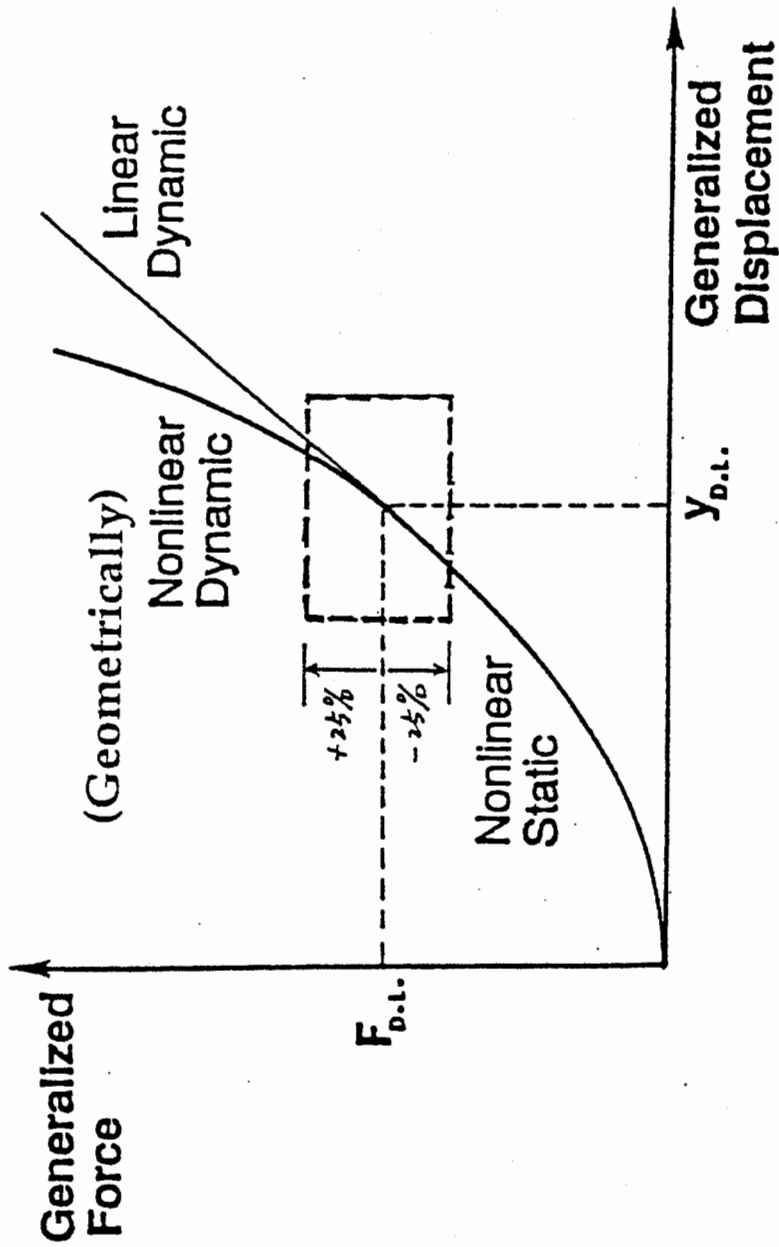
Figure 4.1: Representative Force – Displacement Relationship for Cable Structures
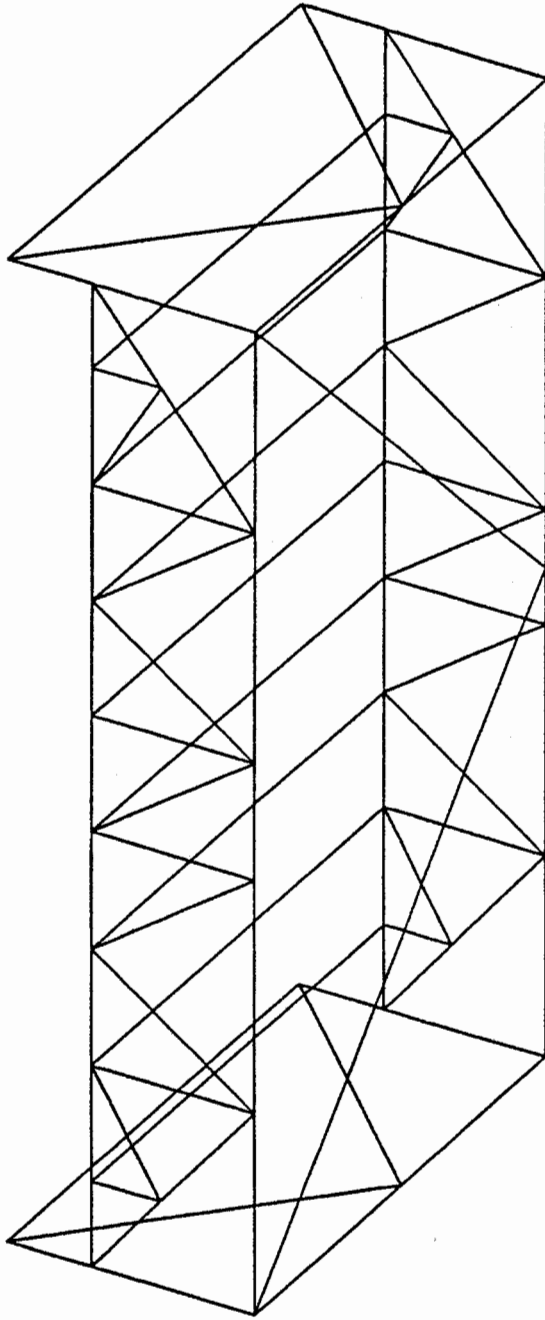
Figure 4.2: Stiffening Truss and Floor Truss System including Longitudinal Stringers
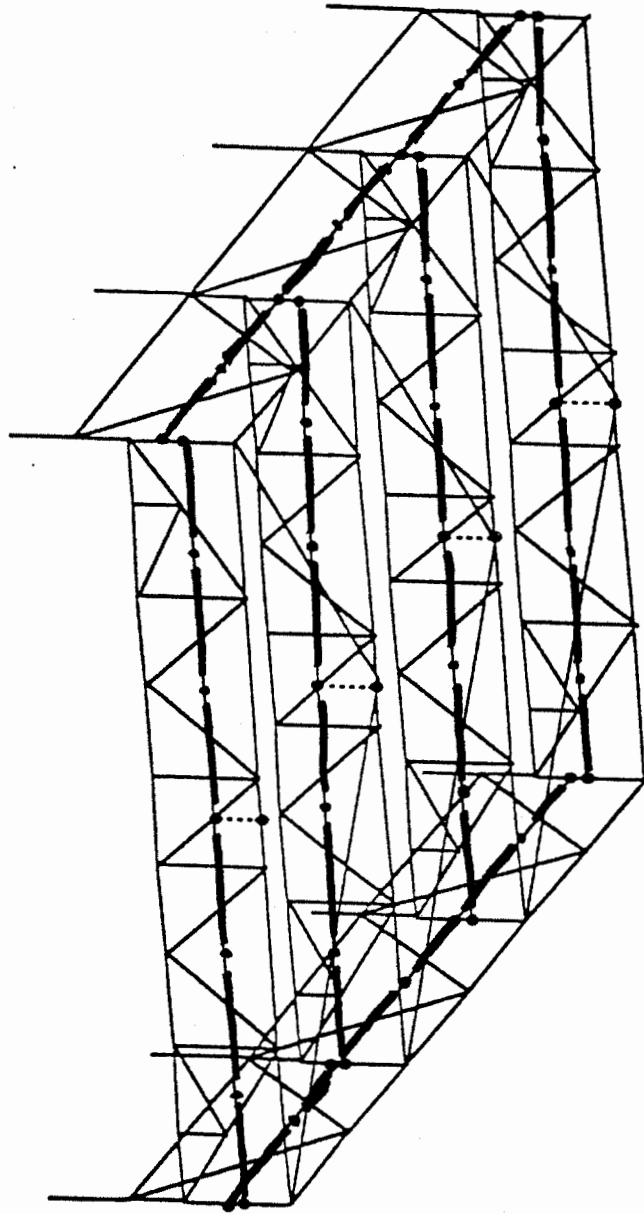
Figure 4.3: Idealization of the Superstructure Stiffening Truss System
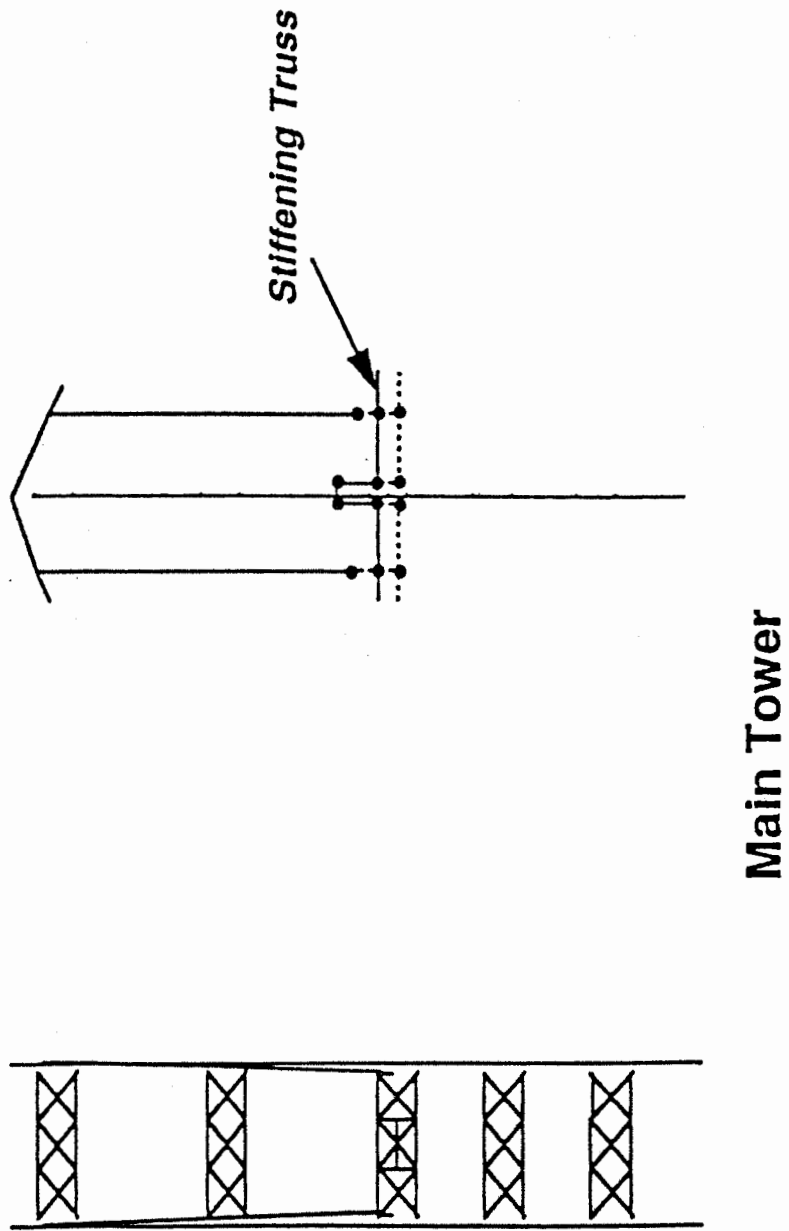
Main Tower

Figure 4.4: Analytical Model of the Main Tower

61
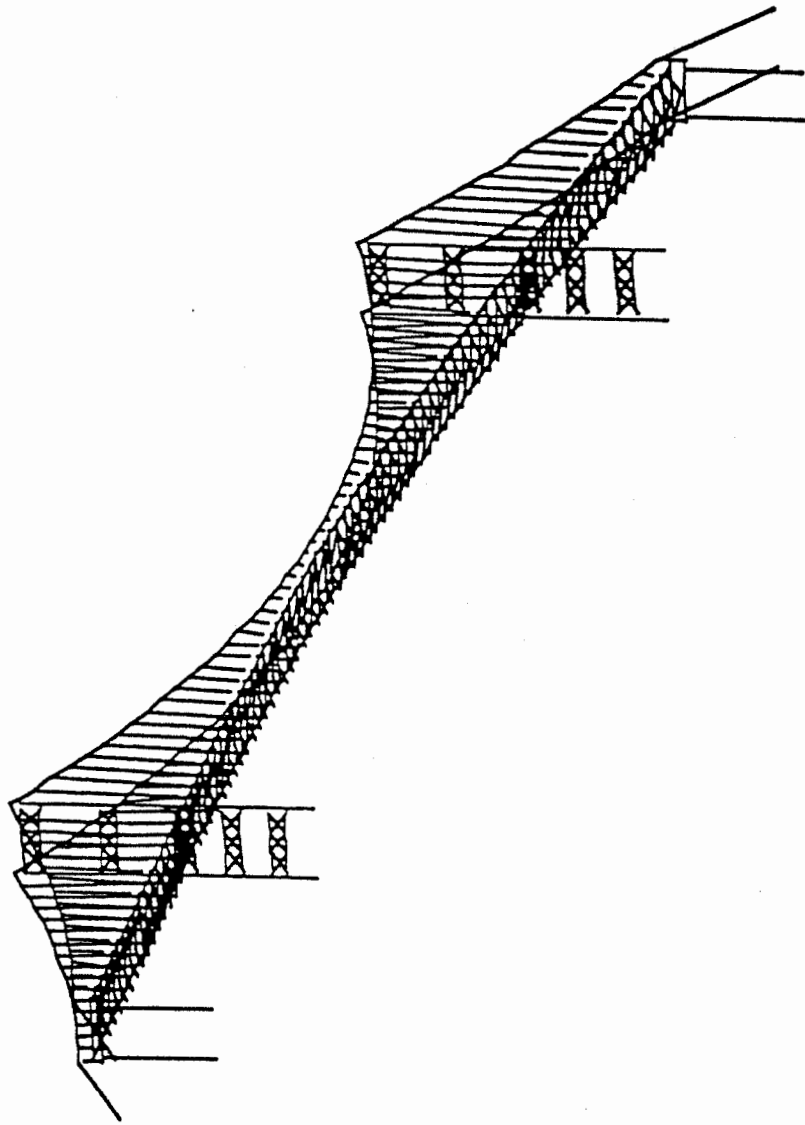
Figure 4.5: Analytical Model of the Bridge

NEABS6
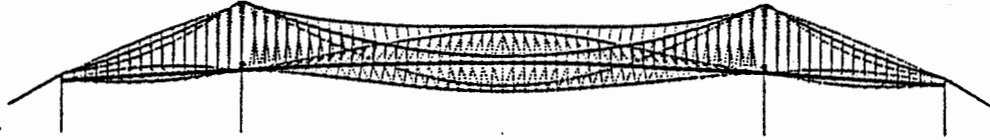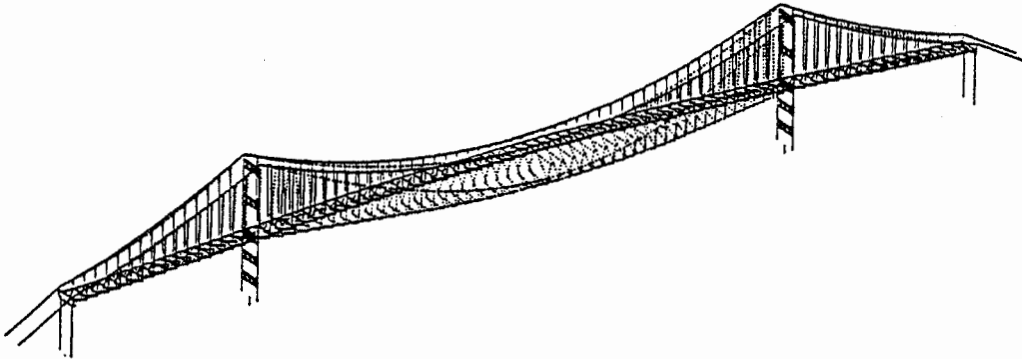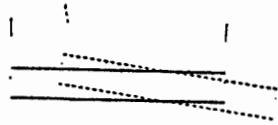
Mode # 1 7.02 Sec

Figure 4.6: Transverse Vibration of the Center Span

NEABS6

Mode # 4 3.69 Sec
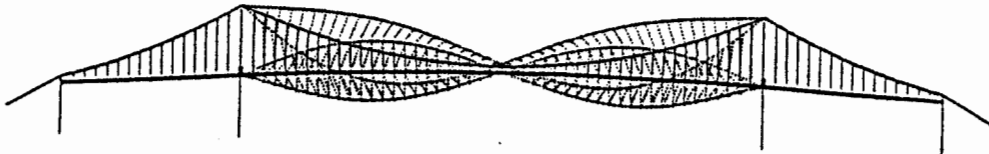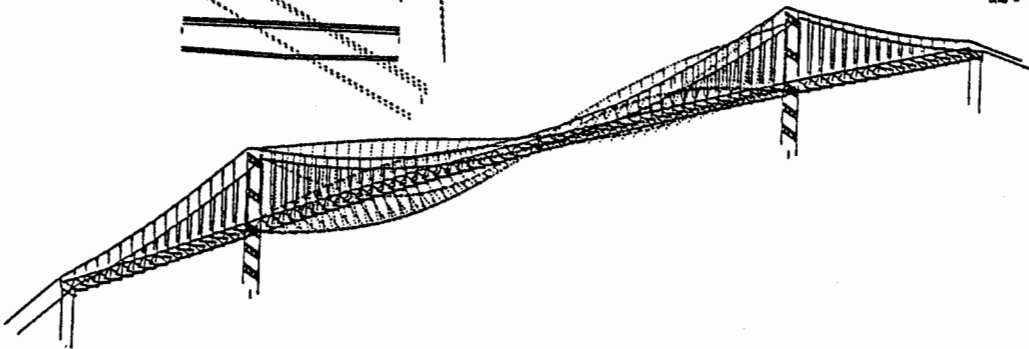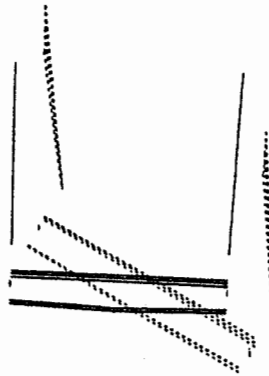
Figure 4.7: Coupled Transverse and Torsional Mode
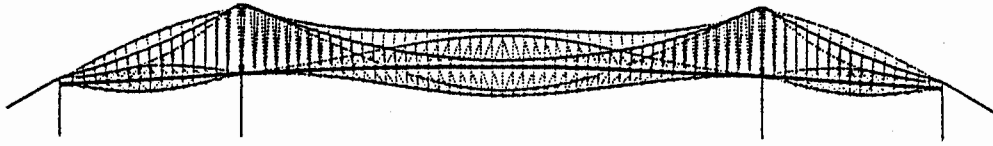
64
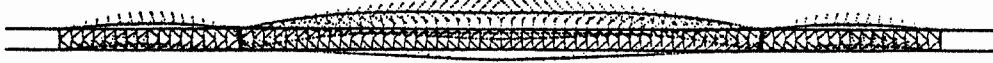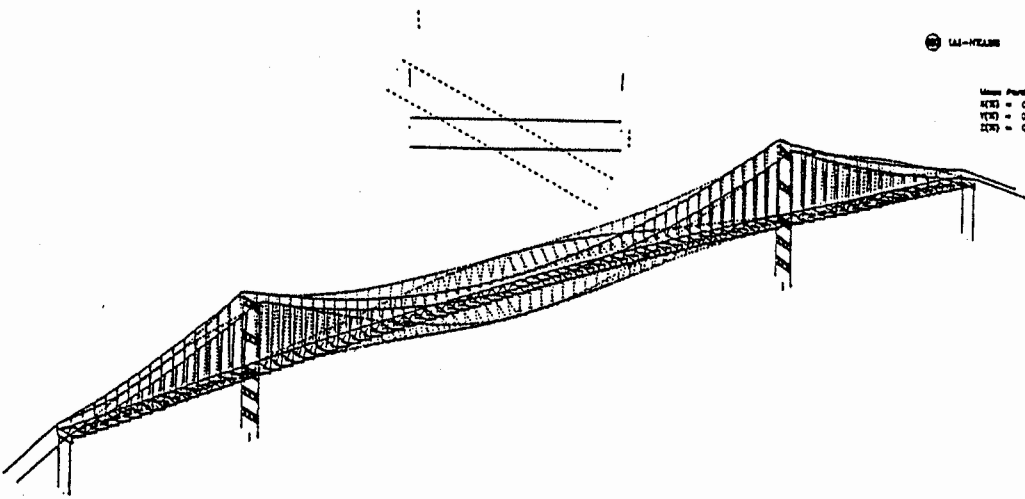
NEABS6

Figure 4.8: Coupled Transverse and Torsional Mode

Mode # 6 2.90 Sec

NEABS6

Mode # 10   2.11 Sec
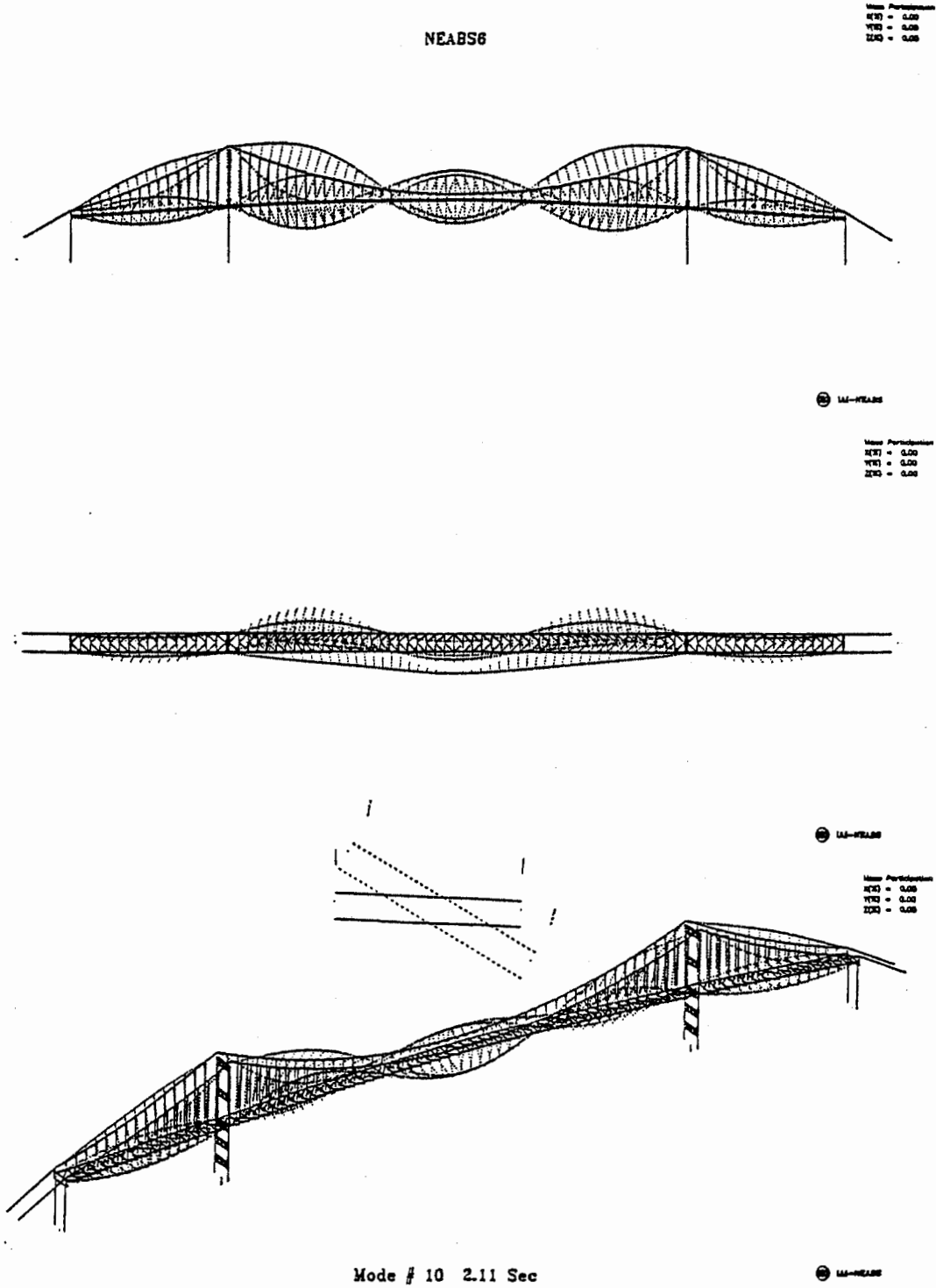
Figure 4.9: Coupled Transverse and Torsional Mode

66
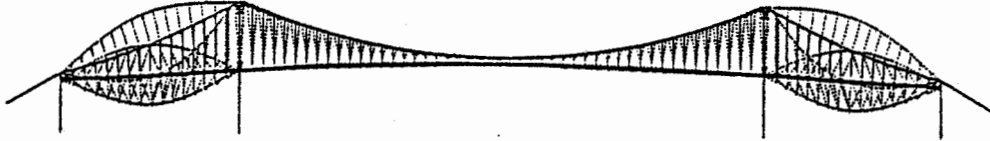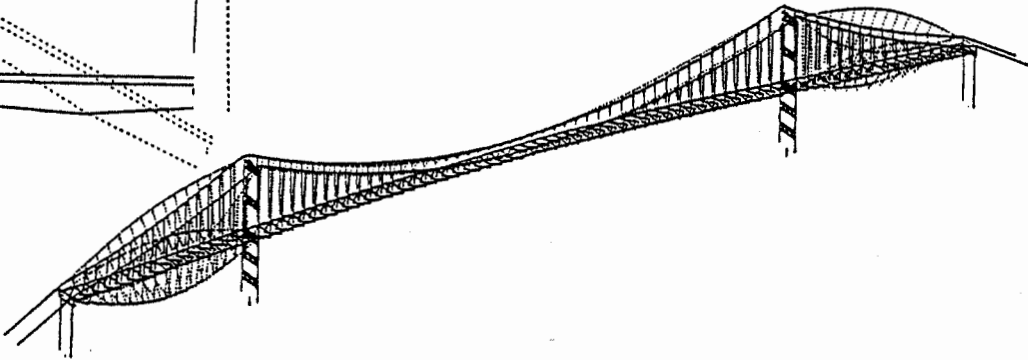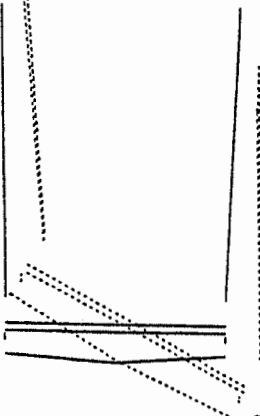
NEABS6

Mode # 11   2.07 Sec

Figure 4.10: Coupled Transverse and Torsional Mode of Side Span

67

NEABS6
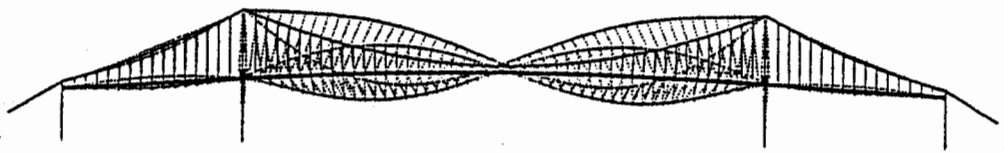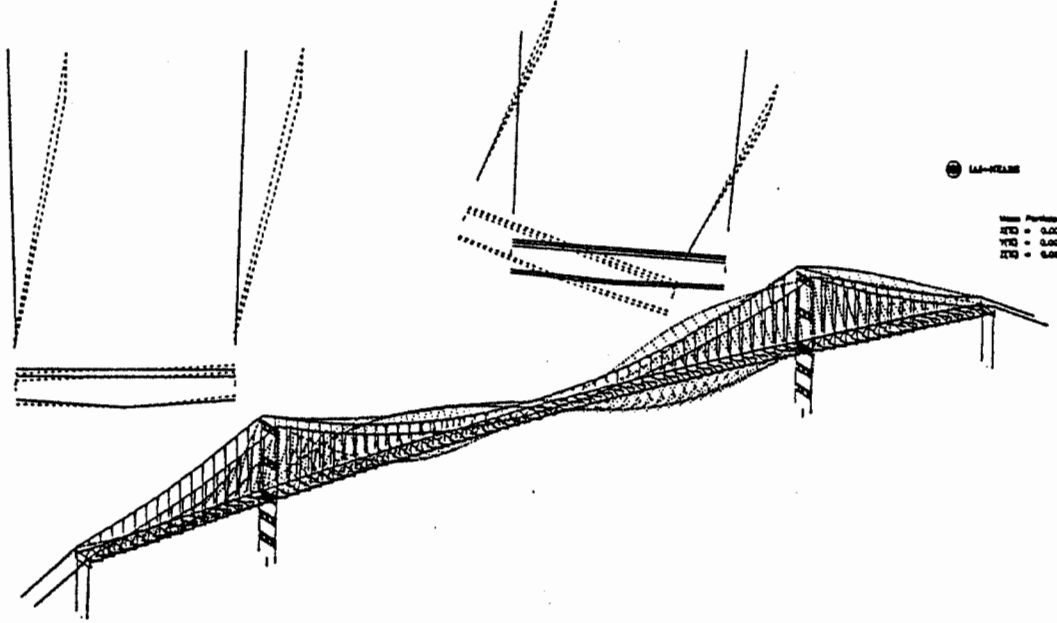
Figure 4.11: Transverse Vibrationa of Center Span and Cables

Mode # 20   1.60 Sec
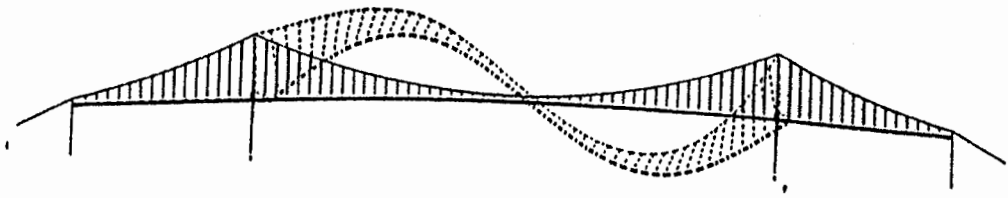
$T_2 = 5.02$ Sec.
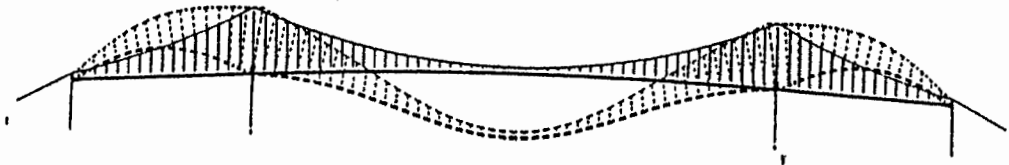
$T_3 = 4.48$ Sec.
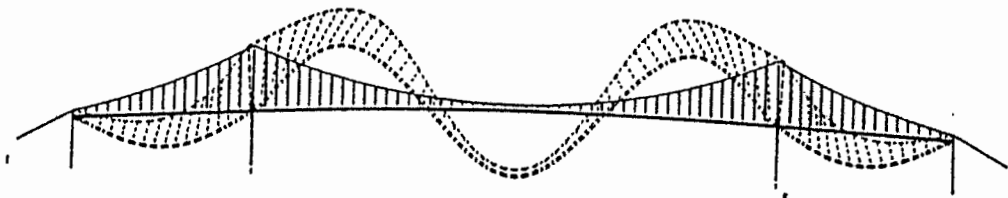
$T_7 = 2.86$ Sec.

$T_8 = 2.79$ Sec.
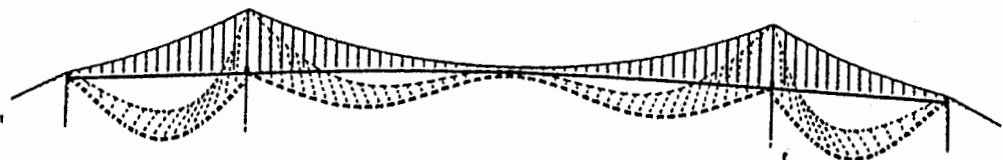
$T_9 = 2.23$ Sec.

Figure 4.12:   Vertical Vibration Modes

69
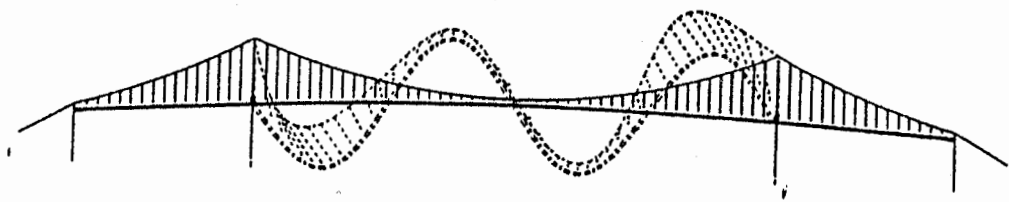
$T_{16} = 1.85$ Sec.
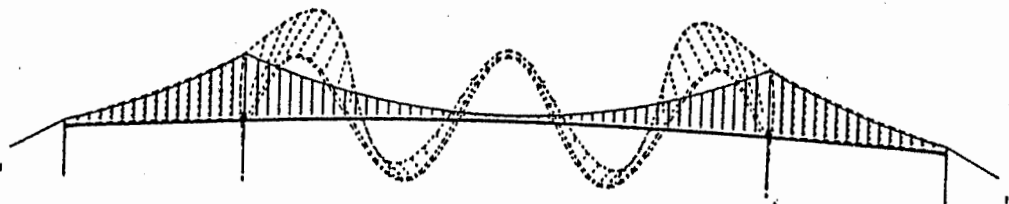
$T_{24} = 1.29$ Sec.
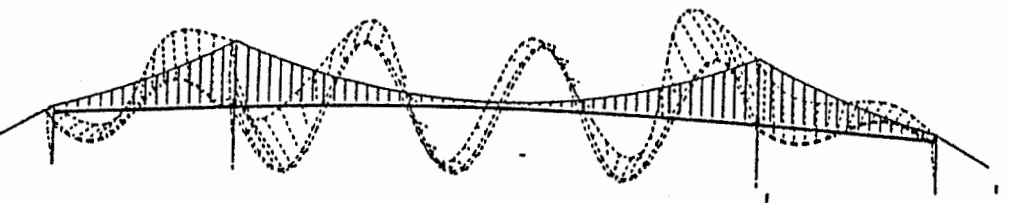
$T_{35} = 0.96$ Sec.
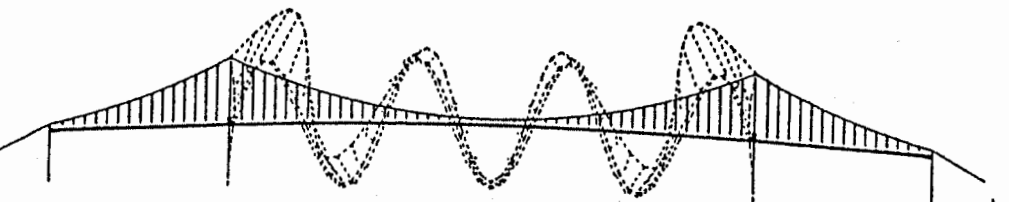
$T_{50} = 0.75$ Sec.
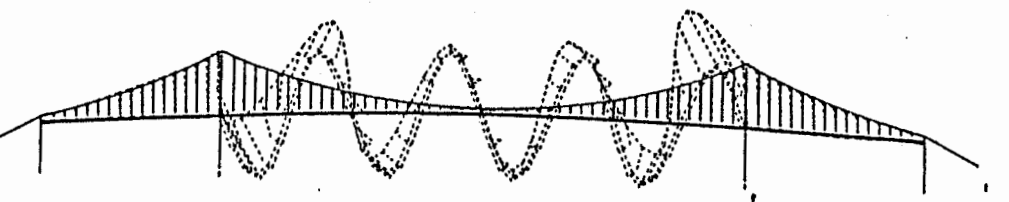
$T_{60} = 0.60$ Sec.

Figure 4.12:   Vertical Vibration Modes (cont.)

$T_5 = 3.42$ Sec.
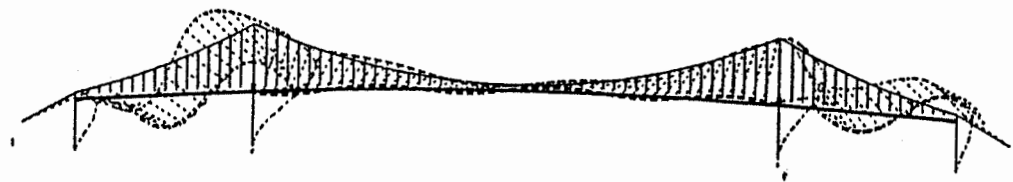
$T_{31} = 1.02$ Sec.
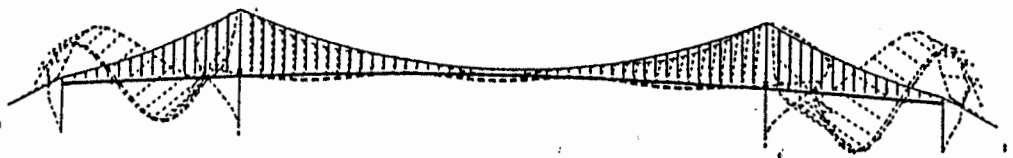
$T_{32} = 1.00$ Sec.
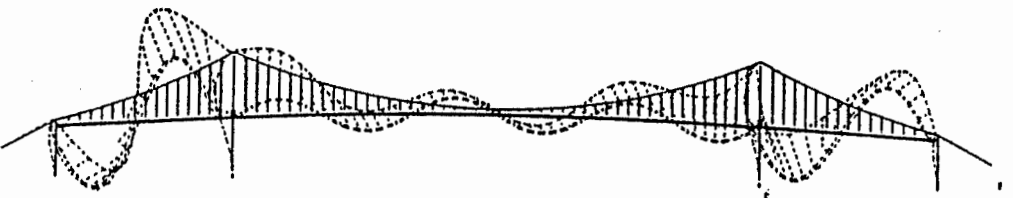
$T_{33} = 0.97$ Sec.

$T_{36} = 0.96$ Sec.

Figure 4.13: Coupled Longitudinal and Vertical Modes for Suspended Structure, Towers and Cable Bents

$T_{39} = 0.88$ Sec.
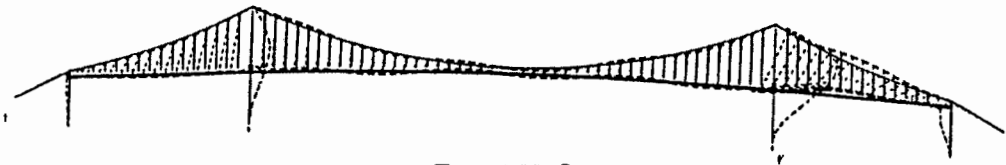
$T_{41} = 0.88$ Sec.

$T_{75} = 0.51$ Sec.

$T_{78} = 0.49$ Sec.

$T_{90} = 0.43$ Sec.

Figure 4.13: **Coupled Longitudinal and Vertical Modes for Suspended Structure, Towers and Cable Bents (cont.)**
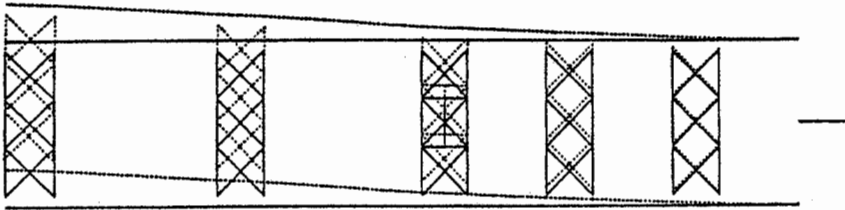
West Tower

West Tower

Mode # 25   1.19 Sec

Mode # 34   0.97 Sec

IAI-NEABS
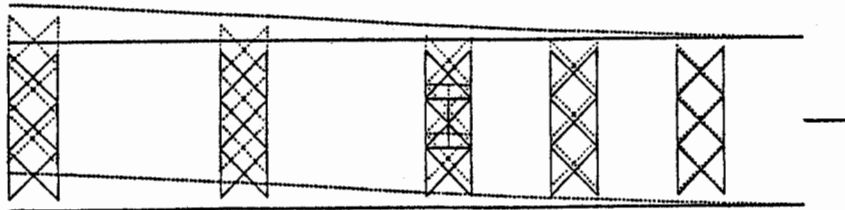
IAI-NEABS

Figure 4.14:   Typical Transverse Vibration Modes of Towers

West Tower

West Tower

Mode # 29 1.05 Sec

Mode # 58 0.64 Sec

West Tower

West Tower

Mode # 20 1.60 Sec

Mode # 57 0.66 Sec
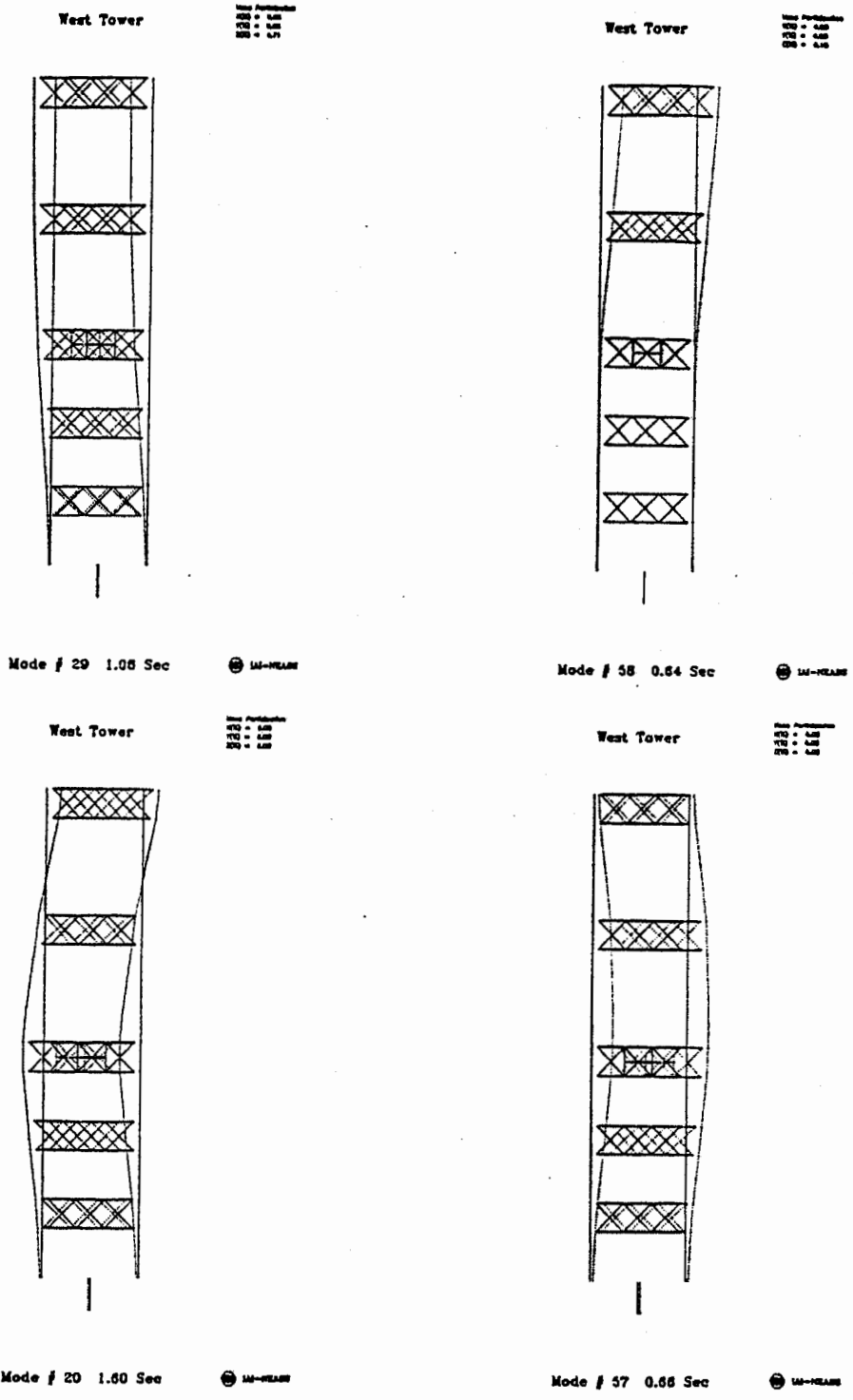
Figure 4.15:   Higher Order Transverse Vibration Modes of Towers

5. Spatially Varying Ground Motions

5.1 General

One of the deficiencies of the instrumentation is the lack of free-field station and the bridge's multiple supports are not fully instrumented. In the correlation study, we have assumed that the foundation motions at the west side of the channel are identical to that at the base of the west tower, and the motions at the east cable bent are identical to that of the east anchorage. The advantage of these motions is that the foundation-soil interaction effects as well as the incoherency effect are both accounted for at the three locations, i.e., west tower, east tower and each anchorage.

To supplement the instrumentation records, it was initially planned to establish a ground motion coherence model based on the ground motion array at the Caltech campus. This will be reported in Section 5.2. The ground motion coherence model would then be used in the multiple-support-response spectrum calculations.

Subsequently, it was recognized that the nature of ground motions recorded at the Caltech campus was quite different from that at the bridge site. In the Long Beach area, the ground motions are dominated at one second period by a wave trapped in the Los Angeles basin (Scriver and Helmberger, 1993) which was not recorded at Caltech stations. The wave form and duration were also quite different indicating different traveling path and local site conditions. Since the structural dynamic responses are characterized by several important vibration modes for towers and suspended spans with periods close to one second, it was decided by IAI and Woodward-Clyde Consultants to derive more relevant ground motion time histories for the multiple supports of the bridge. (This development was funded partially by IAI's in-house research program. Woodward-Clyde Consultants also contributed to this additional study.) These results will be described in Sections 5.3 and 5.4.

5.2 Array Data from Caltech Campus

Strong motion records were obtained for the 1987 Whittier Narrows earthquake on the Caltech campus at spacings of several hundred meters, as shown in Figure 5.1 and Table 5.1. The coherency derived from these records was found to be compatible with the empirical coherency model proposed by Abrahamson et al. (1992). It was concluded that this coherency model is appropriate for use in characterizing the spatial variation at the recording site during the 1987 Whittier Narrows earthquake. Because the Caltech recordings lack absolute time, the horizontal phase velocity cannot be measured. An appropriate horizontal phase velocity for S waves is assumed to be about 2.5 km/sec (8,200 ft/sec).

The comparison of the analytical model with measured coherence for the two horizontal components of the first 5 seconds of motion for two frequencies is shown in Figure 5.2. The radial component is in the direction from the earthquake source to the site (horizontal component of SV motion), and the tangential component is normal to this direction (SH motion). Generally, the Abrahamson model is compatible with the measured values. The subsequent 10 seconds of motion have much lower coherency, as shown in Figure 5.3. If the bridge response from this later motion is important, it may be necessary to consider using a different coherency function.

5.3 Ground Motions in the Long Beach Area from the Whittier Narrows Earthquake

Ground motion recordings of the Whittier Narrows earthquake in the vicinity of the Vincent Thomas Bridge were collected for evaluation. These stations are shown in Figure 5.4 and Table 5.2. Although the separation distances of the recordings are fairly large, and some of them are not in ideal free field locations, they may provide a more appropriate estimate of coherency at the site, especially at periods of around 1 second, than the data from Caltech. This coherency model, together with the time history of the Whittier Narrows earthquake recorded at the east anchor of the Vincent Thomas Bridge, was used to generate time histories for the Whittier Narrows earthquake at the other supports of the Vincent Thomas Bridge.

Data

The eight strong motion recordings used in this study were recorded by the CDMG and the USGS. The recordings used are listed in Table 5.2 and their locations are shown in Figure 5.4. In this figure, the east anchor of the bridge is shown as a hexagon label VTBR near the left side of the figure, and the other supports are shown as dots. Of these recordings, only HADB, LBRC and LBRP are in the free field. Stations LBCH, LBEN, LBHU and LBHA were located in the basements or ground floors of buildings, and VTBG is the east anchor of the Vincent Thomas Bridge. Ideally, we would like to use only free-field stations, but their separations of seven to ten km are too large and too similar to provide a good estimate of spatial coherency. The five recordings from the foundations of structures are all expected to have some effects of soil-structure interaction, and so the measured spatial coherency will be contaminated to some extent.

The time histories of acceleration and velocity in the radial (toward the epicenter) and the tangential (orthogonal to the direction toward the epicenter) directions are plotted as a function of epicentral distance in Figures 5.5 through 5.8. Because station LBHU is very close to stations LBEN and LBRP, and station HADB is very close to station LBHA, the time histories of stations LBHU and LBHA are shown on separate plots.

The time history plots have travel time curves that show the expected time of the direct S wave (16 seconds at 40 km distance) as well as other arrivals. At station LBRC, this direct wave is the largest arrival in both the acceleration and velocity time histories. However, at the more distant stations, a strong pulse with a period of about one second which follows the direct wave by about 5 seconds is almost as large as or larger than the direct S wave in both peak acceleration and peak velocity, especially on the tangential component. This wave has been modeled as a *basin reflected wave* by Scrivner and Helmberger (1993). It is followed by several higher order multiple reflections that have relatively uniform spacing as expected from theory. The geographic region in which these multiples were observed during the Whittier Narrows earthquake is shown in the top panel of Figure 5.9, and includes the Long Beach area and the adjoining region to the north. This basin

reflected wave was associated with larger peak velocities than expected from standard attenuation relations, as shown in the lower panel of Figure 5.9.

Coherency Measurements

The spatial coherency in three time windows were calculated: a six-second interval that includes the direct S wave; an adjacent six-second interval that contains the first basin multiple reflection; and a twenty-second interval that includes both direct S and multiply reflected waves. The separate estimates for the S wave and the first reflection were made to allow comparison of the coherency of these two phases.

The coherency measurements for separations up to three km are shown in Figure 5.10 for frequencies ranging from 0.6 to 2.5 Hz. In general, the first multiple reflection (in the time window 5-11 seconds following the S wave onset) has the largest coherency. The direct S wave has slightly lower coherency than the first reflected wave. The coherency of the 20 second time window, which includes the direct S wave and all of the multiple reflections, has a considerably lower coherency, due to the fact that its long time window includes *scattered* as well as direct waves.

Comparison of Measured Coherency with Model

The coherency model of Abrahamson et al. (1990) is compared with the measured coherency in Figure 5.10. It slightly underestimates the coherency of the direct S wave (0-6 sec) and the first basin reflection (5-11 sec), but overestimates the coherency of the overall time histories (0-20 sec). It is judged that Abrahamson et al. (1990) model is a reasonable representation of the coherency measured in the Long Beach area during the 1987 Whittier Narrows earthquake, given the uncertainties in those measurements due to the presence of many non-free-field sites.

5.4 Generation of Incoherent Time Histories at the Vincent Thomas Bridge

In the preceding section, an appropriate coherency model was established as a representation of the spatial coherency of ground motions at the Vincent Thomas Bridge during the 1987 Whittier Narrows earthquake.

Using the motion recorded at the east anchor of the bridge as the control motion, ground motion time histories were generated that obey the established coherency model at the other supports. These time histories are shown in Figures 5.11 through 5.16 for acceleration, velocity and displacement for the two horizontal components (east – 090 and south – 180). The procedure for ground motion generation was developed by Abrahamson (1992).

The spatial coherency for these generated time histories were calculated as shown in Figure 5.17, which are in reasonably good agreement with the model.

Table 5.1:   Stations at Caltech Campus

Station	East (m)	North (m)
athl	182.4	0
athn	558.6	380.0
brid	129.2	300.2
hous	444.6	235.6
irc	566.2	646.0
keck	273.6	505.4
lura	0	737.2
milk	140.6	368.6
mudd	7.6	281.2

Reference Location: (0,0) shown in Figure 5.1.

Table 5.2: Coherency Study – Whittier Narrows 1987 Earthquake Long Beach Area Stations

Station Identification	Km North of Reference	Km East of Reference	Epicentral Distance (km)	Azimuth
City Hall, Long Beach, ground level (14533) - lbch	1.99	9.85	32.94	198.70
CSULB Engineering Building, basement (14311) - lben	3.66	12.87	29.68	185.55
CSULB Humanities Building, basement (132) - lbhu	2.98	14.54	30.34	185.43
Harbor Administration Building Free Field (14395) - hadb	0.43	6.39	34.55	198.61
Harbor Administration Building, ground level (14323) - lbha	0.54	6.39	34.45	198.66
Rancho los Cerritos, instrument shelter (44242) - lbrc	10.00	6.95	25.46	204.26
Recreation Park, instrument shelter (44241) - lbrp	3.10	12.60	30.47	189.09
Vincent Thomas Bridge, East Anchor (14406) - vtbr	0.00	0.00	37.56	207.95

Figure 5.1: Locations of the Strong Motion Accelerographs on the Caltech Campus

1. Brown Athletic Center (athl)
2. California Boulevard House (hous)
3. Athenaeum Club (athn)
4. Industrial Relations Center (irc)
5. Lura Street House (lura)
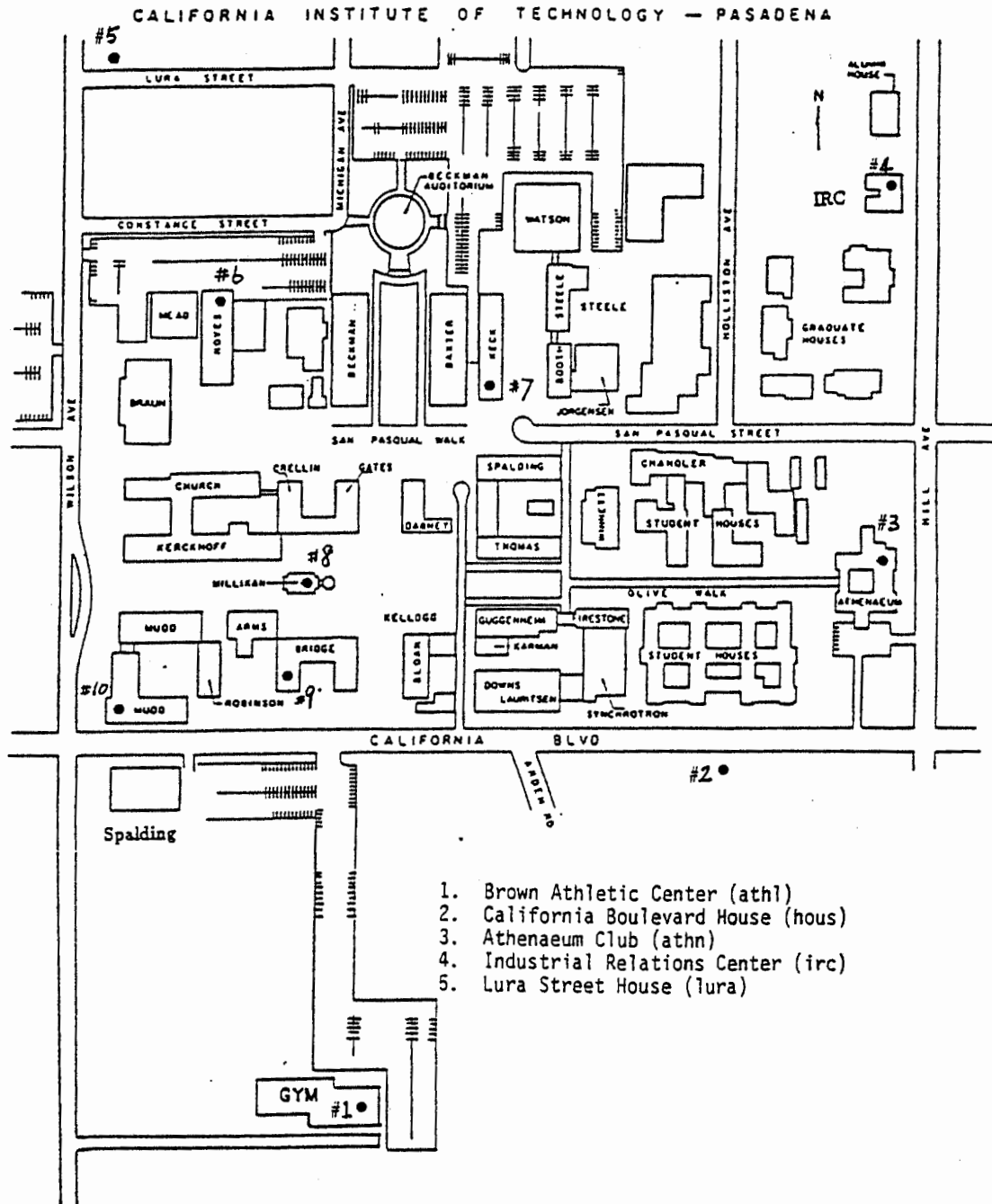
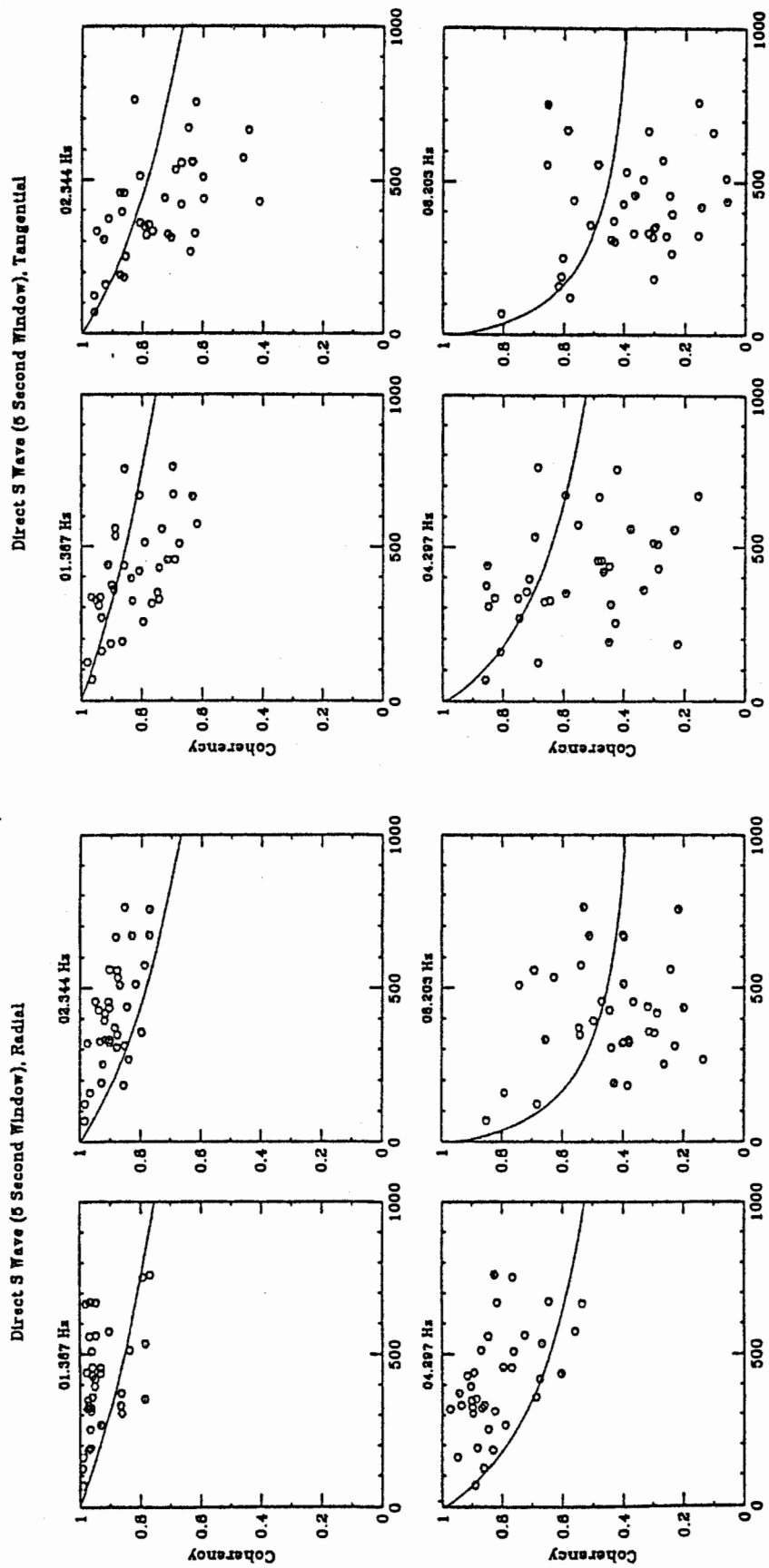Figure 5.2: Ground Motion Coherency – Caltech Stations, 1987 Whittier Narrows Earthquake
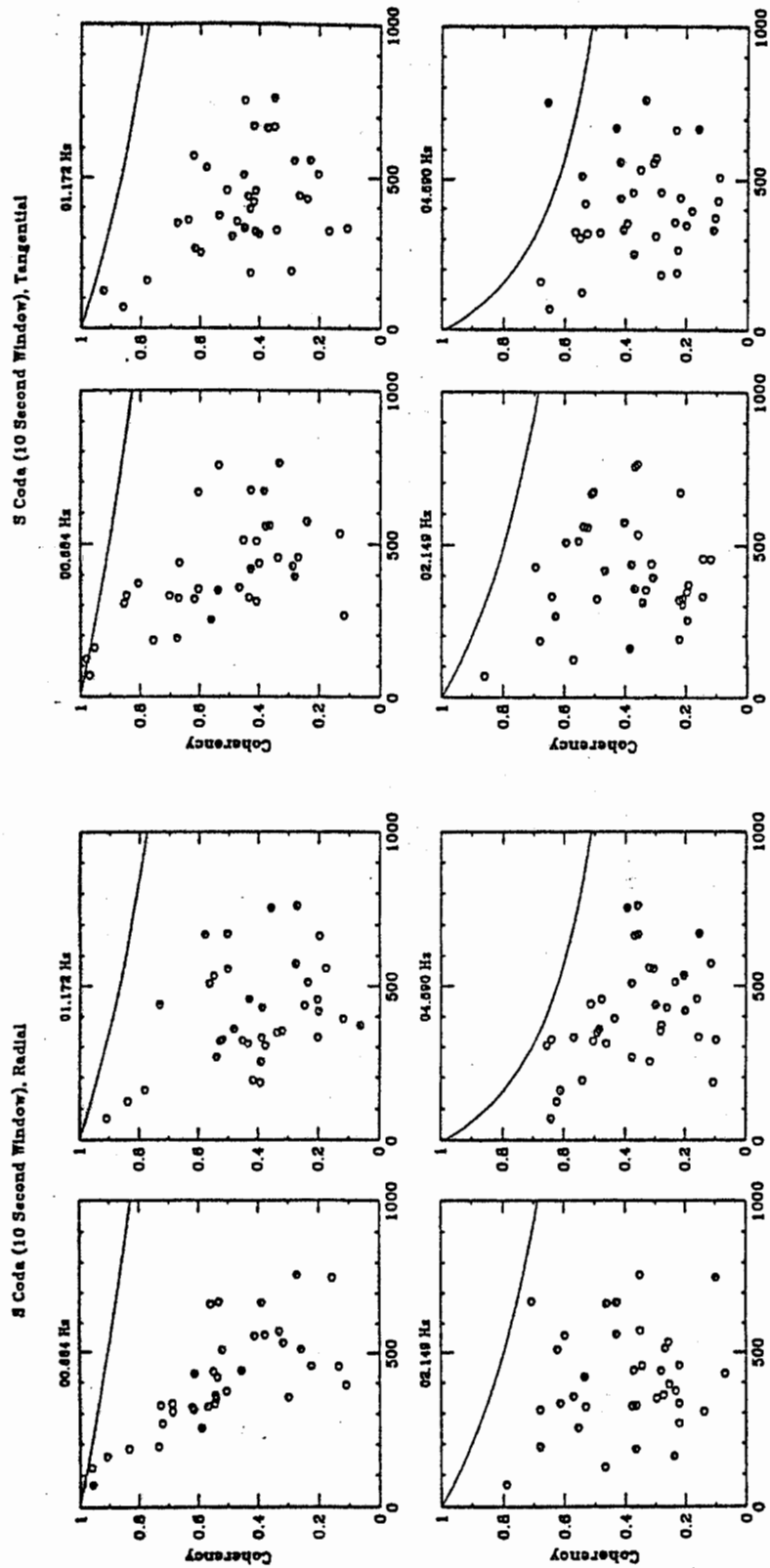
Figure 5.3: Ground Motion Coherency (10 Second Window) — Caltech Stations, 1987 Whittier Narrows Earthquake
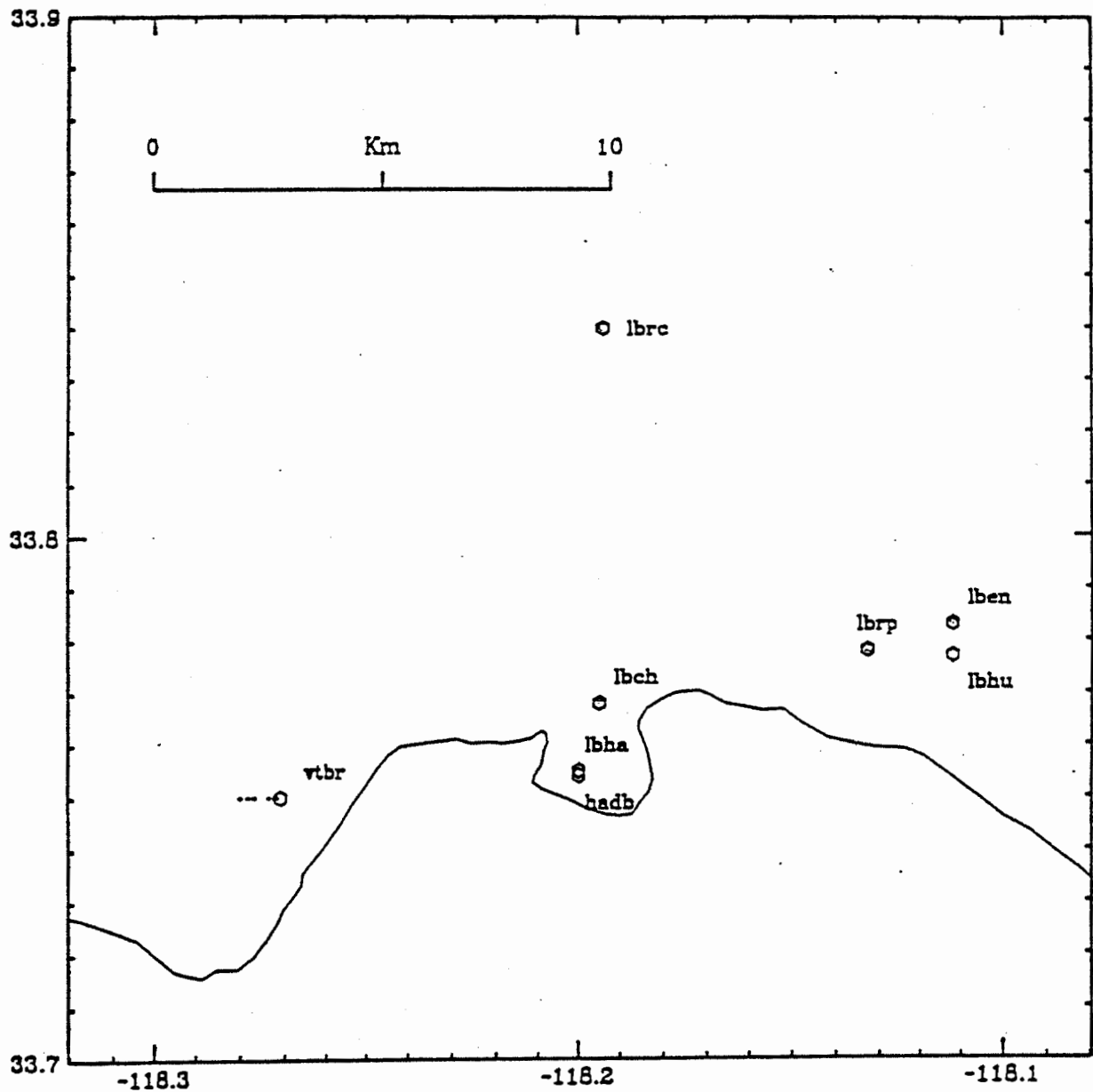
Figure 5.4: Map of Strong Motion Stations in the Free-Field and at the Bases of Structures in the Long Beach Area. The Vincent Thomas Bridge (vtbr) is Located Near the Bottom Left Corner of the Map.
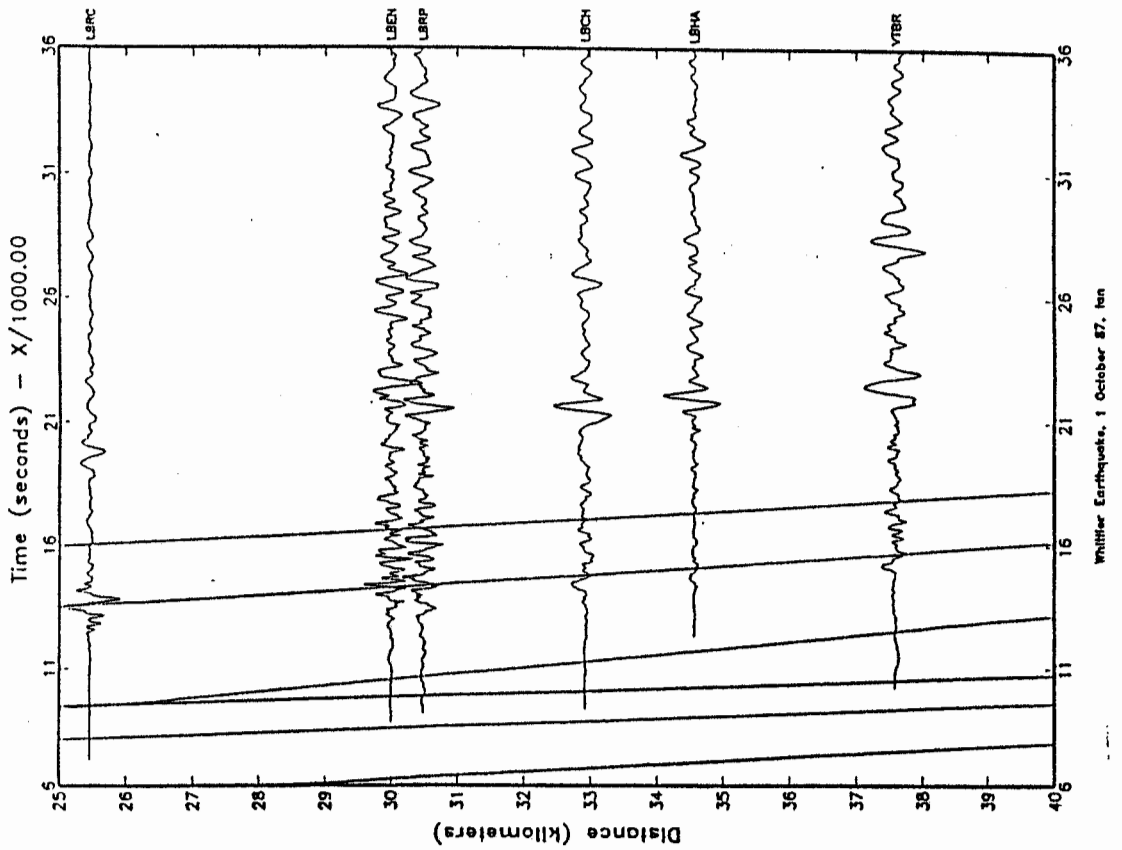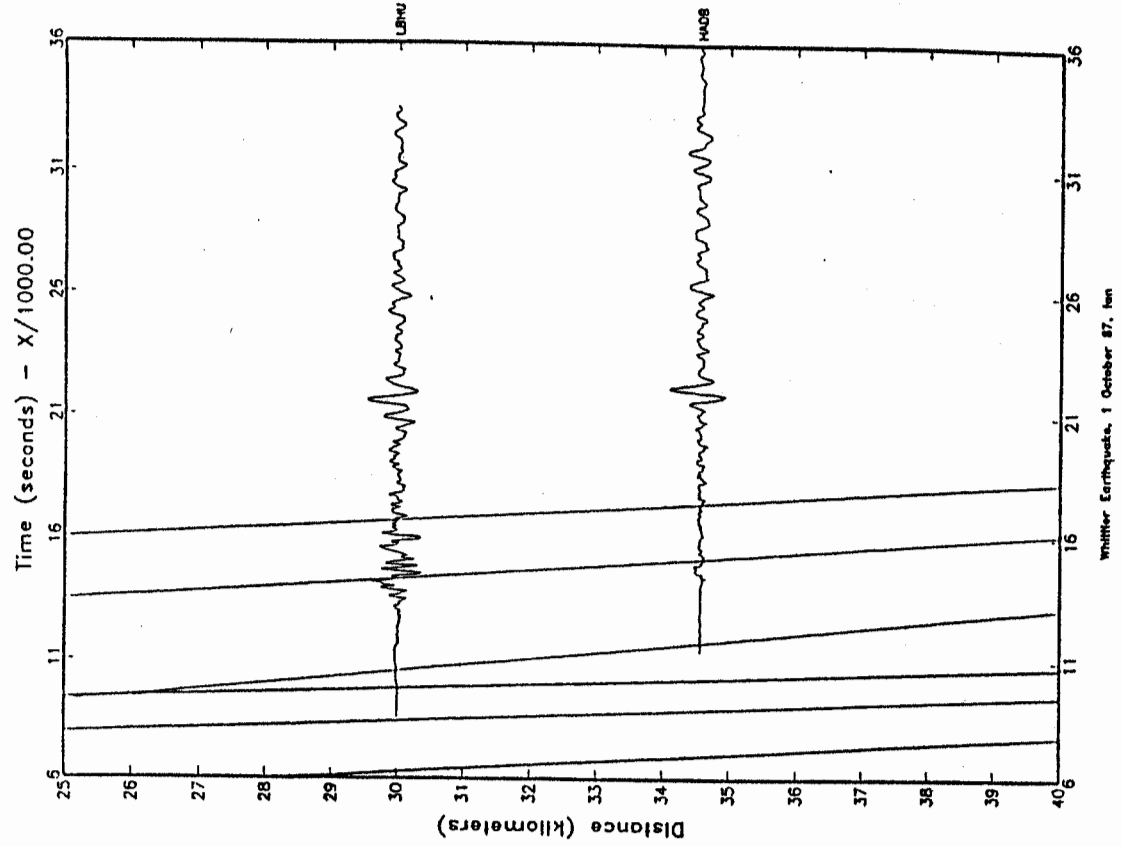
Figure 5.5: Profile of Tangential Component Ground Velocity Recorded at the Stations Shown in Figure 5.4 During the 1987 Whittier Narrows Earthquake

86
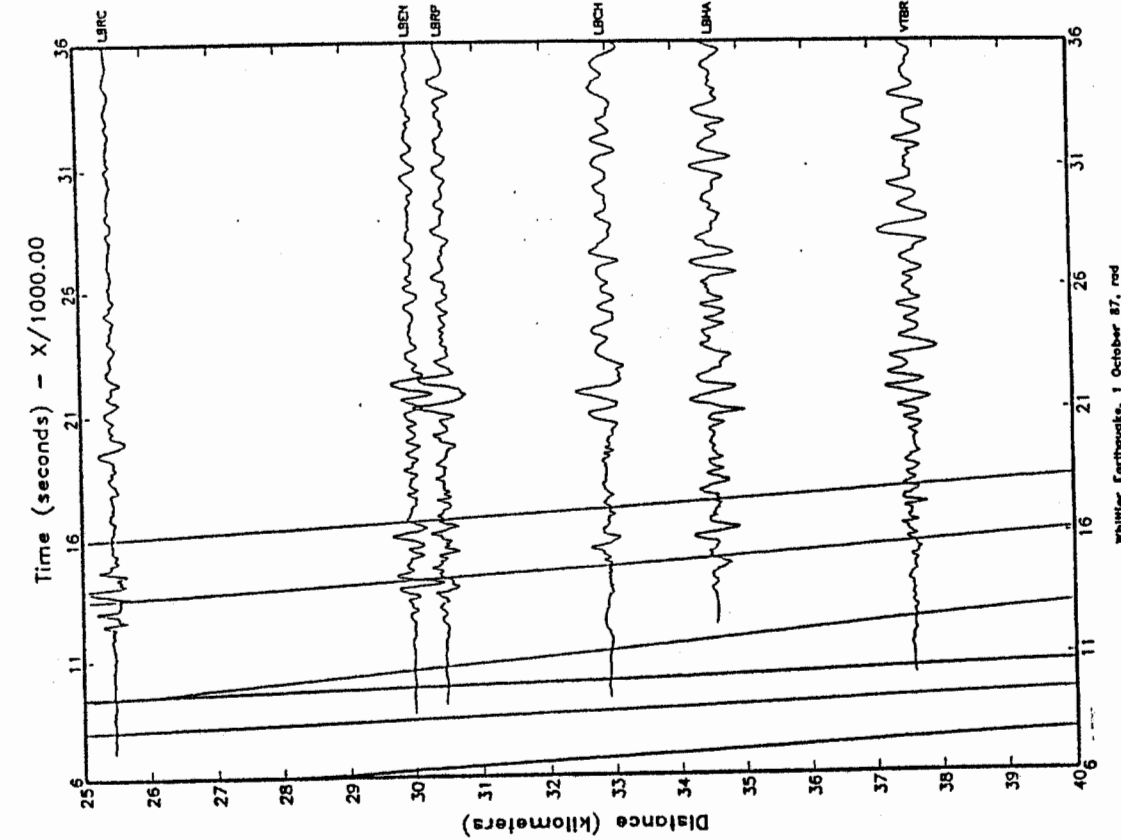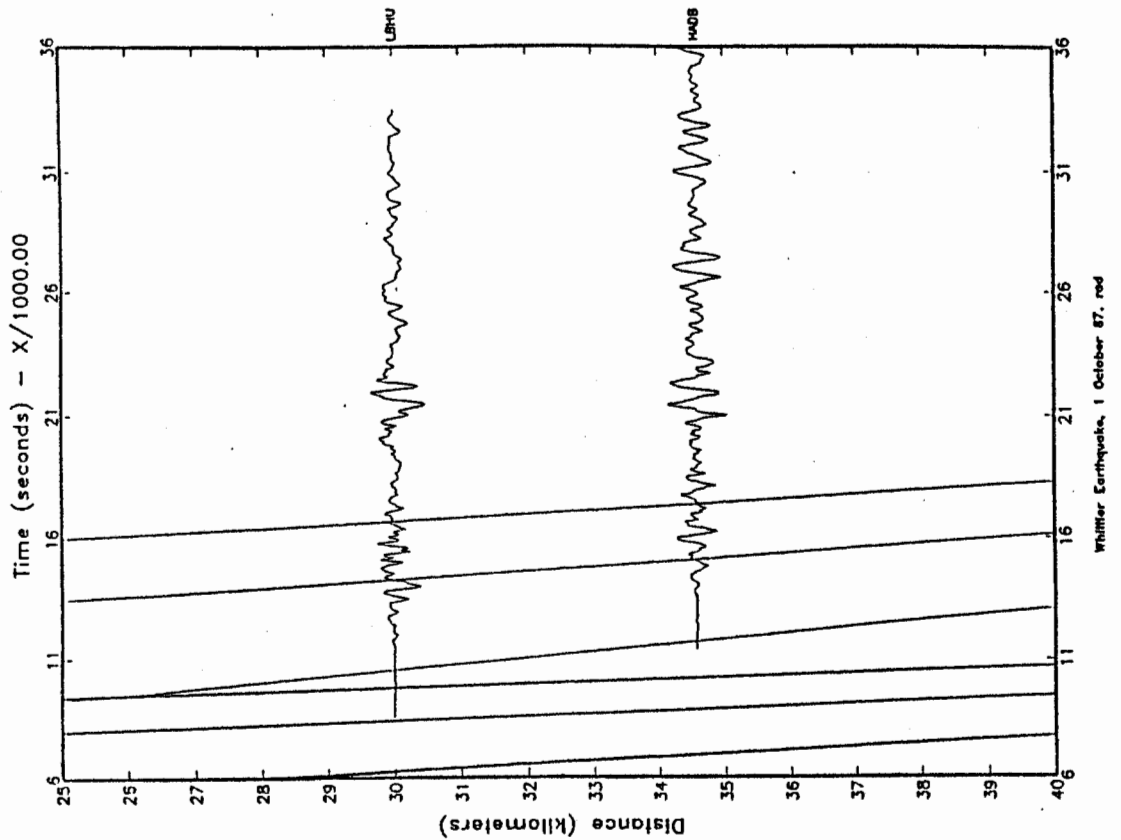
Figure 5.6: Profile of Radial Component Ground Velocity Recorded at the Stations Shown in Figure 5.4 During the 1987 Whittier Narrows Earthquake

87
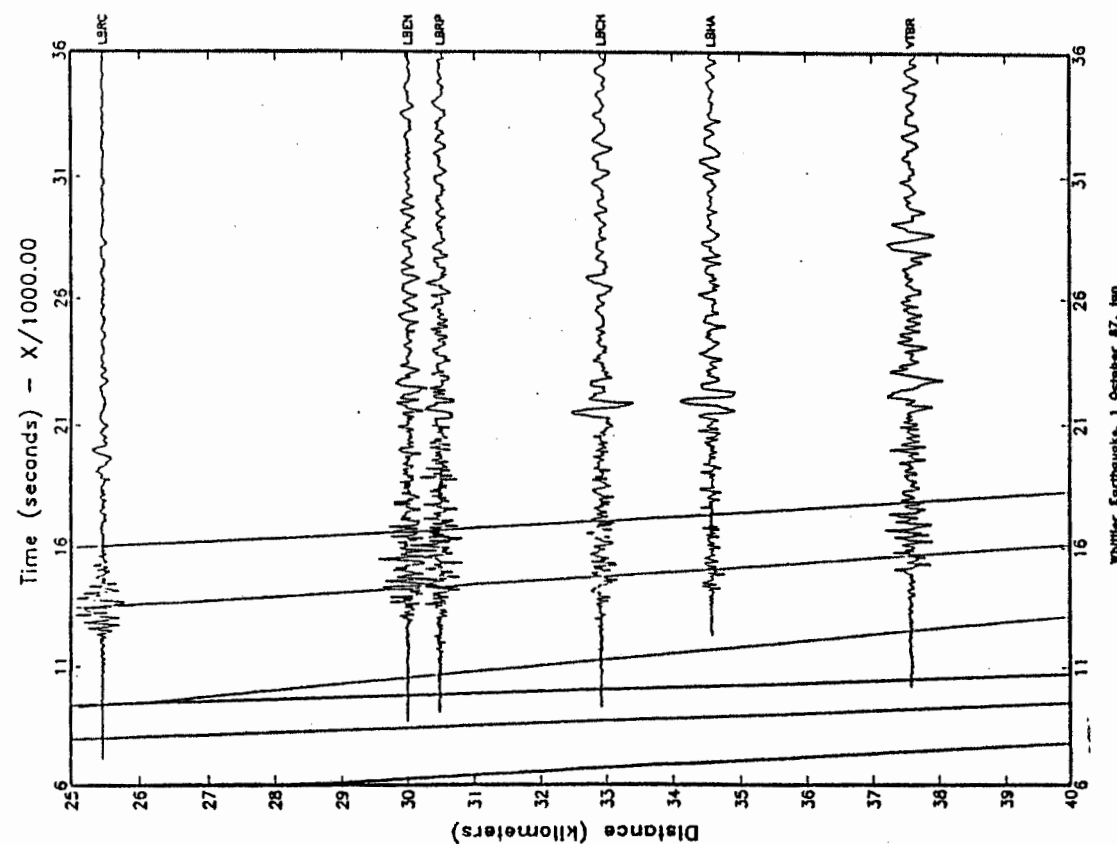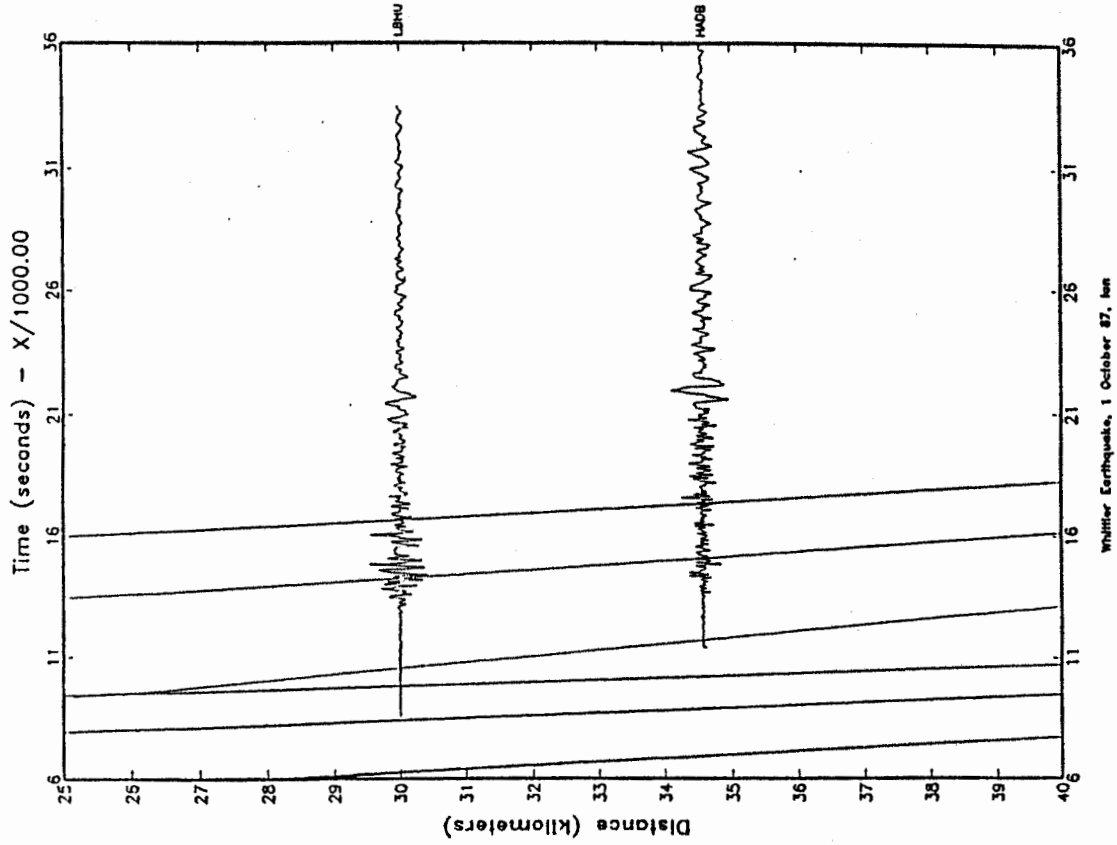
Figure 5.7: Profile of Tangential Component Ground Acceleration Recorded at the Stations Shown in Figure 5.4 During the 1987 Whittier Narrows Earthquake
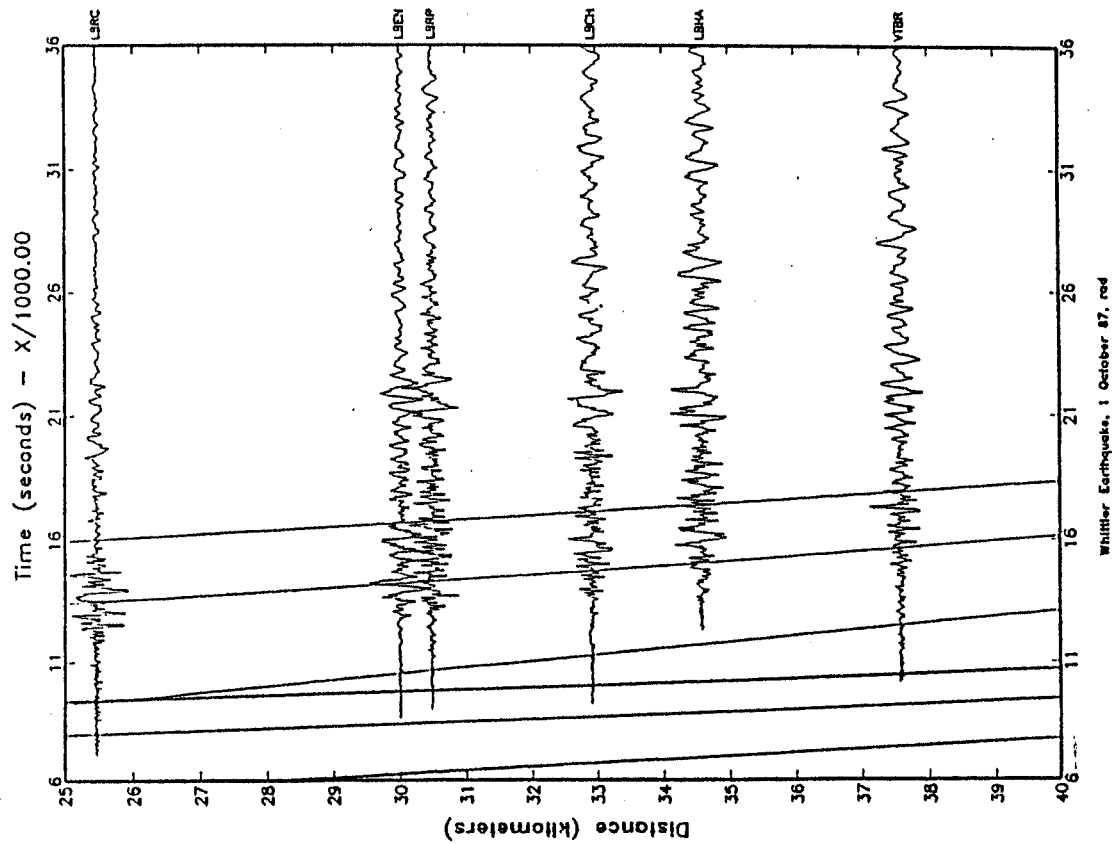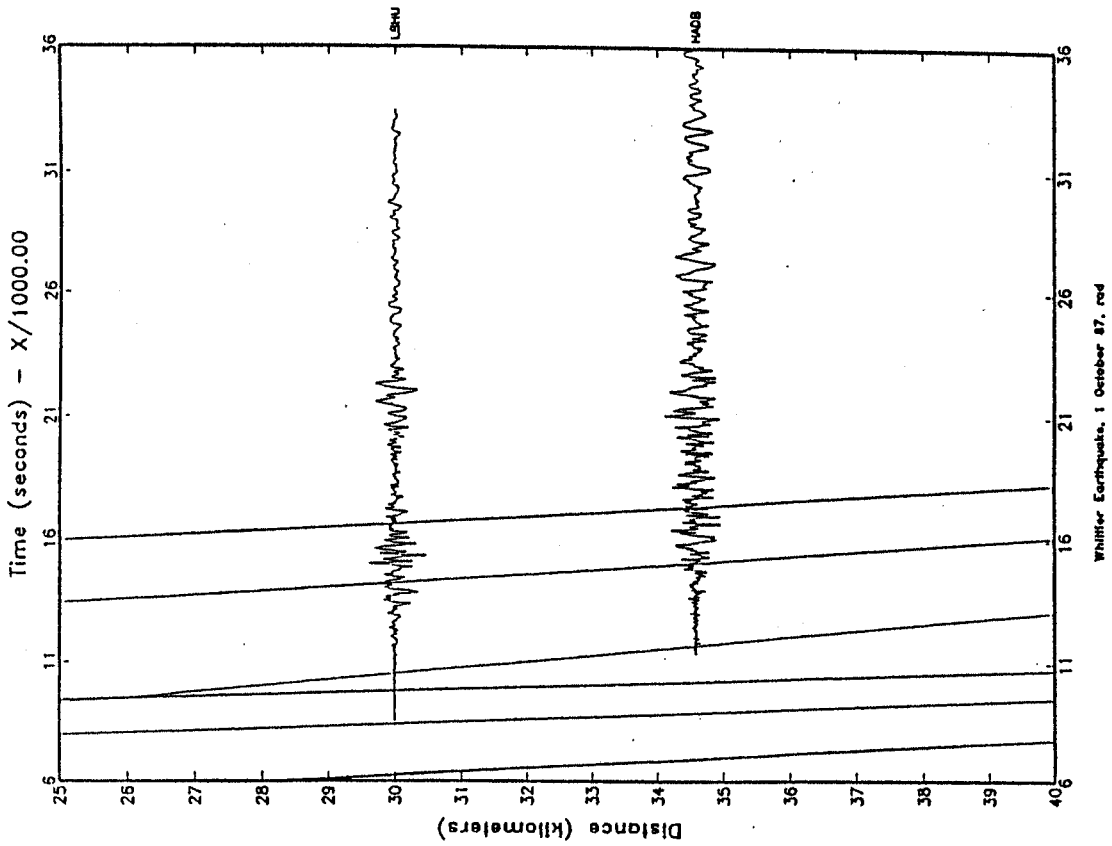
Figure 5.8: Profile of Radial Component Ground Acceleration Recorded at the Stations Shown in Figure 5.4 During the 1987 Whittier Narrows Earthquake
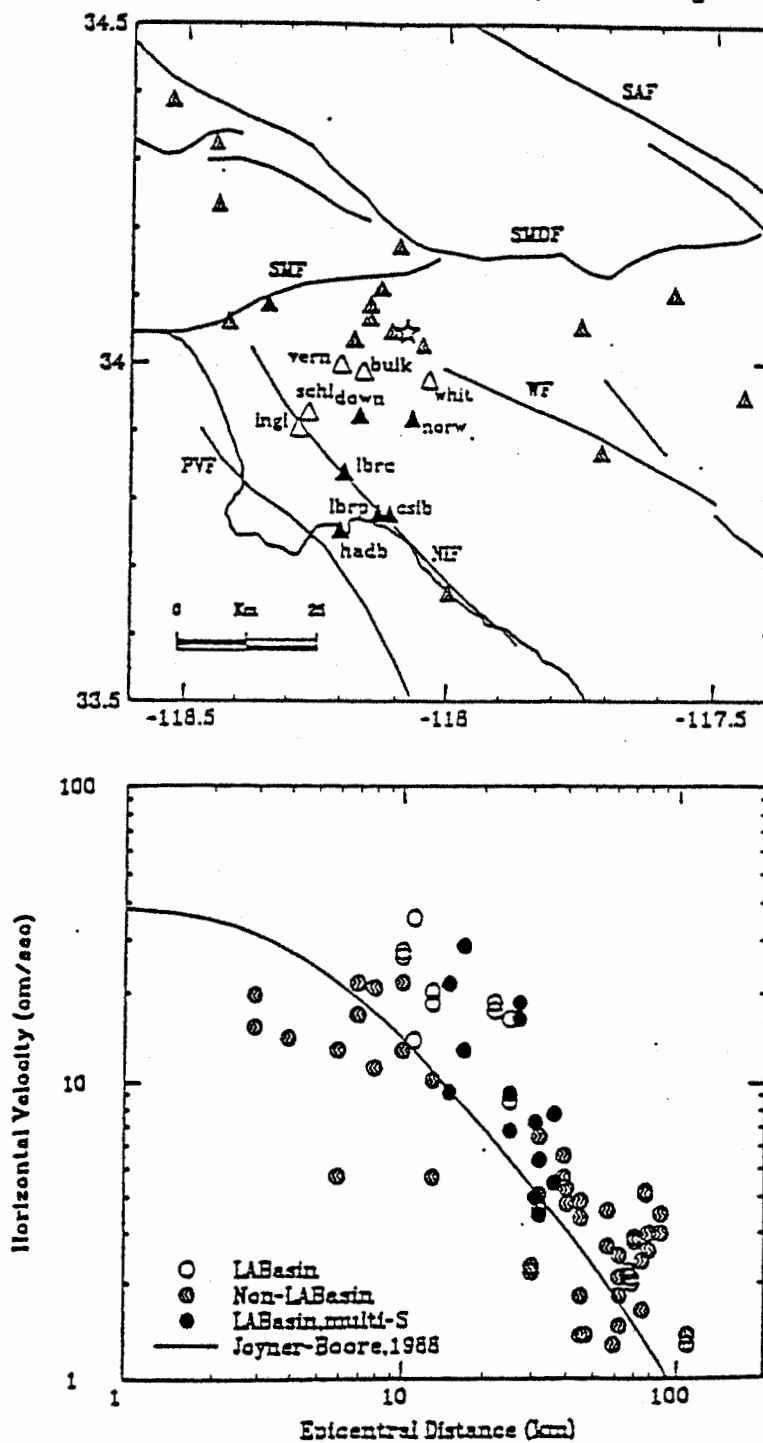
**Figure 5.9:** Top: Location of Strong Motion Recordings of the 1987 Whittier Narrows Earthquake. Stations within the Los Angeles Basin are Shaded Either White or Black. Recordings from the Stations shaded with White Do Not Show Multiple S Phases, While Those Shaded with Black Do Exhibit Strong Multiple S Phases.

Bottom: Comparison of Peak Horizontal Velocity (Both Components) Observed for the Stations Shown at Top with the Empirical Attenuation Relation for Soil Sites of Joyner and Boore (1988).

90
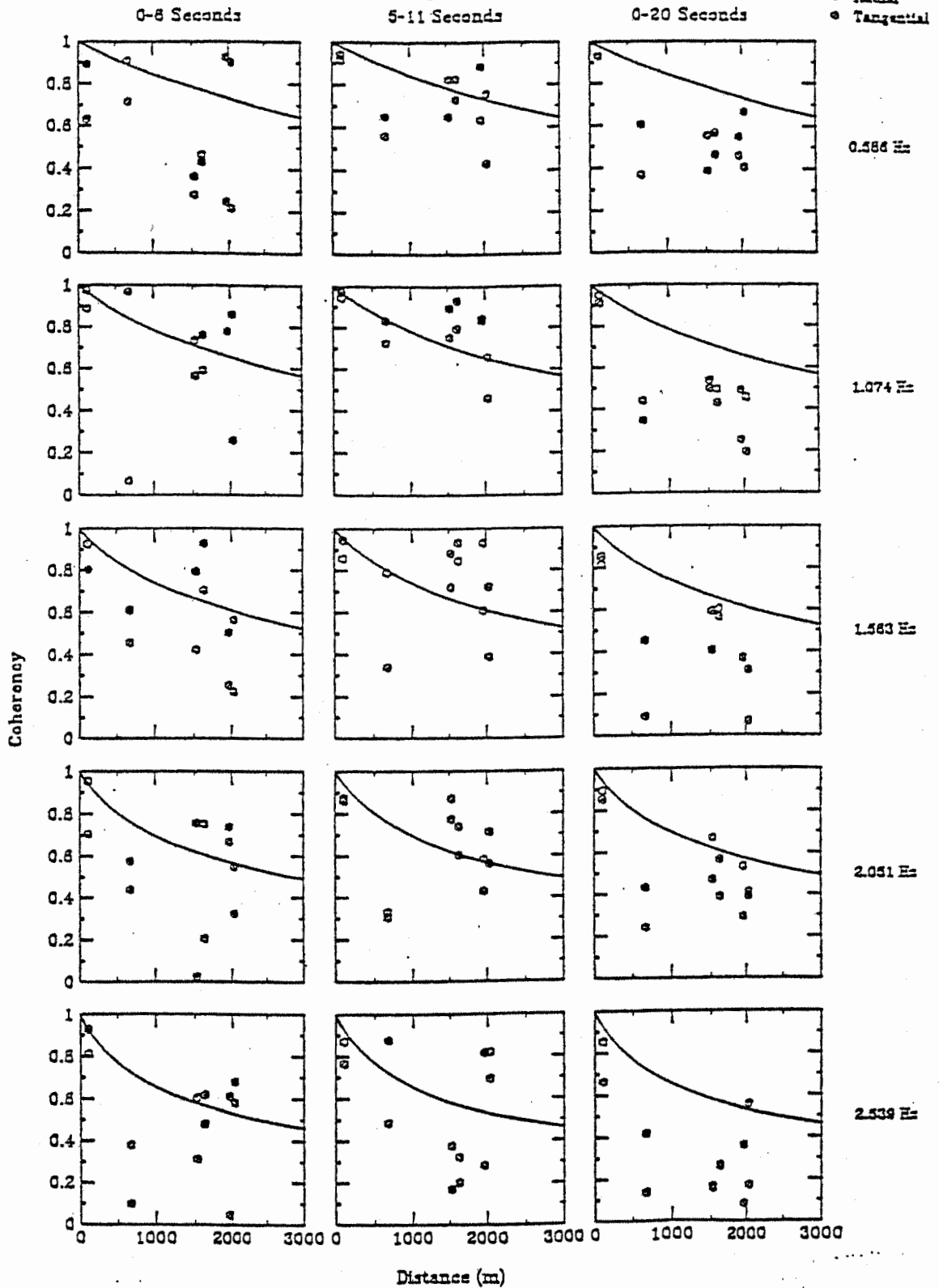
Figure 5.10: Spatial Coherency Measurements of Three Time Windows of the Whittier Narrows Recordings for Station Separations up to 3 km for Frequencies Ranging from 0.586 to 2.539 Hz. The Solid Lines Show the Model of Abrahamson et al. (1990).

Spatially Incoherent Time Histories Vincent-Thomas Bridge

acc: 090 comp.
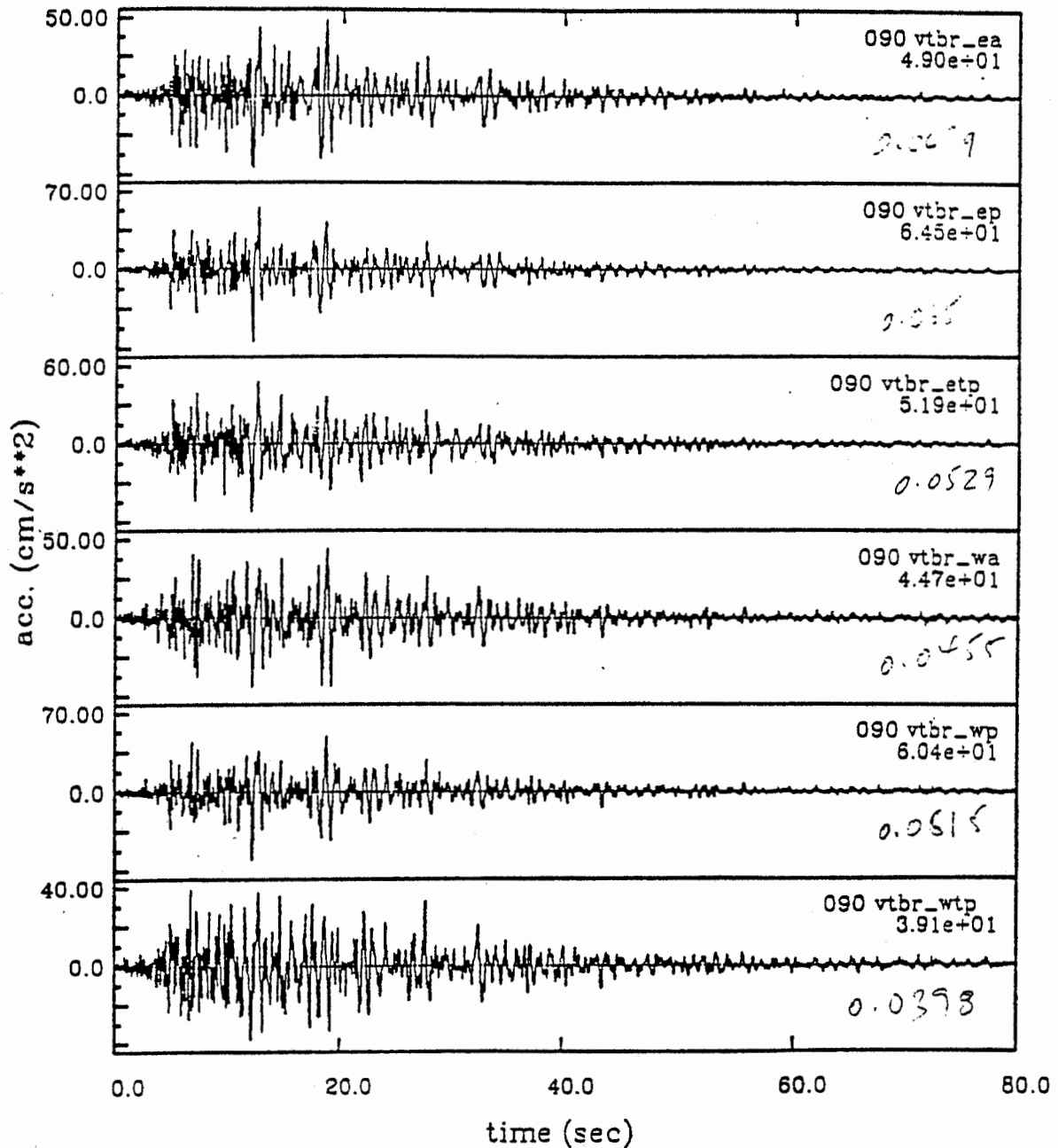
Figure 5.11: Spatially Incoherent Time Histories at the Vincent Thomas Bridge: East Component Acceleration

Spatially Incoherent Time Histories
Vincent-Thomas Bridge

vel: 090 comp.
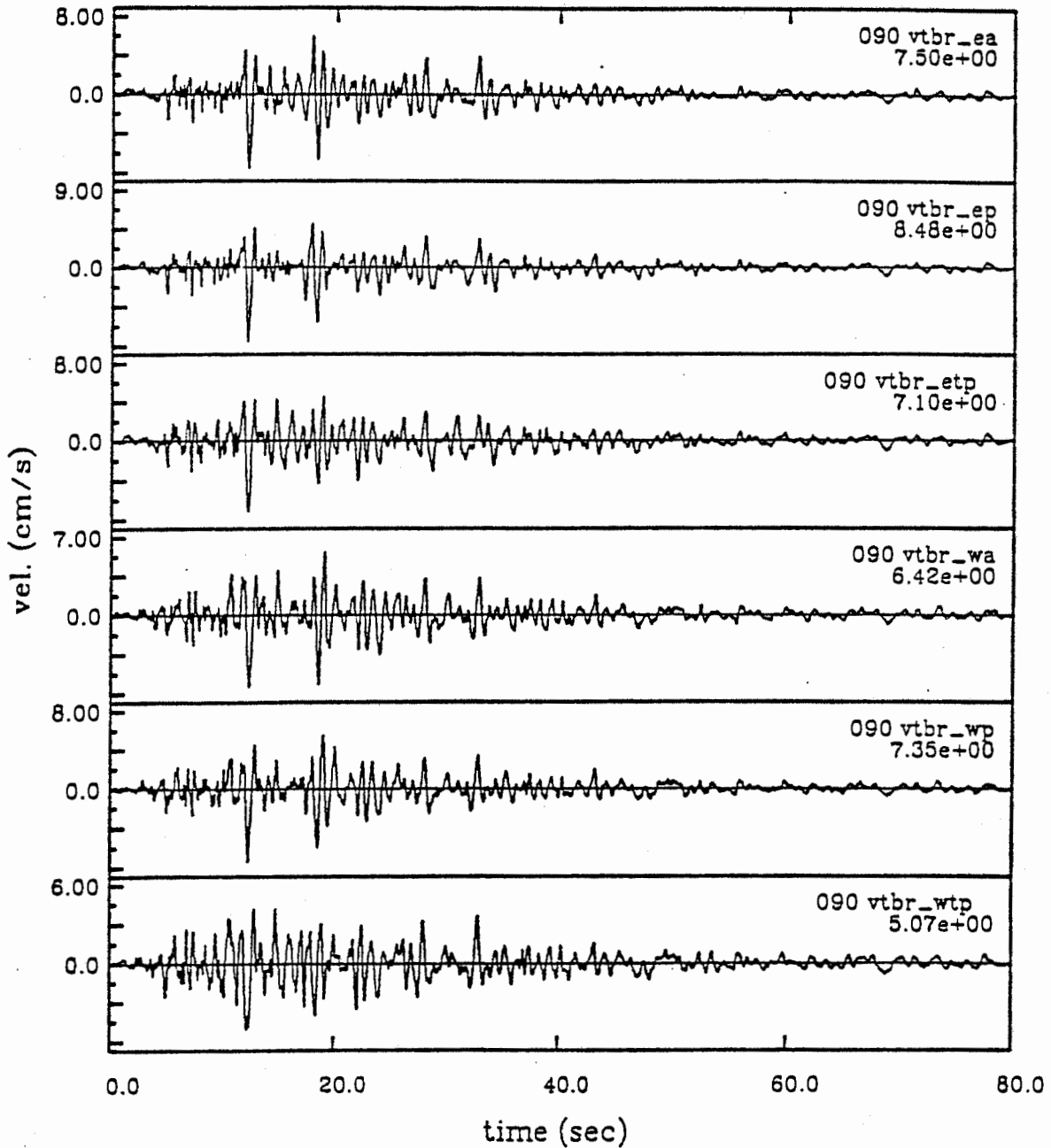
Figure 5.12: Spatially Incoherent Time Histories at the Vincent Thomas Bridge: East Component Velocity

Spatially Incoherent Time Histories
Vincent-Thomas Bridge

disp: 090 comp.
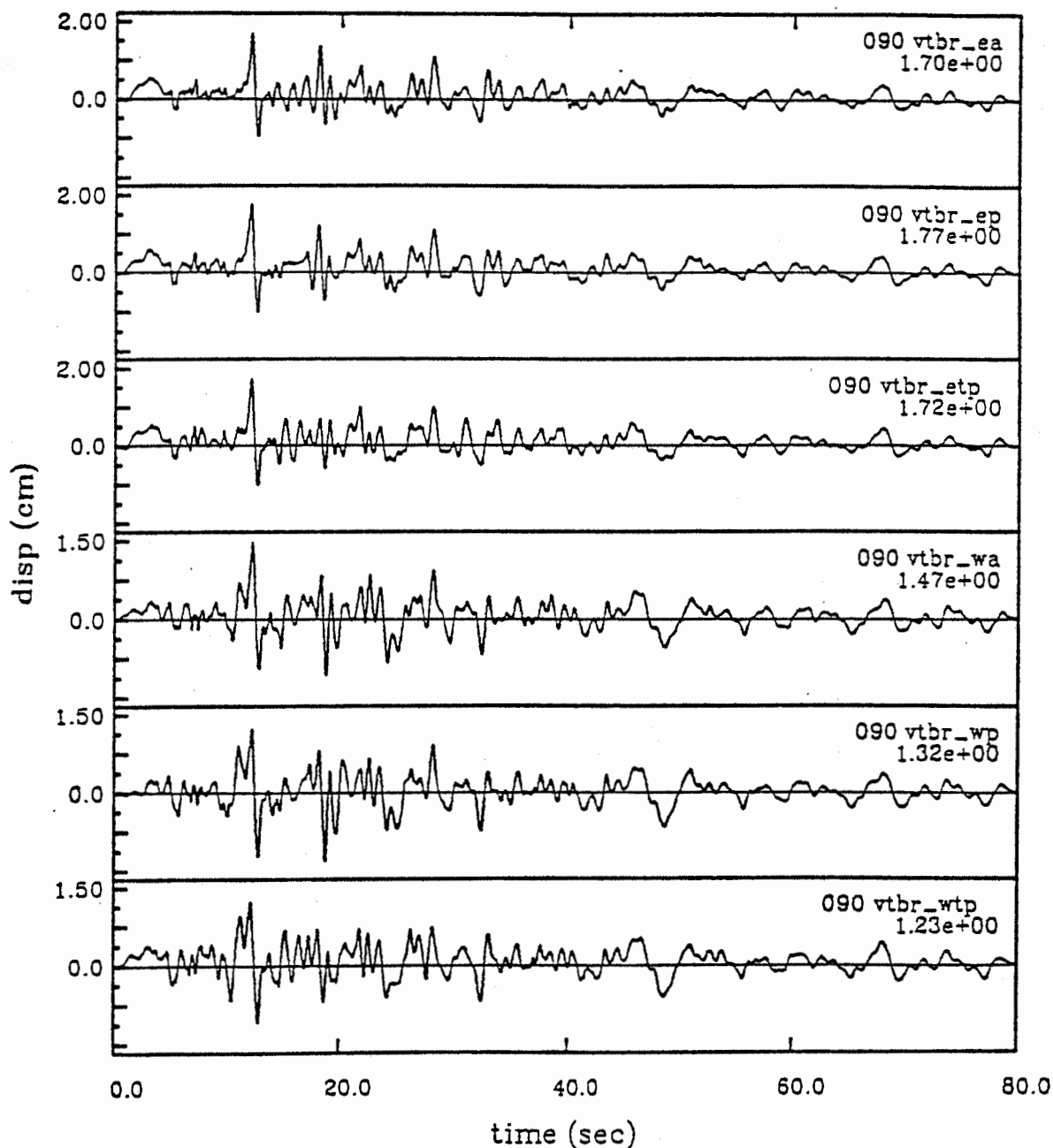
Figure 5.13: Spatially Incoherent Time Histories at the Vincent Thomas Bridge: East Component Displacement

Spatially Incoherent Time Histories
Vincent-Thomas Bridge

acc: 180 comp.
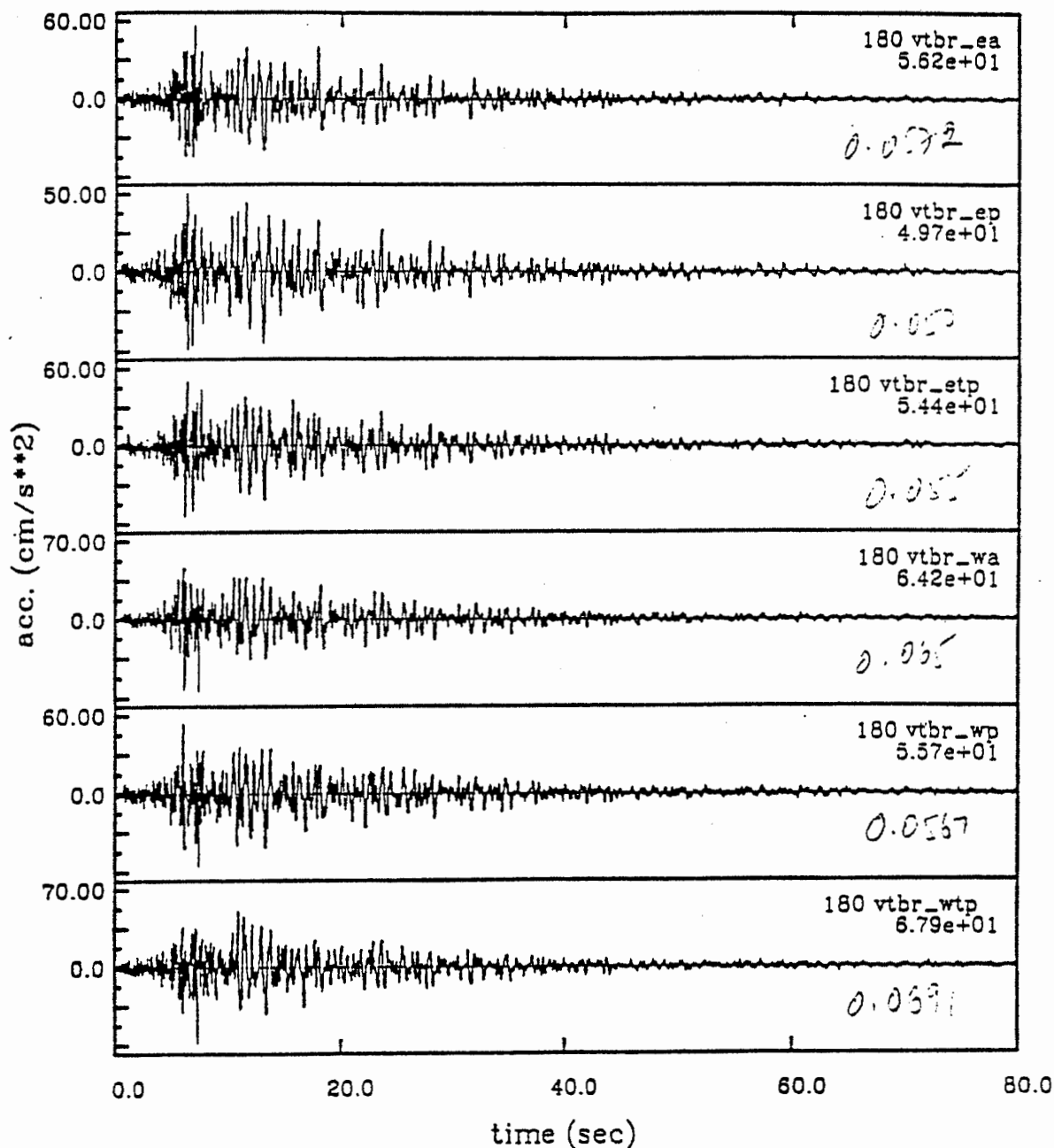
Figure 5.14: Spatially Incoherent Time Histories at the Vincent Thomas Bridge: South Component Acceleration

Spatially Incoherent Time Histories
Vincent-Thomas Bridge

vel: 180 comp.
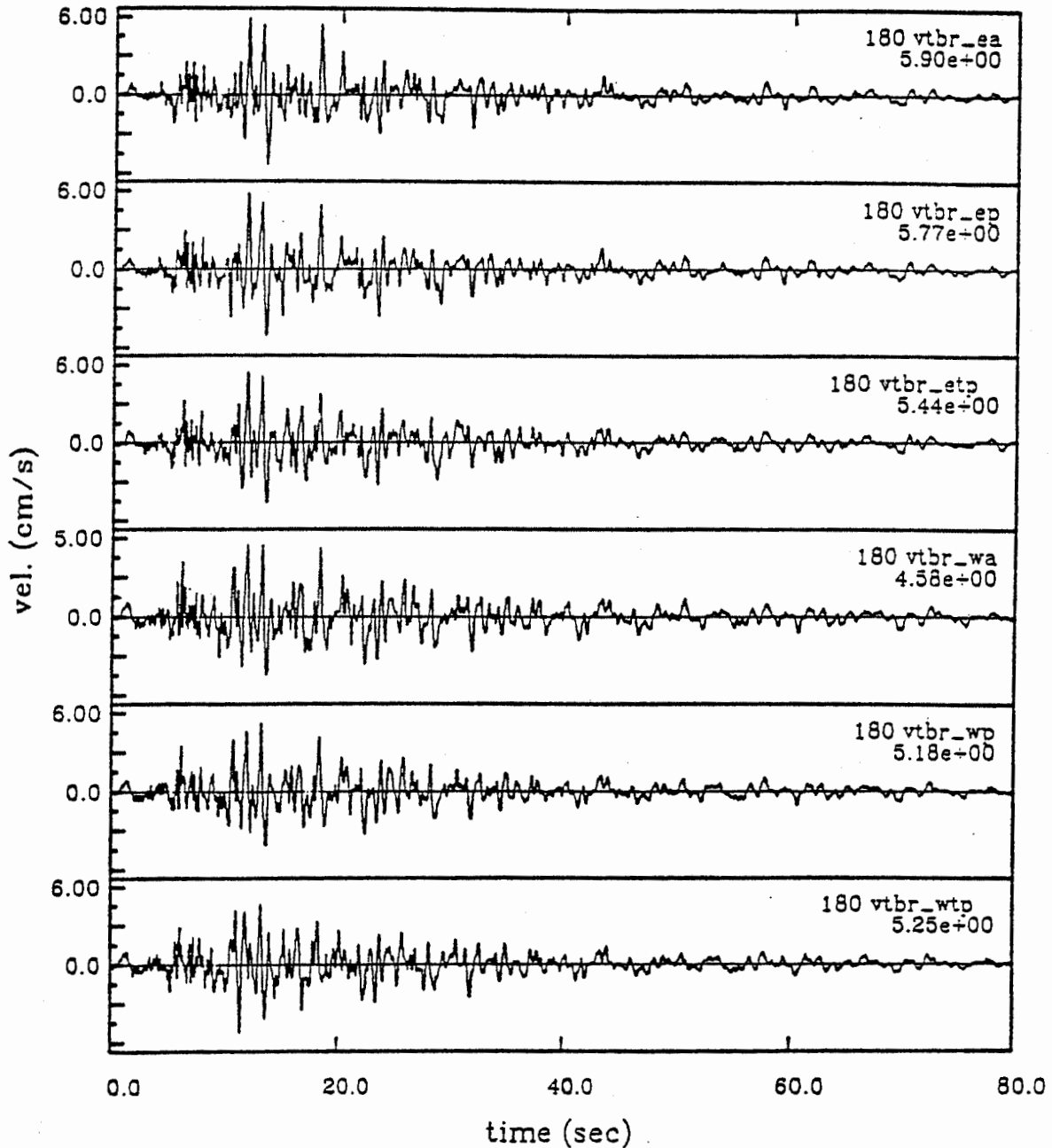
Figure 5.15: Spatially Incoherent Time Histories at the Vincent Thomas Bridge: South Component Velocity

Spatially Incoherent Time Histories
Vincent-Thomas Bridge

disp: 180 comp.
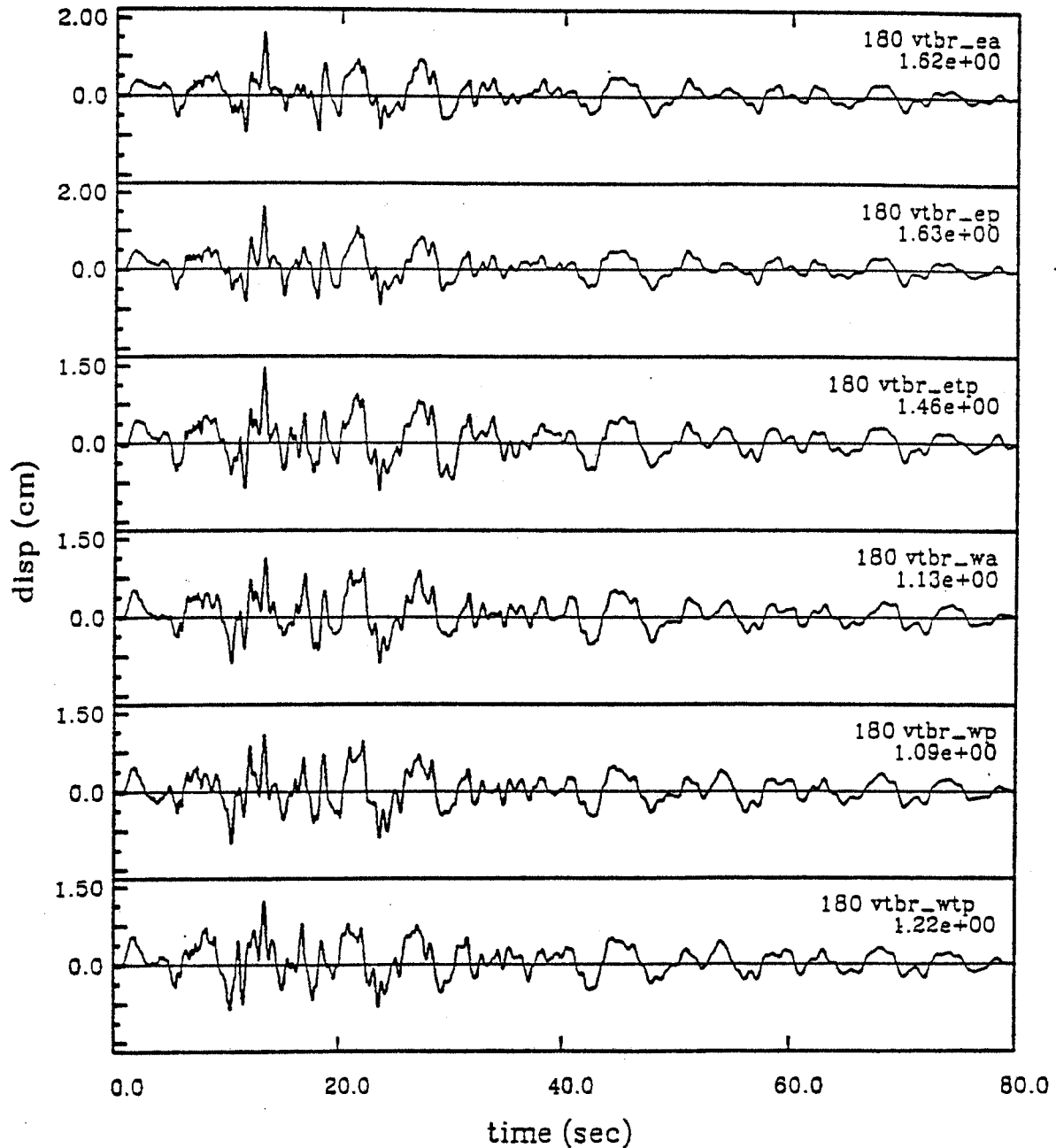
Figure 5.16:   Spatially Incoherent Time Histories at the Vincent Thomas Bridge: South Component Displacement
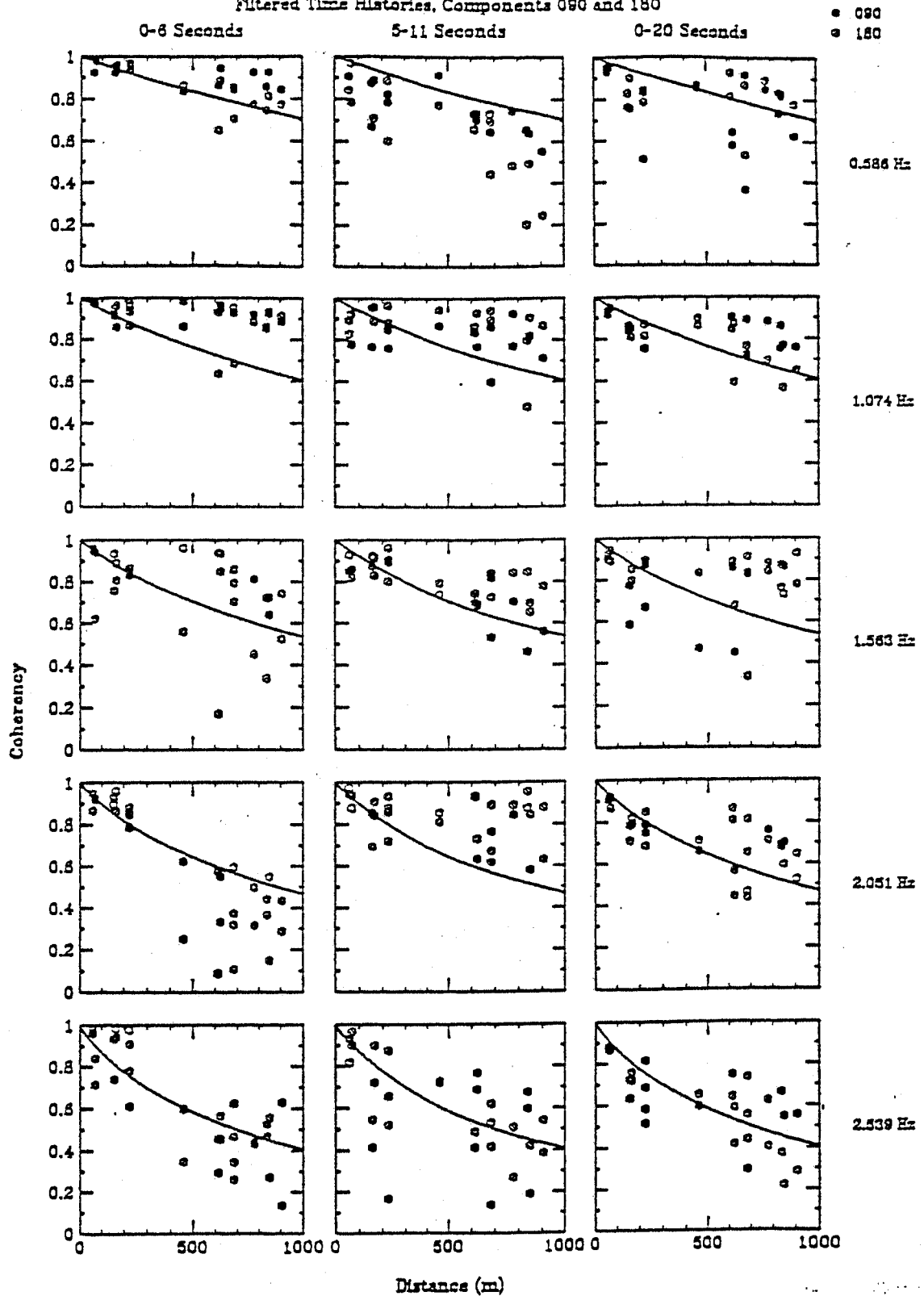
Figure 5.17: Spatial Coherency Measurements of Three Time Windows for Incoherent Time Histories Generated at the Supports of the Vincent Thomas Bridge for Frequencies Ranging from 0.586 to 2.539 Hz. The Solid Lines Show the Model of Abrahamson et al. (1990).

6. Multiple-Support-Excitation Response Analysis

6.1 General

In this chapter, multiple-support seismic response analyses were carried out using the direct-integration time history analysis method. Several studies were conducted using different sets of ground motions at the multiple supports:

1. Motions at the bridge foundations during the 1987 earthquake. It was assumed that the West Anchorage and West Cable Bent foundations have identical motion as the base of the West Tower. The advantage of this set is that the kinematic soil-structure interaction effect was fully accounted for the two towers and the East Anchorage. Results from this analysis will be used to correlate with and to supplement the recorded responses. This is discussed in Section 6.2.

2. Generated support motion time histories were used. As described in Chapter 5, this set was based on ground motion incoherency model derived from the Long beach area data which include the very important Los Angeles *basin effect*. A complete set of motions at the six supports were generated. Since the control motions used were those obtained at the East Anchorage, the resulting motions do not include the proper soil-structure interaction effect for the West Tower. However, this set provides a good basis to compare with the multiple-support response spectrum analysis.

This is discussed in Sections 6.3 and 6.4.

6.2 Correlation Study Using Recorded Motions at the Bridge

The seismic loadings are specified as support displacement time histories:

	Longitudinal	Transverse	Vertical
West Anchorage*	Ch. 23	Ch. 1	Ch. 14
West Cable Bent*	Ch. 23	Ch. 1	Ch. 14
West Tower	Ch. 23	Ch. 1	Ch. 14
East Tower	Ch. 13	Ch. 9	Ch. 19
East Cable Bent*	Ch. 25	Ch. 24	Ch. 26
East Anchorage	Ch. 25	Ch. 24	Ch. 26

* No recording at this location.

In this study, the kinematic interaction effects at the West Tower, East Tower and East Anchorage were fully accounted for in the recorded foundation motion. Using imposed displacement time histories, the total displacement responses including the quasi-static effect are calculated.

Correlation with Measured Responses

In a previous study (Niazy, 1991), the time history analysis was conducted using *modal* time integration. Once the dominant model frequencies were identified, the modal damping ratios can be adjusted to match the measured responses.

In the direct integration time history analysis, the structural damping matrix is specified as Rayleigh damping which is defined as:

$$C = \alpha M + \beta K_T$$

Since there are only two parameters, it is impossible to fit appropriate damping ratios at all modes. The alternative is to conduct several analyses each with appropriate damping ratios at different frequency ranges. In this study, no attempt was made to establish the optimized match. The Rayleigh damping parameters used are:

$$\alpha = 0.0747$$
$$\beta = 0.0061$$

The damping ratio is shown in Figure 6.1 as a function of period. This would correspond to a damping ratio of 2.5% at one second, and 5% damping at 0.4 second period. For the period range of interest, from 0.5 to 6 seconds, the damping ratio is between 2% to 4%. For periods shorter than 0.4 second, the damping ratio will be too high.

Side Span Responses – Comparisons of Fourier amplitude spectra for measured and calculated motions are sown in Figures 6.2a, 6.2b and 6.2c for vertical, transverse and torsional responses of the deck, respectively. As shown in Figure 6.2a, very good correlation was obtained for the vertical vibration in both the vibration frequency and amplitude. This correlation was also obtained in the natural modes of the bridge (Chapter 4). For transverse vibration, the dominant frequency of 1 Hz was captured very well as shown in Figure 6.2c. However, the calculated amplitude is less. This 1 Hz frequency component is a coupled transverse and torsional mode of the truss. The torsional response is shown in Figure 6.2b as the difference of two channels (Ch. 21 - Ch. 22). The 1 Hz frequency is captured well by the analytical model except the amplitude is overestimated. This may be caused by the assignment of structural damping and how the stiffening truss box was modeled. The obvious improvement is to model all structural members explicitly in the analytical model. A better approach is to fully understand the coupled torsional-lateral response from the measurements to provide a benchmark for modeling, and to derive a simplified representation of the 3D truss system.

Main Span Responses – Comparisons of Fourier amplitude spectra for measured and calculated responses are shown in Figures 6.3 and 6.4. The vertical responses at the midspan and the one-third span locations (based on Ch. 15 + Ch. 16 and

Ch. 17 + Ch. 18) correlate very well with analytical prediction in both the frequency and amplitude (Figure 6.3).

For the transverse vibration at the midspan, the analytical model predicted the frequency of the first mode ($f_1 = 0.16$ Hz), but overestimate the amplitude as shown in Figure 6.4a. The correlation of torsional response was not as good as shown in Figure 6.4b. The frequency components at 1 to 1.1 Hz were captured. However, several low frequency modes were not predicted. This is due to the coupling effect of transverse and torsional vibration as in the span truss.

East Tower Structures – For the transverse vibration, measured and calculated responses at top of the south leg and at the roadway level are shown in Figure 6.5. The correlation was very good. The dominant frequency was predicted. The amplitude was somewhat overestimated.

The longitudinal responses at the roadway level (Ch. 12) are compared in Figure 6.6. The frequency content was well predicted. The amplitude is overestimated.

The twisting response of the two tower legs is shown in Figure 6.7. Both the frequency and the amplitude are predicted well.

Additional Response Predictions

1. West Tower – Since only the East Tower is instrumented, it would be of interest to compare the responses of the two towers. Displacement response time histories along the height of each tower are shown in Figures 6.8 through 6.11. From the amplitudes and the dominant frequency, the dominant tower vibration mode shapes in the longitudinal and the transverse direction can be identified. The maximum displacement responses at five elevations are shown Table 6.1. The longitudinal displacement at the West Tower is about 30% higher than the East Tower; while the transverse displacement at the top of the East Tower is 50% higher that the West Tower. This is apparently affected by the kinematic soil-structure interaction effect and the spatial variation of ground motion.

102

Maximum moments developed at the base section of tower legs are:

West Tower		East Tower
M_T	30,000 kip-ft	20,000 kip-ft
M_L	8,700 kip-ft	10,000 kip-ft

M_T corresponds to longitudinal shear.

M_L corresponds to transverse shear.

Again, the moment in the West Tower is about 50% higher than that in the East Tower. This has also been observed in the previous study of the Golden Gate Bridge (Liu and Imbsen, 1990) and was attributed to the several closely-spaced in-phase and out-of-phase tower vibration modes (as shown in Chapter 4) and the multiple-support excitations.

The average stress in tower leg under dead load is about 10 ksi. The flexural stress is about 20 ksi caused by the maximum moment about the transverse axis in the West Tower. Given the low amplitude of the ground motion during the 1987 Whittier Narrows earthquake, this calculated stress level is not low.

2. Relative Displacements at Tower-Deck Joints – Longitudinal displacement time histories at the main span, tower and side span are shown in Figures 6.12 and 6.13 for East Tower and West Tower, respectively. The maximum relative displacements are about 5 ~ 6 inches during the 1987 Whittier Narrows earthquake.

3. Additional Earthquake Induced Cable Force – Maximum cable forces during the excitation are calculated. The additional earthquake induced cable forces are 2.5% to 3% the initial dead load cable force in the side span, less than 2% in the main span. However, in the backstay, the additional cable forces are 9% to 10% of the initial cable tension. This is a very significant increase given the low intensity of ground motion input. The increased cable force in the backstay may be due to the angle change of the cable profile at the cable bent, and the interaction between the cable and the much stiffer cable bent.

The cable force in the west side backstay increased to 8,600 kip (from an initial T_0 of 7,800 kip).

4. Cable Bent Response – The cable bents are 180 feet tall concrete structure the equivalent of a 15 story building and are very critical to the integrity of the bridge. At top of each column, the maximum longitudinal shear developed was 580 kip at the West cable bent and 220 kip at the East cable bent. These shear forces will have to be transferred through the cable bent saddles. Time histories of the longitudinal and transverse shear at top of each cable bent column were shown in Figures 6.14 and 6.15.

In recent investigation of the Golden Gate Bridge and the San Francisco-Oakland Bay Bridge, the concrete pylons are found to be very vulnerable. It would be of interest to monitor the response of the cable bents in future earthquakes.

6.3 Multiple-Support Seismic Analysis Using Generated Motions

As discussed in Chapter 5, generated ground motion time histories at the six supports were developed to follow the appropriate coherency model for the Long Beach area. However, since the recorded motions at the East Anchorage of the bridge were used as control motions, the generated motions all have included similar soil-structure interaction effect as that of the East Anchorage. The apparent varying local site effects at the East and West sides of the channel are not accounted for. Two multi-support time history analyses were carried out corresponding to the following assumptions:

1. All foundations have the same kinematic interaction effect. The generated motions were applied at top of the foundations.

2. All foundation motions were assumed to be free-field motion and were applied at the ground. The kinematic soil-structure interaction were ignored.

The results of these two analyses for the Tower displacements are shown in Table 6.2. These results indicate that with different assumptions regarding the

support input motions, results obtained could be drastically different. Even though the spatial incoherency and the foundation impedance effects are the same in both analyses, the kinematic interaction effects were handled differently.

6.4 Multiple-Support Response Spectrum Analysis

The multiple-support response method was recently developed by Der Kiureghian and Neuenhofer (1992) that would account for the multiple-support input. This is a direct extension of the CQC modal combination method under uniform input (Der Kiureghian, 1980). Based on random vibration theory, the mean value of maximum responses (any displacement and member force component) can be expressed in terms of:

- peak ground displacements at each support,
- response spectrum at each support, and
- several cross-correlation coefficients.

In equation form, this is expressed as the sum of three terms as follows:

$$
\begin{aligned}
E\left[\max|z(t)|\right] = \Bigg\{ &\sum_k \sum_l a_k a_l \rho_{u_k u_l} u_{k,max} u_{l,max} \\
&+ 2\sum_k \sum_l \sum_j a_k b_{lj} \rho_{u_k s_{lj}} u_{k,max} D_l(\omega_j,\xi_j) \\
&+ \sum_k \sum_l \sum_i \sum_j b_{ki} b_{lj} \rho_{s_{ki} s_{lj}} D_k(\omega_i,\xi_i) D_l(\omega_j,\xi_j) \Bigg\}^{\frac{1}{2}}
\end{aligned}
$$

where

$z(t)$ = response quantities of interest.

a_k, a_l = effective quasi-static influence factors associated with supports k and l, respectively.

b_{ki}, b_{lj} = effective modal influence factors for mode i (j) and support degree of freedom k (l).

$u_{k,max}$ = peak ground displacement at support k.

$D_k(\omega,\xi)$ = displacement response spectrum associated with support k.

$\rho_{u_k u_l}$, $\rho_{u_k s_{lj}}$, and $\rho_{s_{ki} s_{lj}}$ = cross-correlation coefficients.

The three terms in the above equation account for:

1. the quasi-static effect,
2. the coupled quasi-static and dynamic effect, and
3. the dynamic effect.

The cross-correlation coefficients used account for the effects of spatial ground motion variation and the cross modal correlation. The method has been used in the study of the Golden Gate Bridge (Nakamura et al. 1993). The data flow diagram for the multiple-support response spectrum analysis is summarized in Figure 6.17.

This method was applied to a study using motions recorded at Caltech stations. Good agreement was obtained for the displacement responses. However, as mentioned earlier in Chapter 5, the Caltech records do not represent the bridges site particularly with regard to the basin effect with a dominant period of about one second.

Ground motions based on the Long Beach area data are being used to compare with results obtained in Section 6.3.

Table 6.1: Maximum Total Displacement Response along the Tower Height

Vincent Thomas Bridge
Whitter Earthquake
Tower Displacement

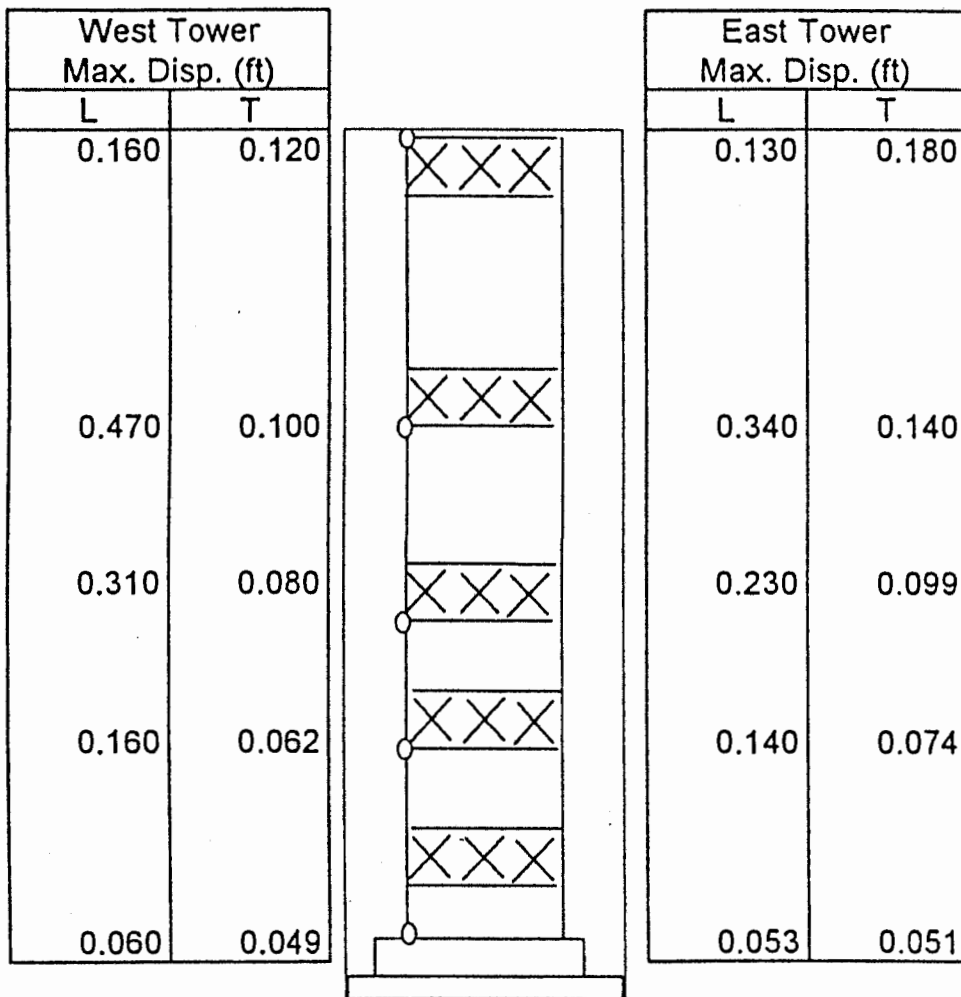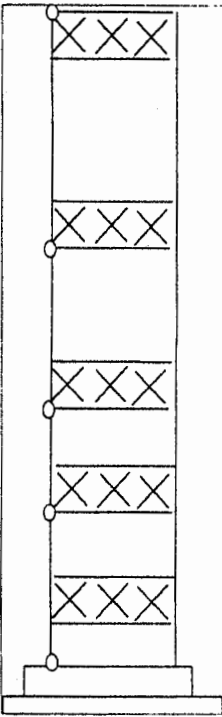| West Tower Max. Disp. (ft)		East Tower Max. Disp. (ft)	
L	T	L	T
0.160	0.120	0.130	0.180
0.470	0.100	0.340	0.140
0.310	0.080	0.230	0.099
0.160	0.062	0.140	0.074
0.060	0.049	0.053	0.051

Table 6.2: Maximum Total Displacement Response along the Tower Height Using Simulated Earthquake Time Histories

Vincent Thomas Bridge
Whitter Earthquake
Tower Displacement

West Tower Max. Disp. (ft)			
LongBeach (2)		LongBeach Pier (1)	
L	T	L	T
0.078	0.120	0.084	0.120
0.220	0.090	0.190	0.094
0.150	0.061	0.150	0.064
0.083	0.054	0.096	0.052
0.043	0.048	0.040	0.040

East Tower Max. Disp. (ft)			
LongBeach (2)		LongBeach Pier (1)	
L	T	L	T
0.075	0.130	0.094	0.200
0.180	0.099	0.290	0.150
0.110	0.068	0.210	0.097
0.070	0.054	0.130	0.070
0.058	0.049	0.056	0.048

(1) Motion applied at top of foundations
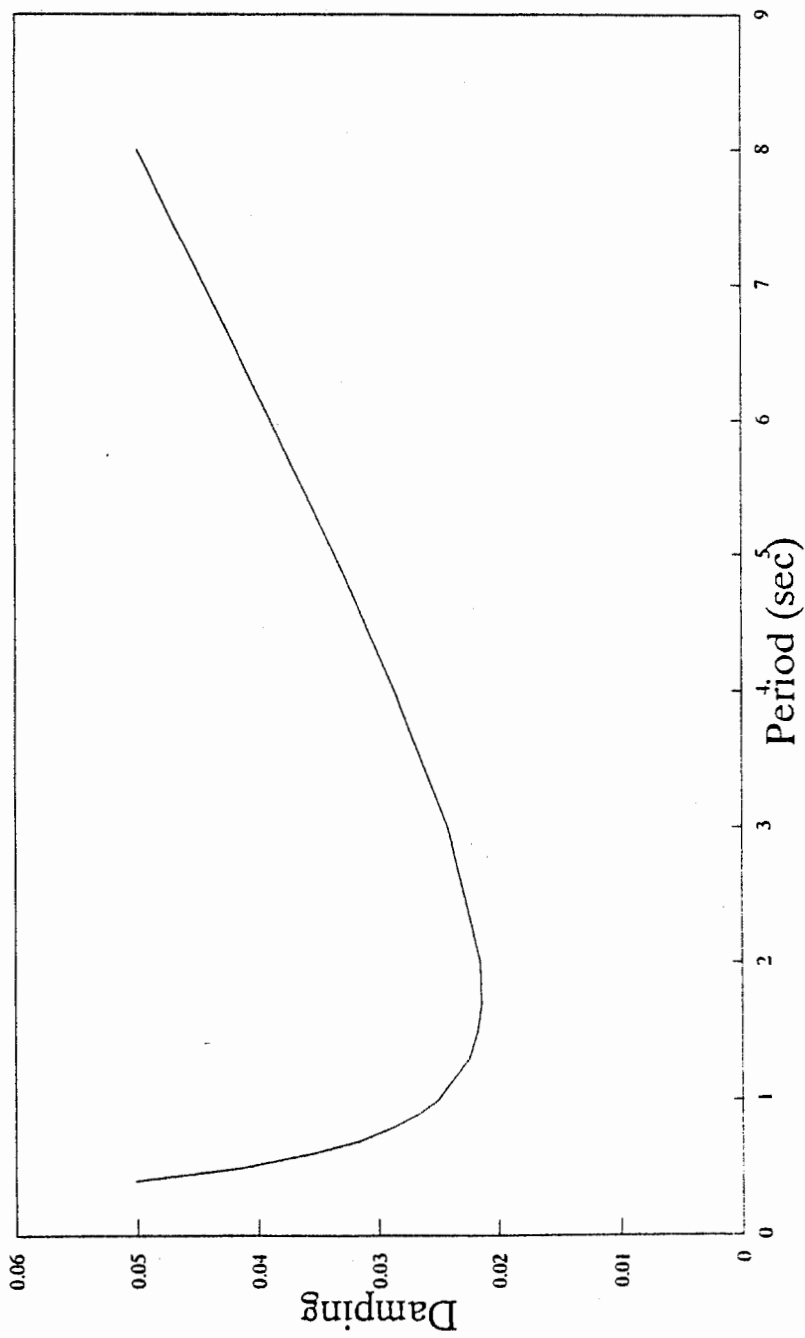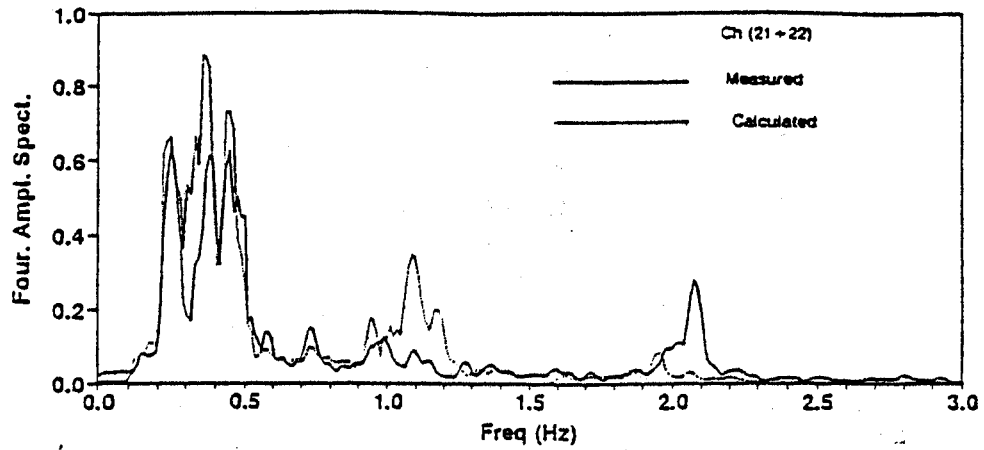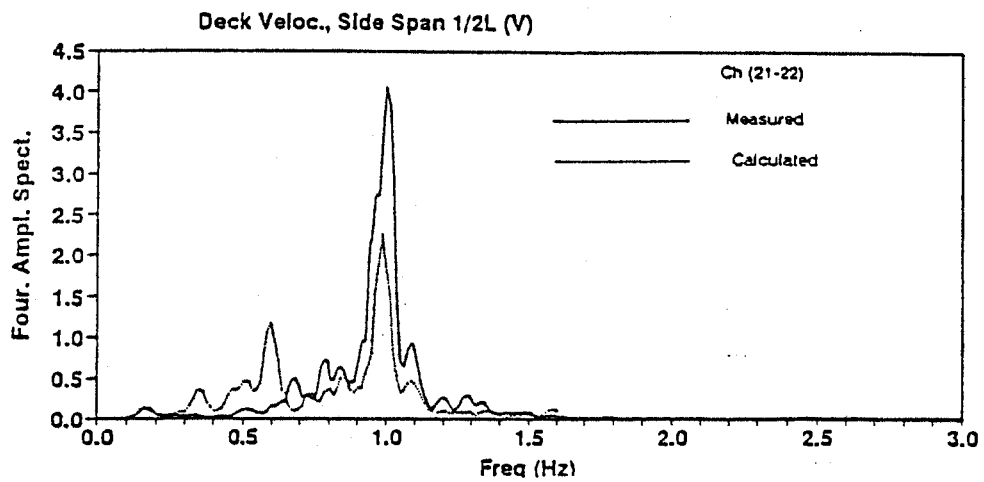(2) Motion applied at the ground

108

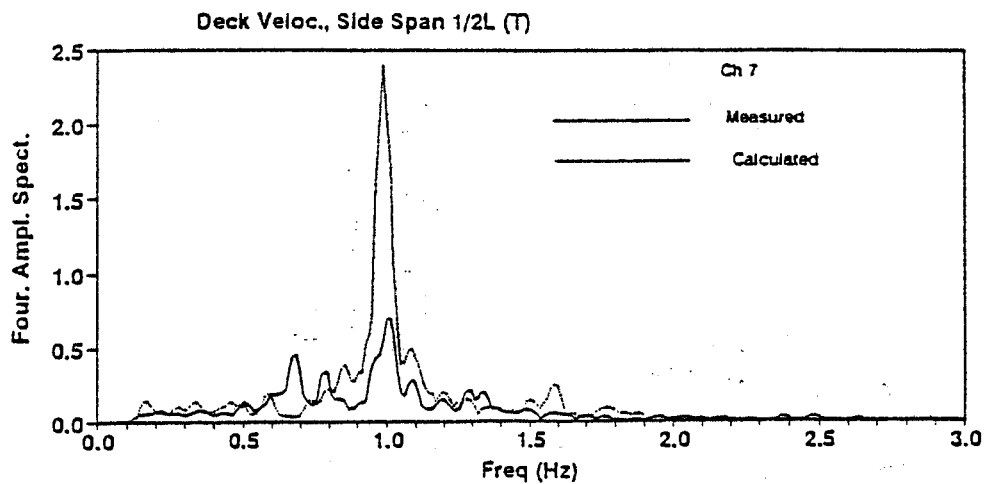**Figure 6.1:   Structural Damping Ratio as a Function of Period**

a. Vertical Response (Ch. 21 + Ch. 22)

b. Torsional Response (Ch. 21 - Ch. 22)

c. Transverse Response (Ch. 7)

Figure 6.2: East Side Span – Comparison of Vertical, Transverse and Torsional Responses

110
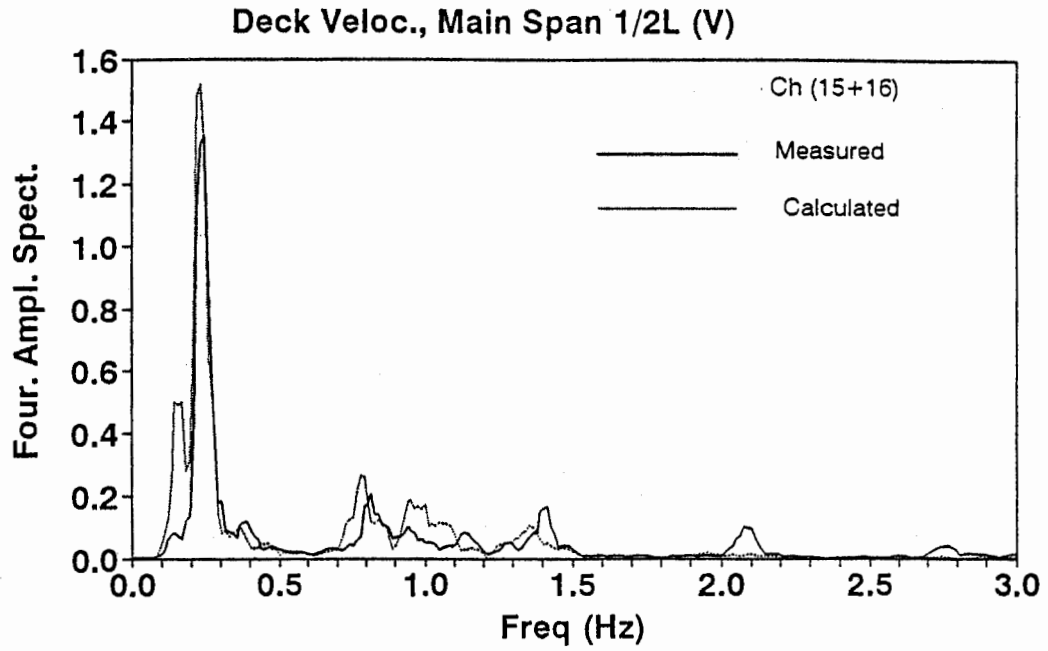
a. Midspan (Ch. 15 + Ch. 16)
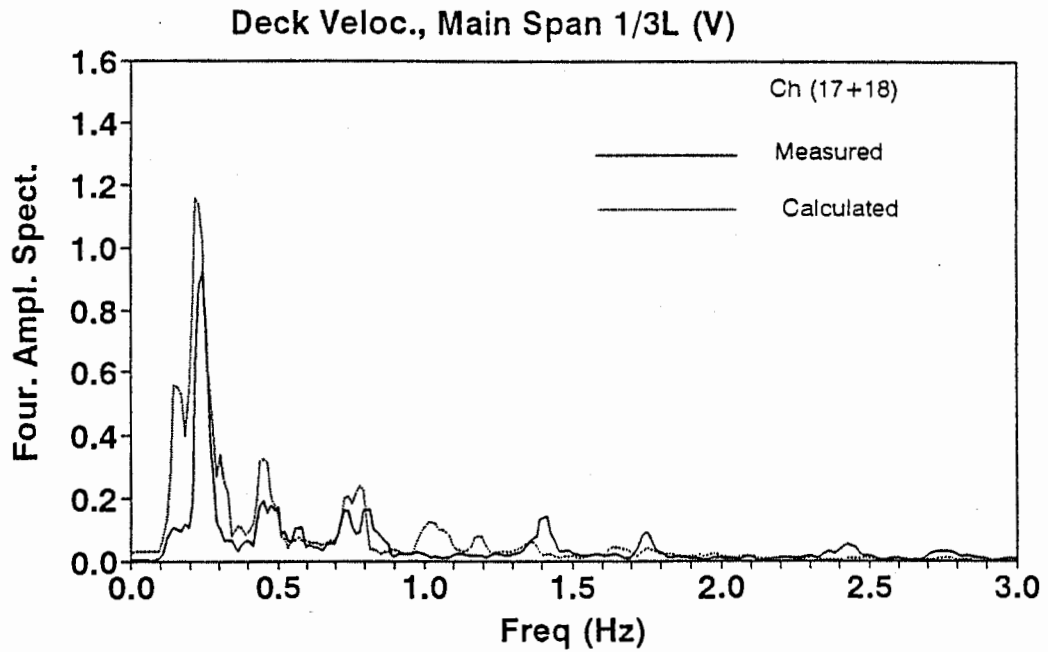
b. One-third Span (Ch. 17 + Ch. 18)

Figure 6.3:   Main Span – Comparison of Vertical Response
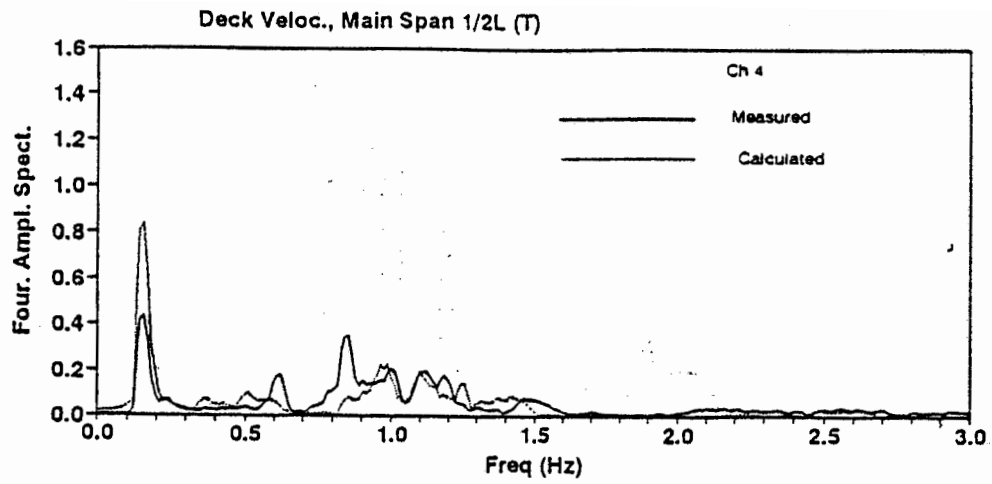
a. Transverse Response at Midspan (Ch. 4)
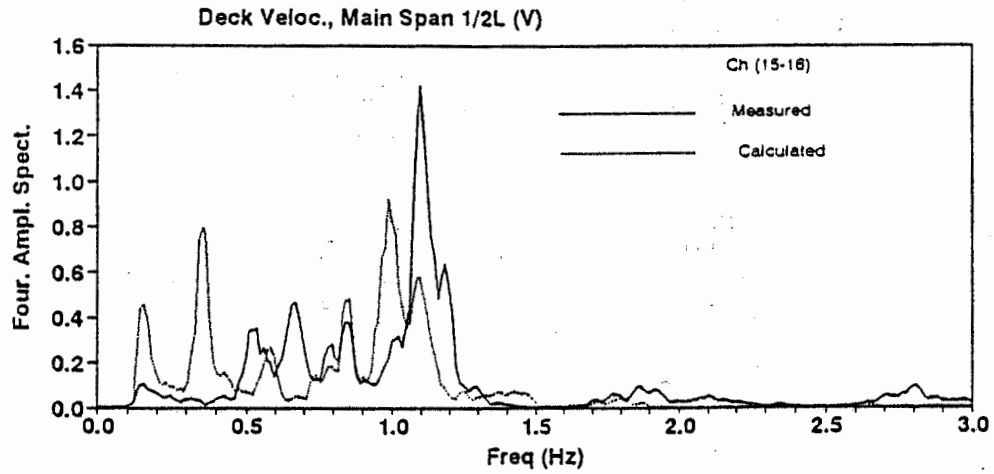
b. Torsion at Midspan (Ch. 15 - Ch. 16)
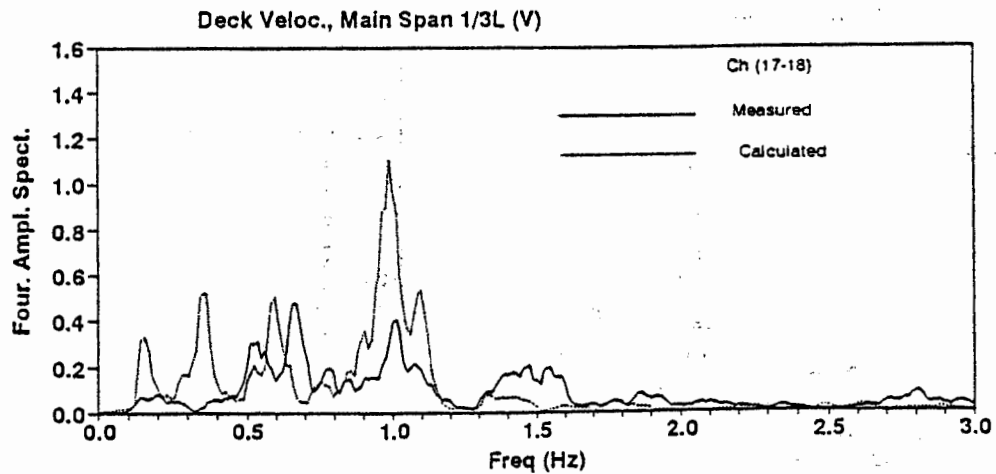
c. Torsion at One-third Span (Ch. 17 - Ch. 18))

Figure 6.4: Main Span – Comparison of Torsional and Transverse Responses

112
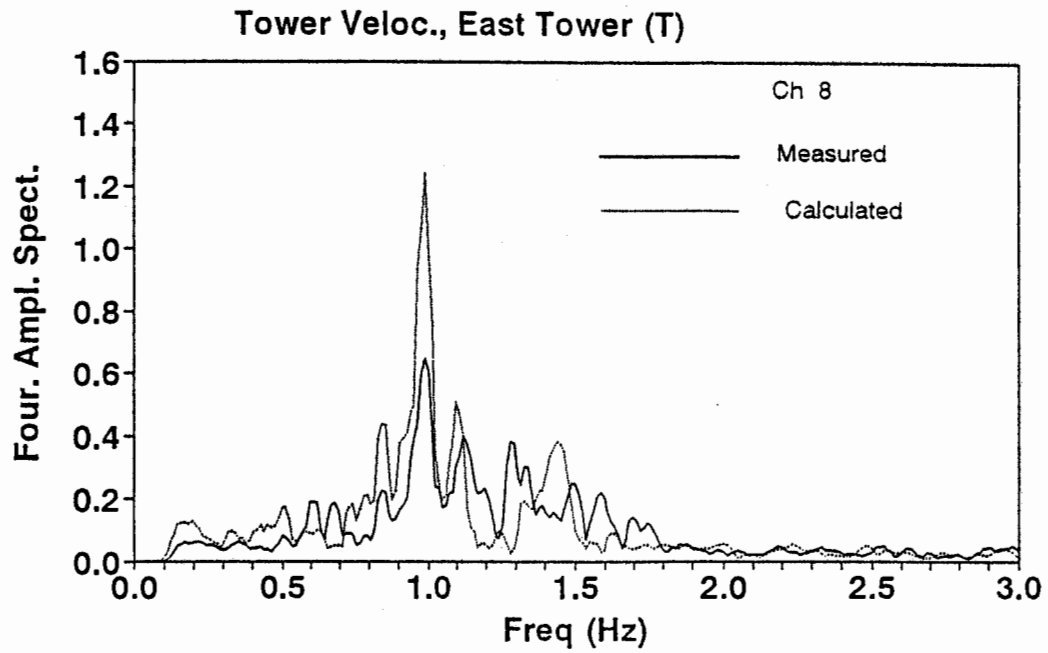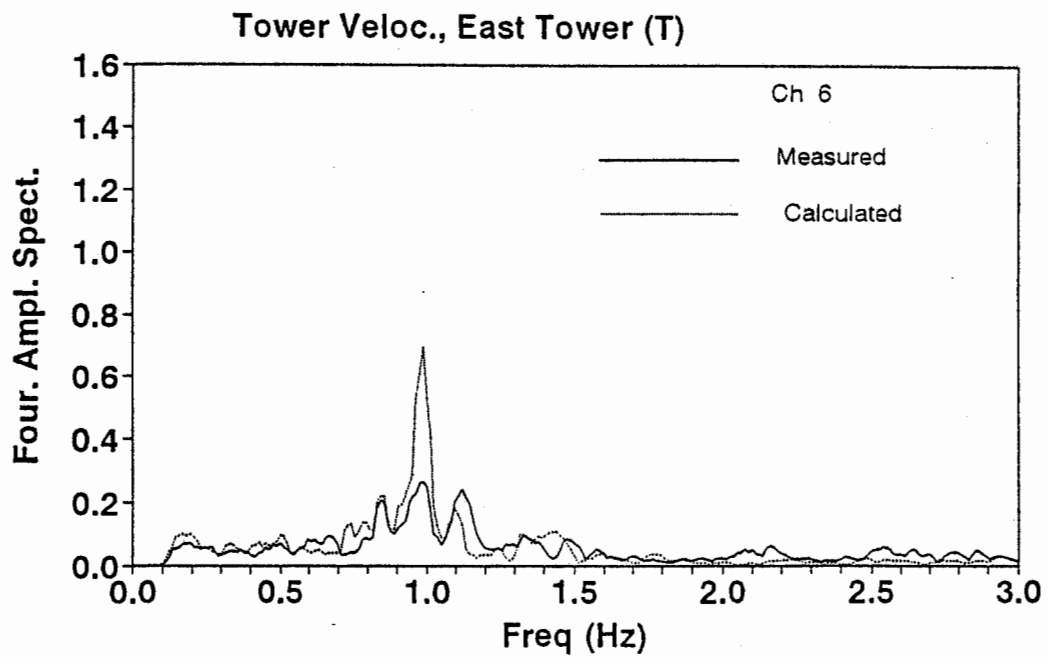
a. Top of Tower (Ch. 8)

b. Roadway Level (Ch. 6)

Figure 6.5: East Tower – Comparison of Transverse Response of South Leg

Tower Veloc., East Tower (L)

Ch 10

Measured

Calculated

Four. Ampl. Spect.

Freq (Hz)

a. Top of Tower (Ch. 10)

Tower Veloc., East Tower (L)

Ch 12

Measured

Calculated

Four. Ampl. Spect.

Freq (Hz)
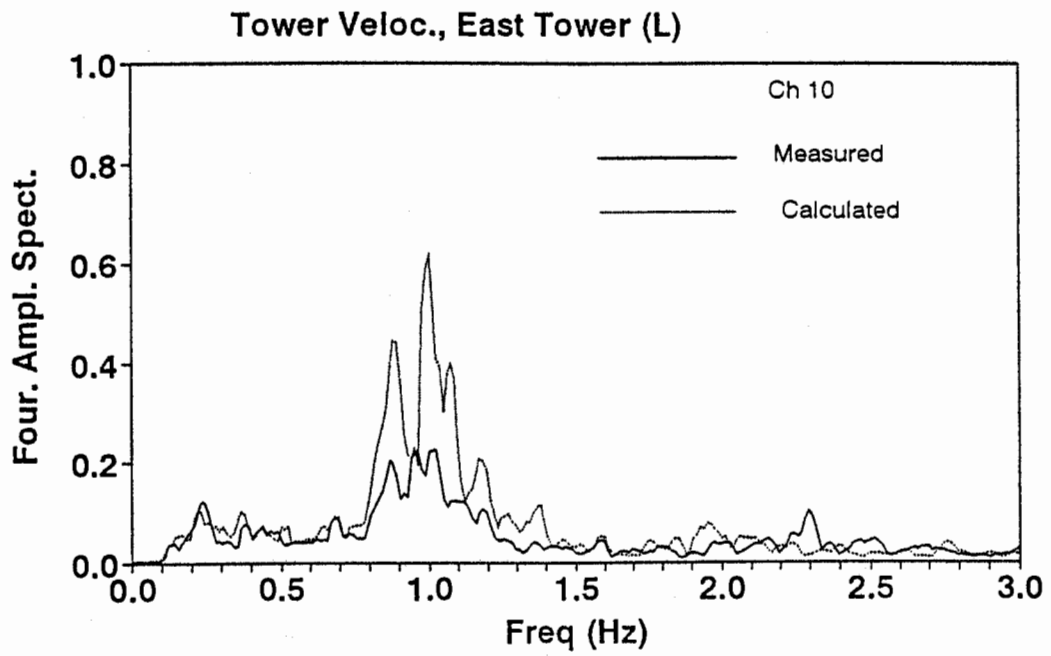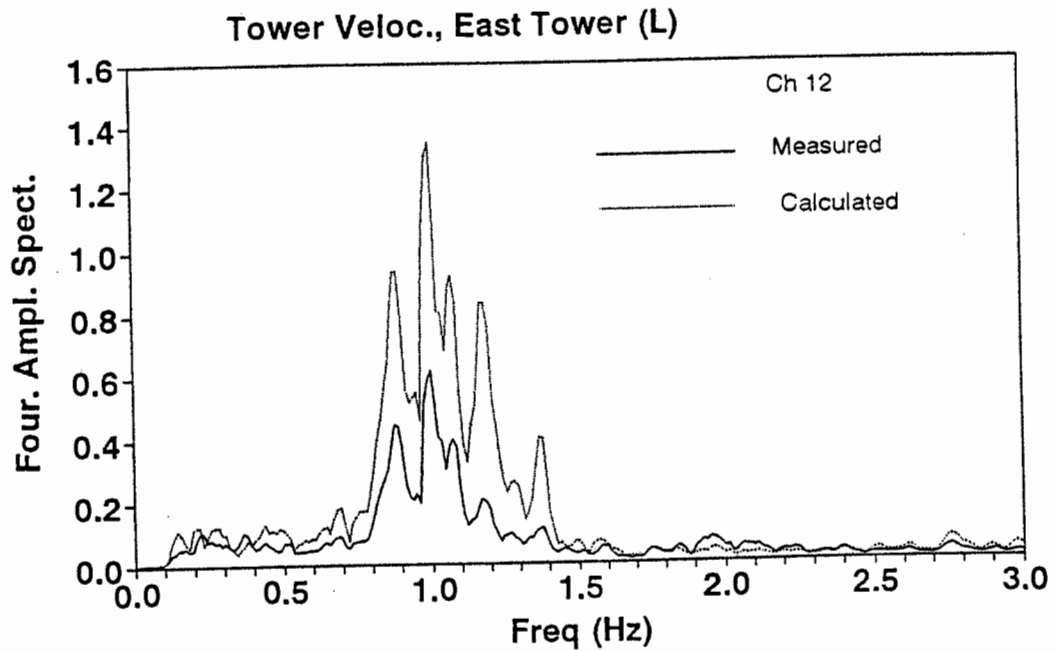
b. Roadway Level (Ch. 12)

Figure 6.6:   East Tower – Comparison of Longitudinal and Torsional Responses
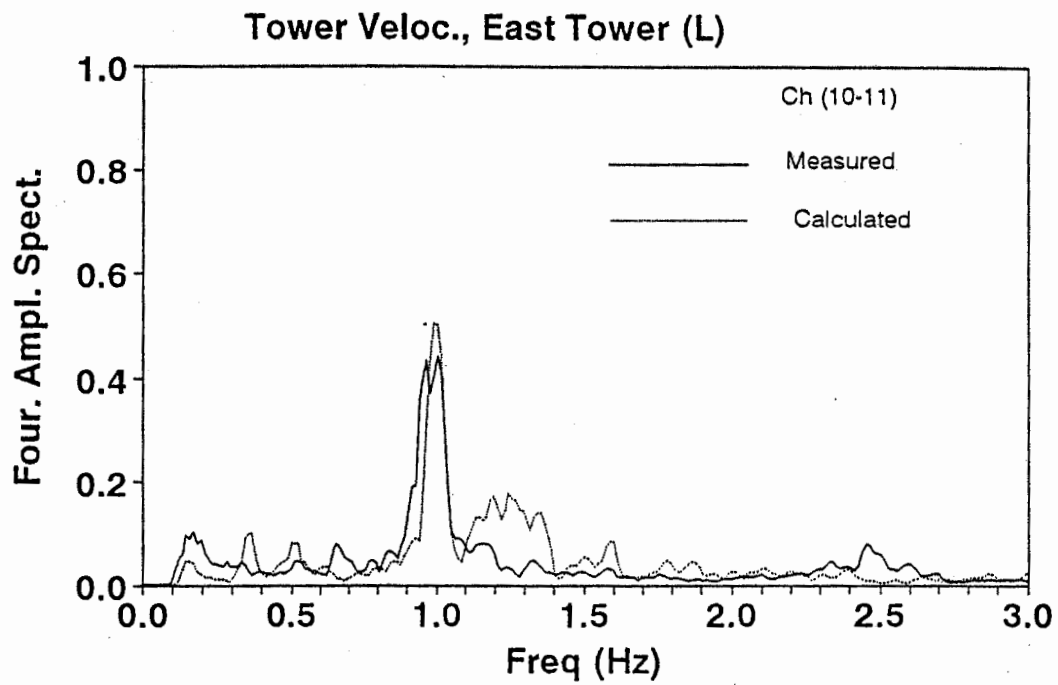
Figure 6.7: East Tower – Torsional Response at Top of Tower Legs (Ch. 10 - Ch. 11)
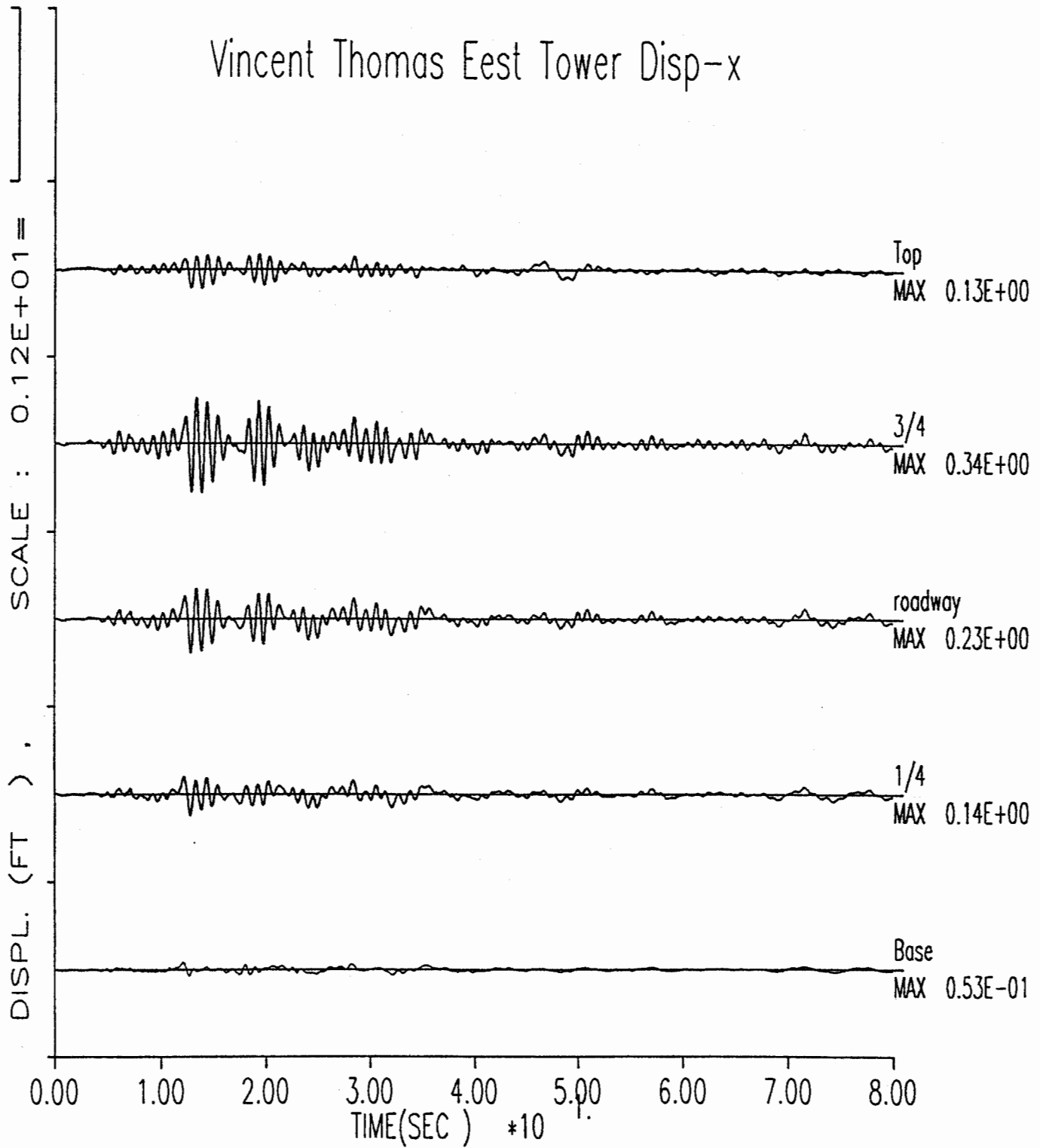
Figure 6.8: Longitudinal Displacement Time Histories of the East Tower

116
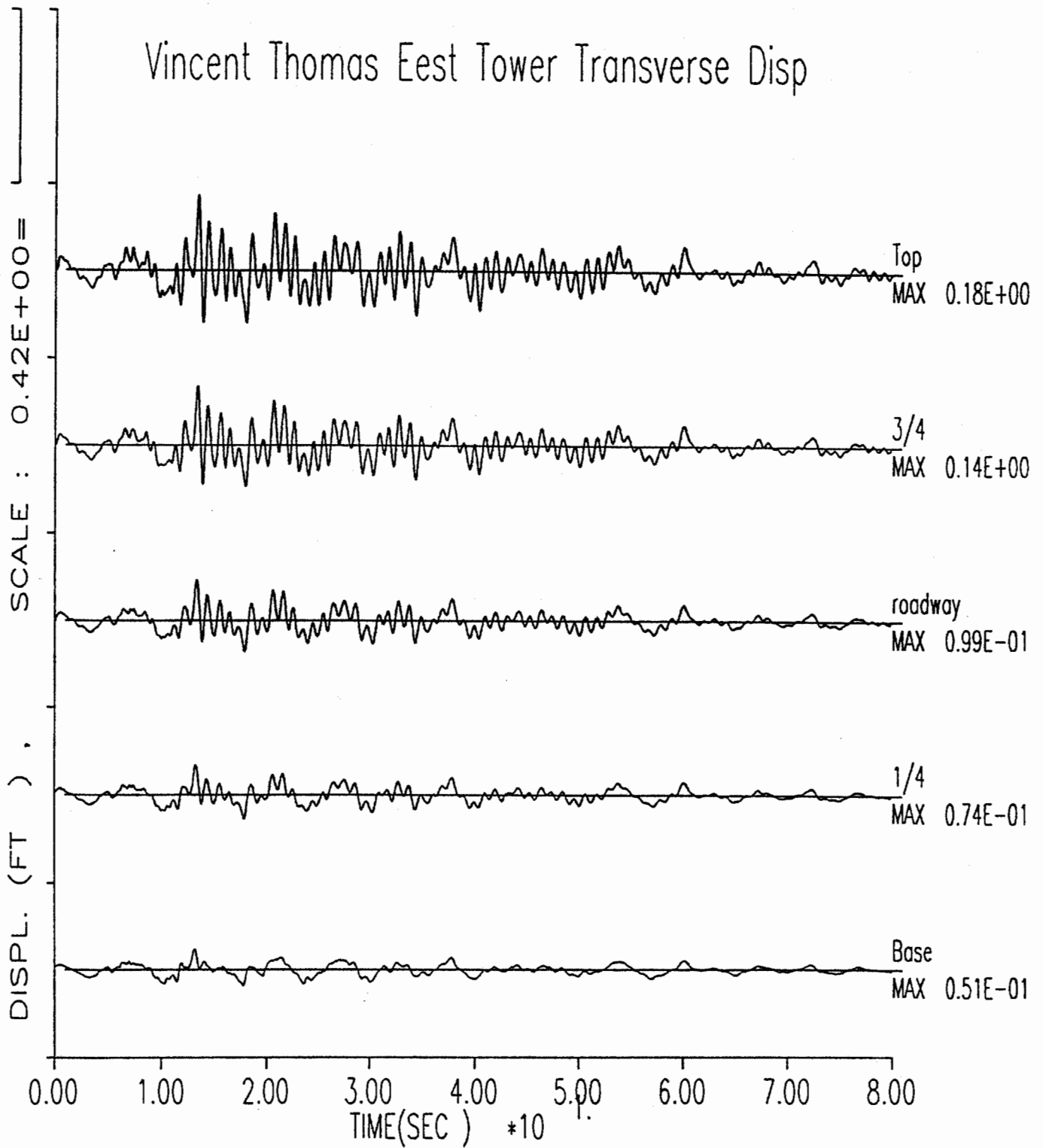
Figure 6.9: Transverse Displacement Time Histories of the East Tower

117
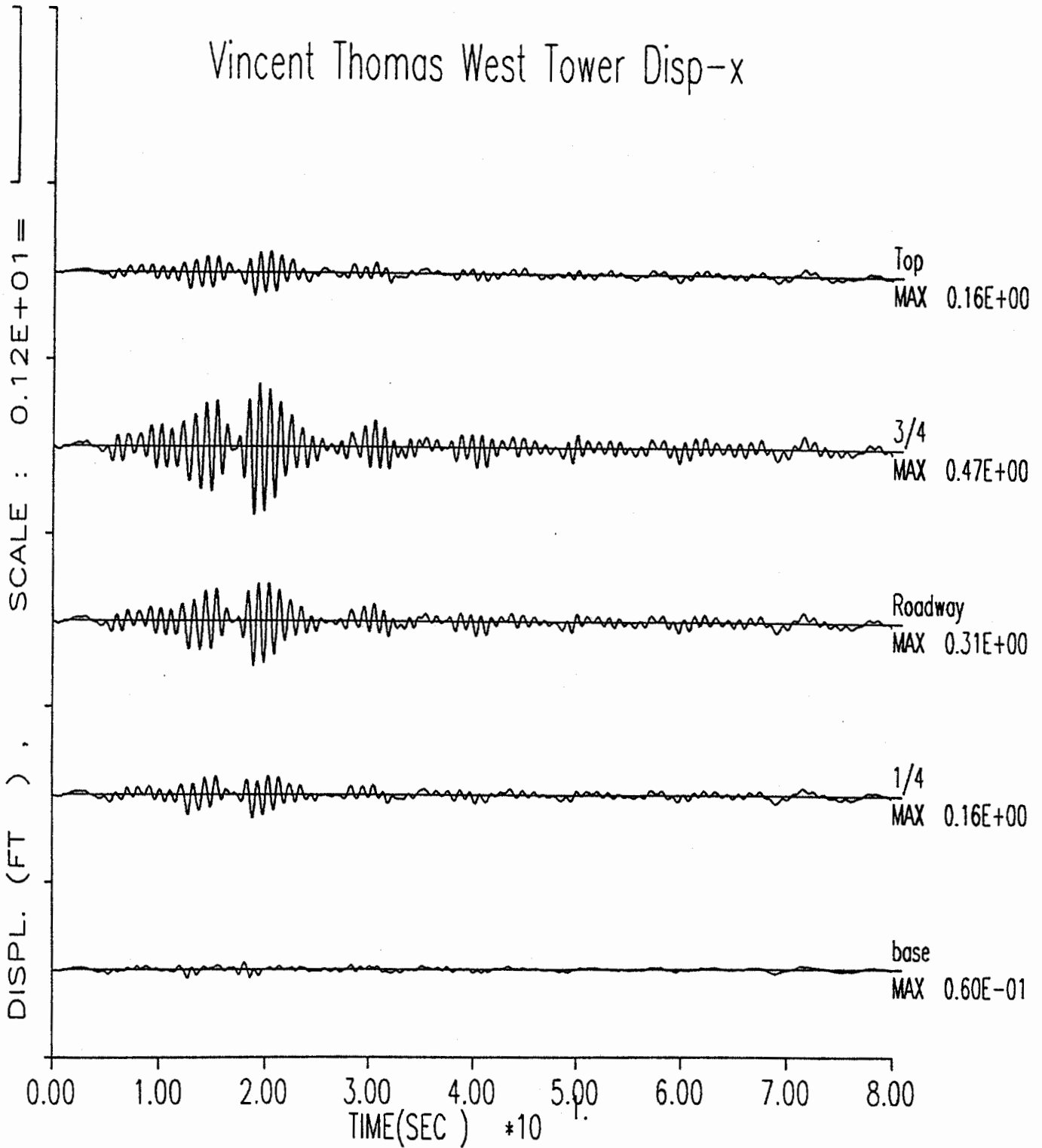
Figure 6.10: Longitudinal Displacement Time Histories of the West Tower

118
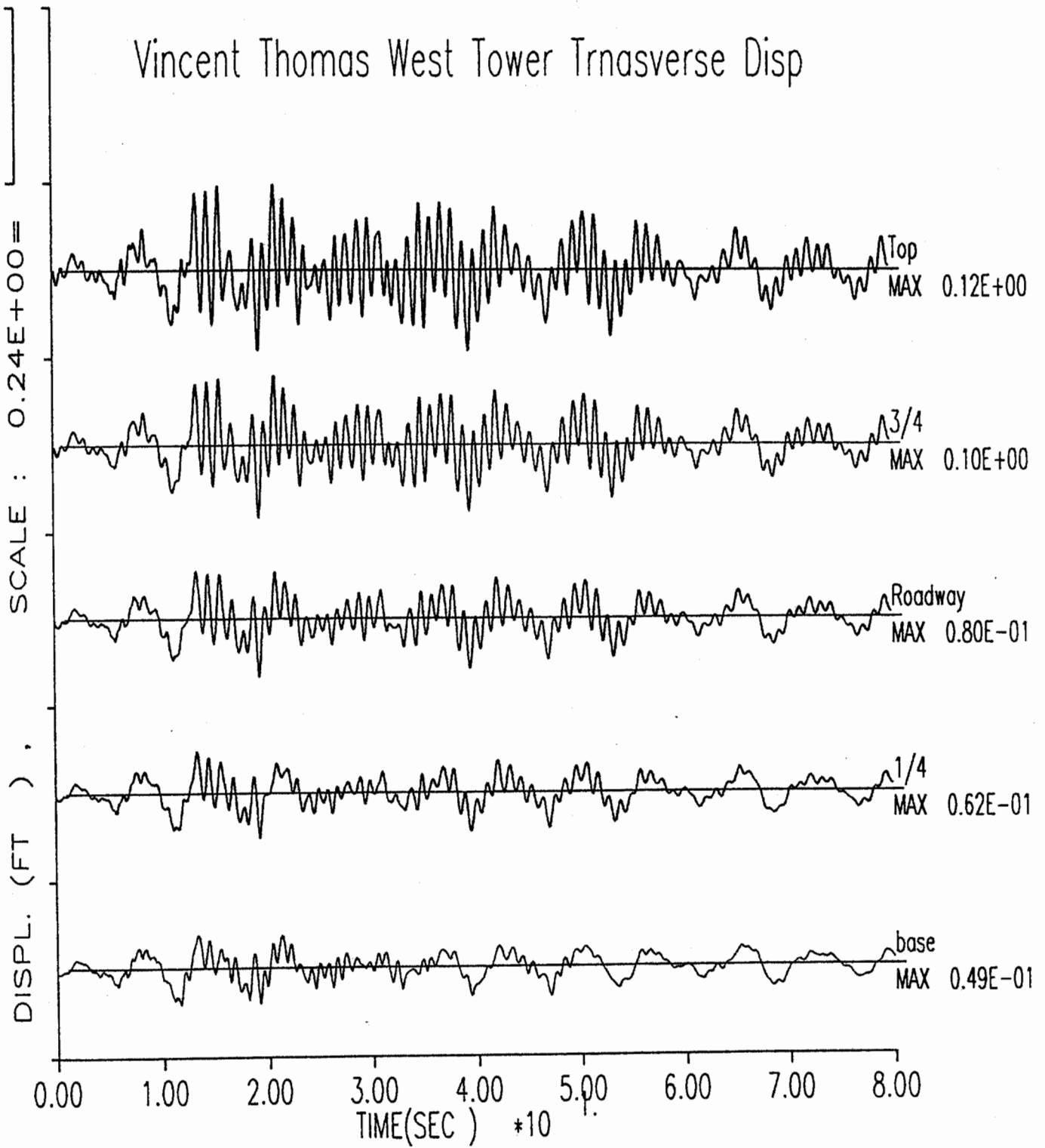
Figure 6.11: **Transverse Displacement Time Histories of the West Tower**
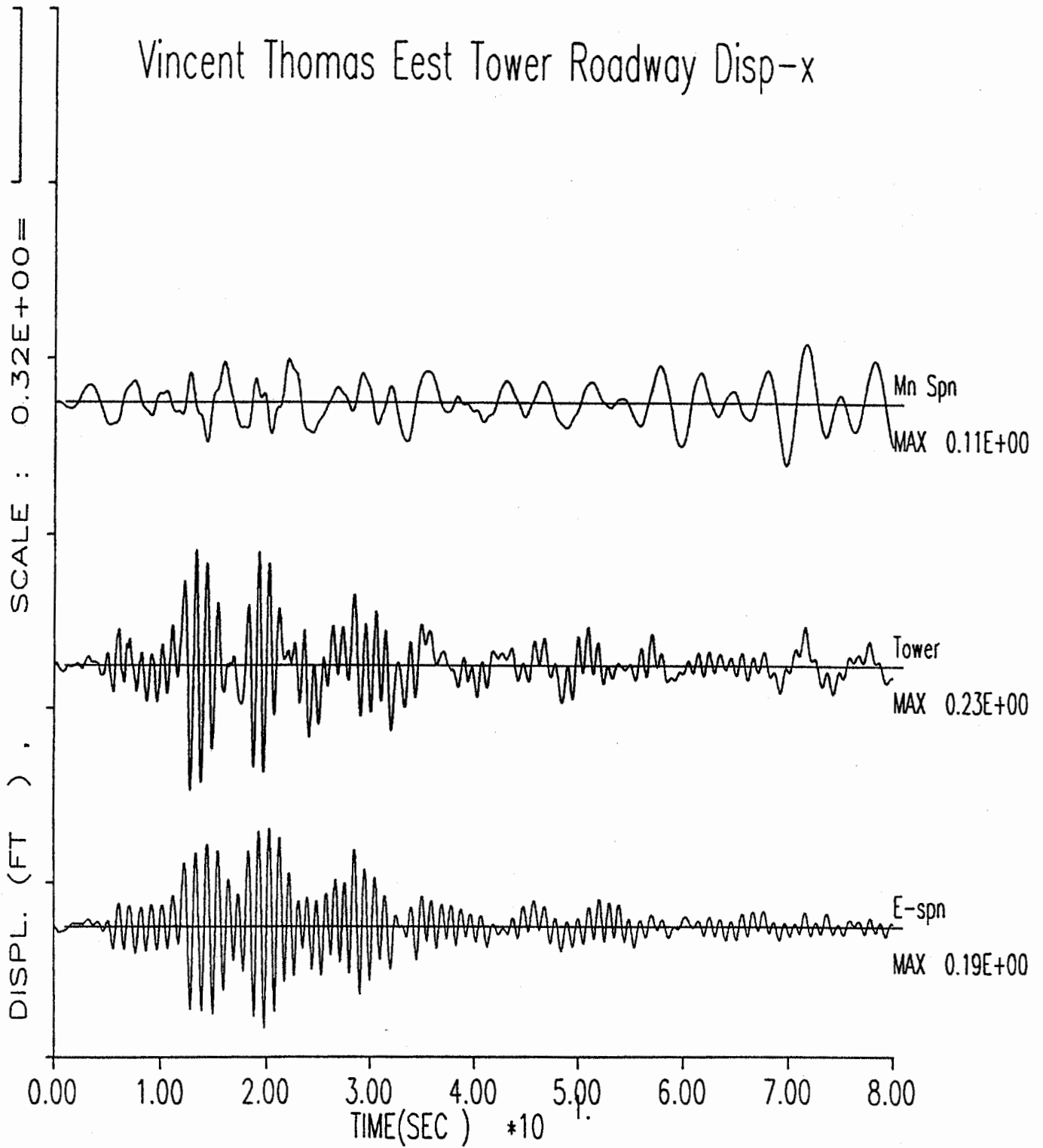
Figure 6.12: Longitudinal Displacement Response Time Histories at the Junction of the East Tower and Trusses

120
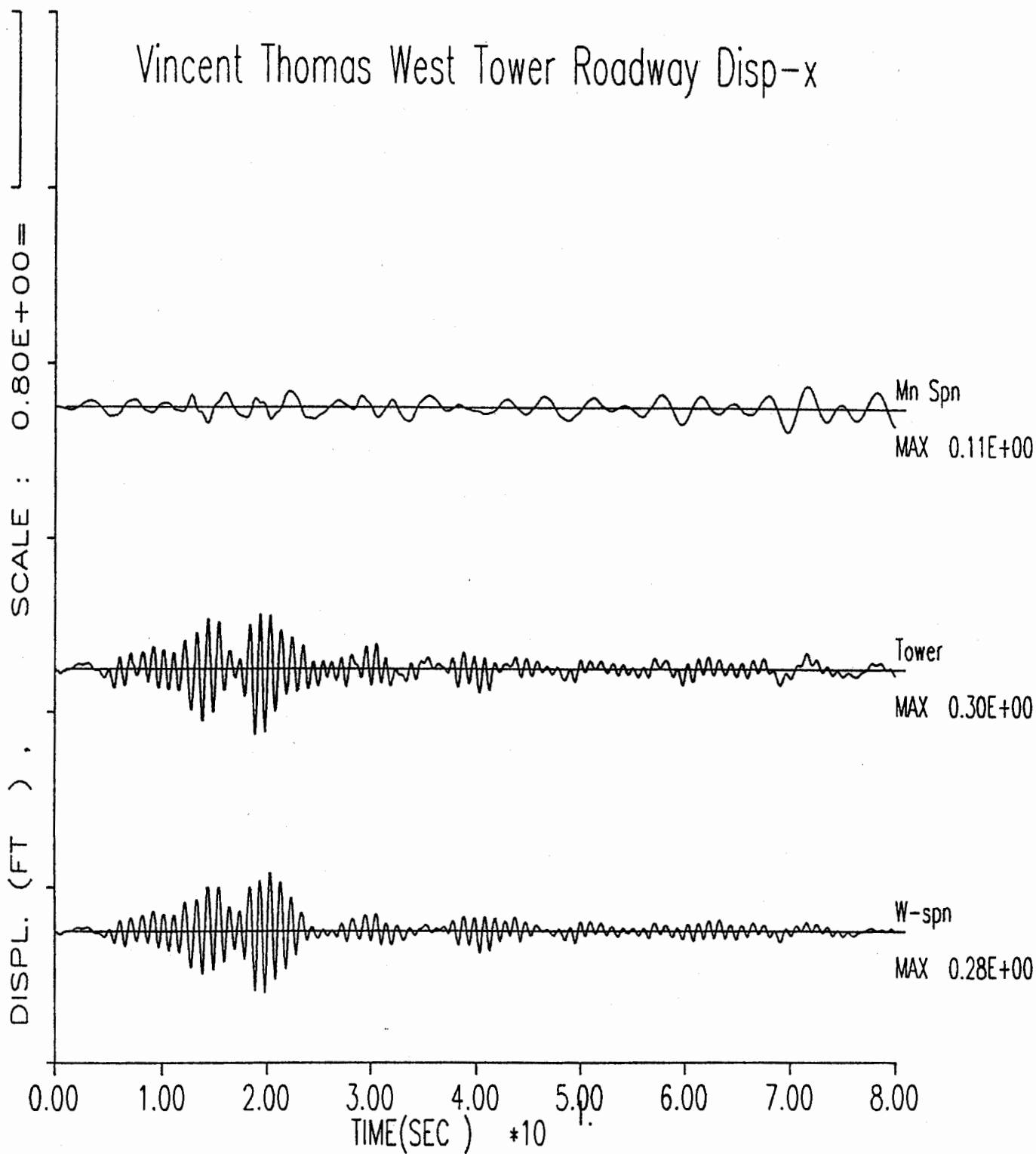
Figure 6.13: Longitudinal Displacement Response Time Histories at the Junction of the West Tower and Trusses

121

Vincent Thomas Cable Bent Top Long. Shear Force

East-S
MAX 0.35E+03

East-N
MAX 0.38E+03

West-S
MAX 0.58E+03

West-N
MAX 0.53E+03

SCALE : 0.10E+04=

FORCE (KIP) ,

TIME(SEC) *10
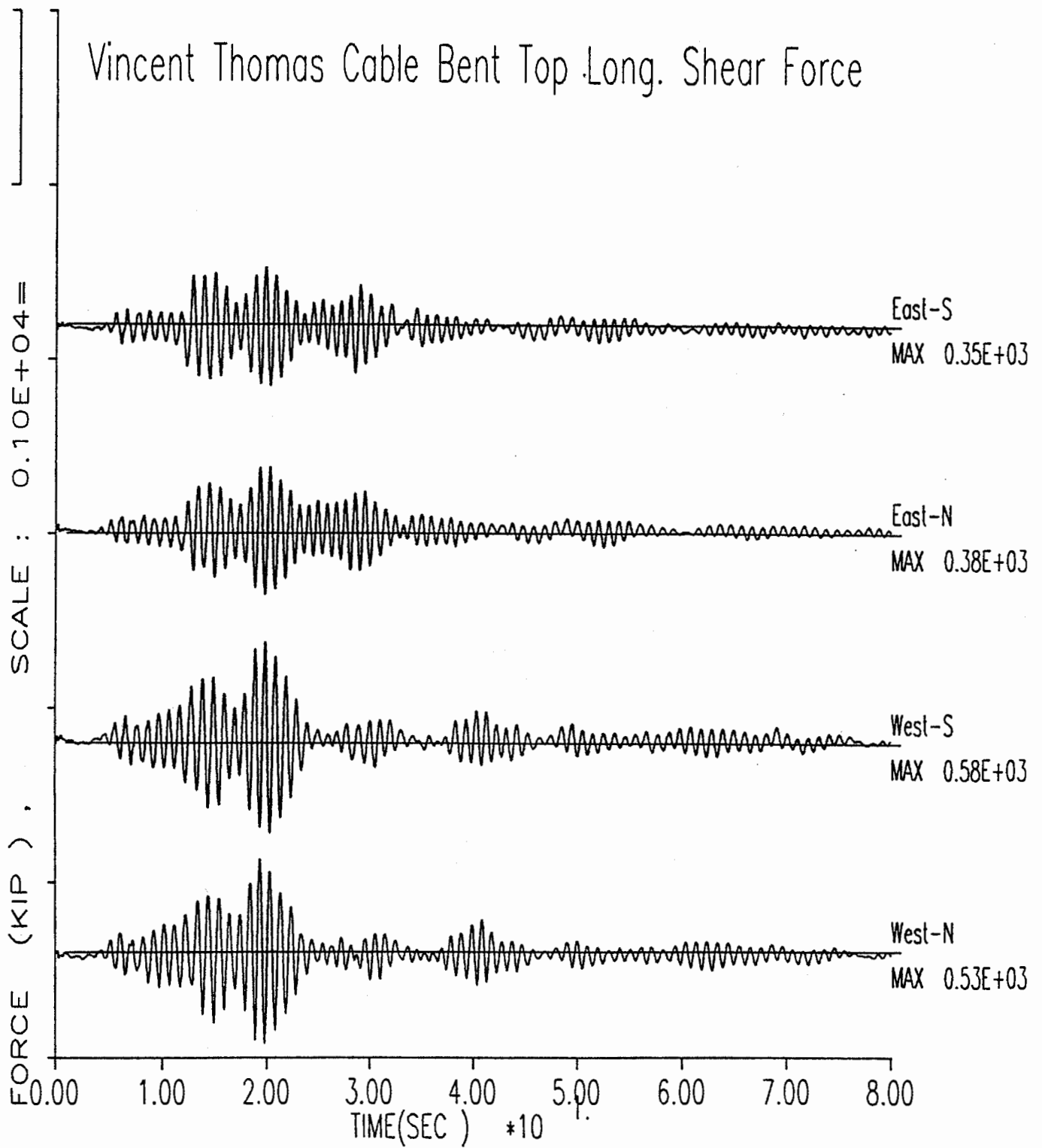
Figure 6.14:   Longitudinal Shear Time History at Top of Cable Bent Columns

122
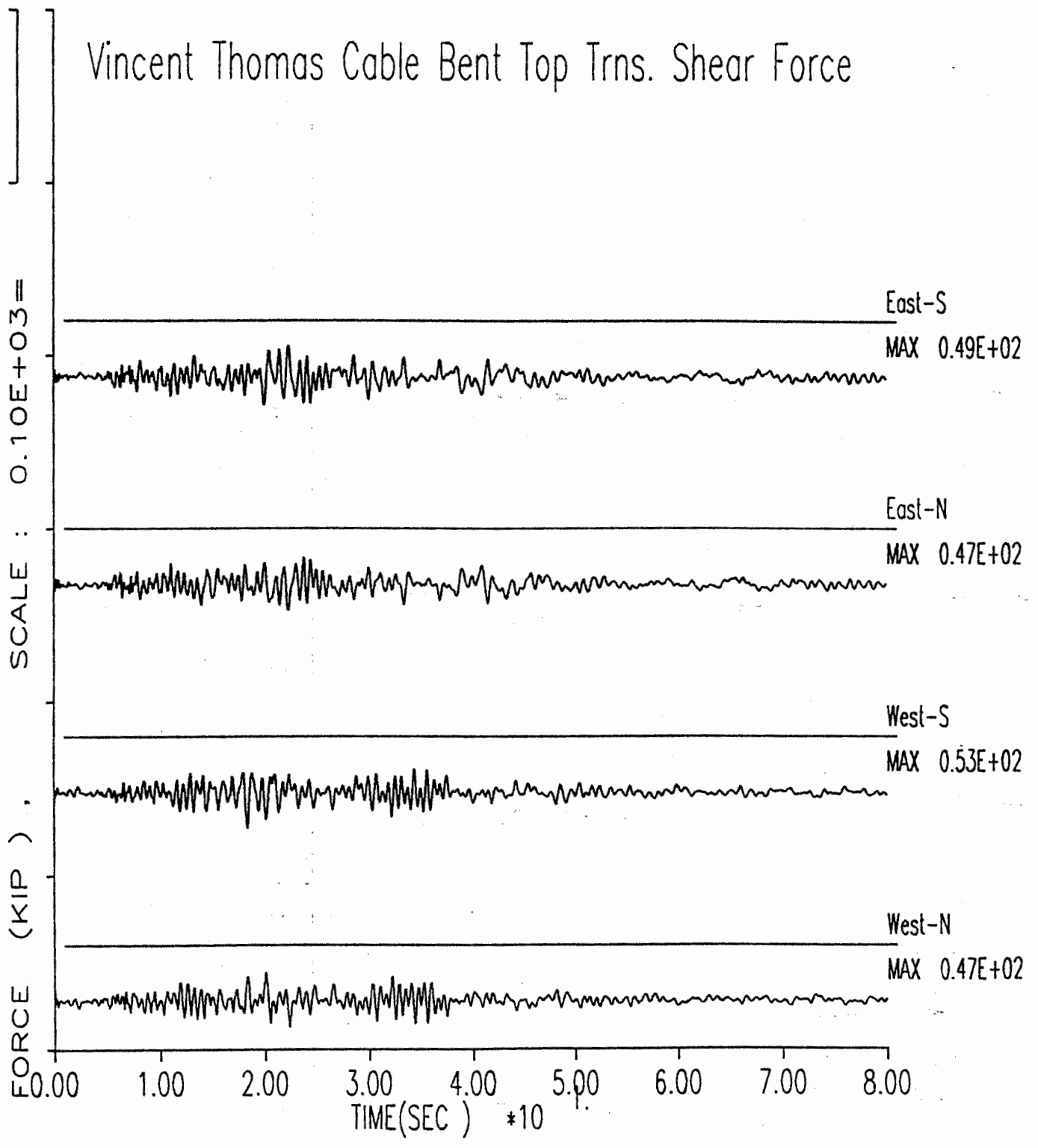
Figure 6.15:   Transverse Shear Time History at Top of Cable Bent Columns

123

7. Conclusions and Recommendations

Based on data reduction from the 1987 Whittier Narrows earthquake records and structural seismic analysis the following conclusions can be made:

1. Based on motions obtained in several Long Beach stations and bridge foundations, a dominant period of 1 second can be identified in the ground motion which is attributed to the Los Angeles *basin effect*. This has also been observed in the recent 1994 Northridge earthquake.

   The structure also has several important modes in the towers and suspended spans with 1 second natural period.

   In the seismic vulnerability assessment for a future maximum earthquake, this aspect of ground motion input must be accounted for. An attempt has been made in Chapter 5 to generate appropriate ground motion time histories at the bridge's multiple supports based on motions recorded in the Long Beach area.

2. Motions recorded at East Tower and West Tower were quite different in both amplitude and frequency content. This is caused by the different subsurface soil conditions and the soil-structure interaction effect. The two vertical sensors at the base of the East Tower provided a quantitative assessment of the rocking motion of the pile-supported foundation. However, the torsional motion (about the vertical axis) of the foundation cannot be quantified.

   It would be desirable to establish nearby free-field stations at the east and the west sides of the channel to quantify the local site response effect.

3. Based on structural response measurements obtained at East Side Span, Main Span and East Tower, several important vibration modes were identified. Some of these modes correlate very well with the analytical model (Chapters 3, 4 and 6).

   The lateral and torsional vibration of the truss box are coupled. Data collected at the side span and main span provided very valuable information

to benchmark the simplified analytical model (i.e., using superelement representation for the 3D truss system).

4. If one ignores the rotational foundation input motion, the data collected at the two tower bases represent both the spatial variation of ground motion and the kinematic interaction effect of the foundation. Using these foundation motions as input, the responses at the two towers are predicted. Significant differences existed in the responses of the two towers. This is caused by the presence of pairs of in-phase and out-of-phase longitudinal vibration modes.

5. The "additional" cable tension due to seismic load was a 10% increase in the backstay, but only a 3% increase in the side spans. This is probably caused by the angle change of cable profile at the cable bent and resulted in the interaction of cable and cable bent. As a result, the longitudinal shear force developed at each cable bent column is about 600 kip. This is a very critical component in the structure system because it supports the main cables. (Note that the cable bent is equivalent to a 15-story building in height.) However, there is no measurement available to quantify the response prediction at cable bent. In the Golden Gate Bridge and other major suspension bridges, the concrete pylons or cable bents have been shown to be vulnerable under seismic loads. It is recommended to instrument one of the cable bents in both the longitudinal and transverse directions to verify the interaction of main cable and cable bents.

6. The multiple-support response spectrum analysis was carried out using the Caltech records as input. Displacement responses were comparable to the time history results. However, because the motions do not include the site effect at the bridge site, no further comparison was made. Additional studies are being conducted using the Long Beach motions (reported in Chapter 5).

8. References

Abdel-Ghaffar, A.M. and G. W. Housner (1978), Ambient Vibration Tests of a Suspension Bridge. *Journal of Engineering Mechanics, ASCE*, 104(EM5):983-999, October 1978.

Abdel-Ghaffar, A.M. and L.I. Rubin (1982), Suspension Bridge Response to Multiple-Support Excitations. *Journal of Engineering Mechanics*, ASCE, 108(EM2):291-308, April 1982.

Abdel-Ghaffar, A.M. and R.H. Scanlan (1985), Ambient Vibration Studies of the Golden Gate Bridge: I. Suspended Structure, II. Pier Tower Structure. *Journal of Engineering Mechanics, ASCE,* 111:483-499, 1985.

Abrahamson, N.A., J.F. Schneider, and J.C. Steep (1990), Spatial Variation of Strong Ground Motion for Use in Soil-Structure Interaction Analyses, Earthquake Spectra, Vol. 7, No. 1.

Abrahamson, N.A., J.F. Schneider, and J.C. Steep (1991), Empirical Spatial Coherency Functions for Applications to Soil-Structure Interaction Analysis, *Earthquake Spectra*, Vol. 7, No. 1.

Bathe, K.J. and S. Bolourchi (1979), "Large Displacement Analysis of Three-Dimensional Beam Structures," International Journal for Numerical Method in Engineering, Vol. 14, pp. 961-986.

California Department of Conservation (1987), CSMIP Strong-Motion Records From the Whittier, California Earthquake of October 1, 1987. Technical Report OSMS 87-05, Division of Mines and Geology, Office of Strong Motion Studies, 1987.

Clough, R.W. and J. Penzien (1992), Dynamics of Structure, McGraw-Hill, New York, NY.

Der Kiureghian, A. (1980), Structural Response to Stationary Excitation. *Journal of Engineering Mechanics, ASCE,* Vol. 106 1195-1213.

Der Kiureghian, A. and A. Neuenhofer (1991), A Response Spectrum Method for Multiple-Support Seismic Excitations, Report No. UCB/EERC-91/08, Earthquake Engineering Research Center, University of California, Berkeley, August 1991.

Der Kiureghian, A. (1994), "Model for Coherency Function for Spatially Varying Ground Motion," 5th U.S. National Conference on Earthquake Engineering, Chicago, Illinois, July 1994.

Housner, G.W., et. al. (1990), Competing Against Time, Report to Governor George Deukmejian from The Governor's Board of Inquiry on the 1989 Loma Prieta Earthquake, State of California, Office of Planning and Research, May 31, 1990.

Imbsen, R.A. and W.D. Liu (1991), Seismic Evaluation of Large and Unusual Bridge Structures. *8th Annual International Bridge Conference,* Pittsburgh, Pennsylvania, June 10-11 & 12, 1992.

Konishi, I. and Y. Yamada (1969), Studies on the Earthquake Resistant Design of Suspension Bridge Tower and Pier Systems, *Proceedings 4th WCEE,* Vol. 1, 1969.

Liu, W.D., F.S. Nobari, and R.A. Imbsen (1989), Dynamic Response Prediction for Earthquake Resistance Design of Bridge Structures, in *Seismic Engineering*: Research and Practice, Edited by C.A. Kirchner and A.K. Chopra, ASCE Structure Congress '89, San Francisco, CA, 1989, pp. 1-10.

Liu, W.D. and R.A. Imbsen (1990), Seismic Evaluation of Golden Gate Bridge and Tower Structure. Technical Report, T.Y. Lin International, Golden Gate Bridge, Highway and Transportation District, San Francisco, California, November 1990.

Liu, W.D. et. al. (1990), Response of a Major Freeway Bridge During the Whittier Earthquake, *Proceedings of 4th National Conference on Earthquake Engineering,* Palm Springs, CA, May 20-24, 1990.

Liu, W.D., F.S. Nobari, R. Hamidi, and R.A. Imbsen (1991), "Modeling of Golden Gate Bridge Tower Structures," Earthquake Response of Highway Bridges – Testing and Modeling, ASCE Structural Congress, Indianapolis, Indiana, April 1991.

Liu, W.D. et al. (1994), "Seismic Evaluation of the Tied-Arch Bridge Across the Mississippi River on I-40," Proceedings of the Structural Congress, ASCE, Atlanta, Georgia, April 1994.

Naizy, A-S.M. (1991), Seismic Performance Evaluation of Suspension Bridges, Ph.D. Dissertation, Department of Civil Engineering, University of Southern California, December 1991.

Nakamura, Y., A. Der Kiureghian and W.D. Liu (1993), Multiple-Support Response Spectrum Analysis of the Golden Gate Bridge, Earthquake Engineering Research Center, University of California, Berkeley, 1993.

Scrivner, C.W. and D.V. Helmberger (1993), Two Dimensional Modeling of Deep Sedimentary Basin Effects for Two Los Angles Earthquakes, Manuscript Submitted to Bull. Seism. Soc. Am.

Wald, D.J., P.G. Somerville, and L.J. Burdick (1988), Simulation of Recorded Accelerations of the 1987 Whittier Narrows Earthquake. *Earthquake Spectra,* Vol. 4 139-156.

Yamamura, N. and H. Tanaka (1990), Response Analysis of Flexible MDF Systems for Multiple-Support Seismic Excitations. *International Journal of Earthquake Engineering and Structural Dynamics,* Vol. 19 345-357, 1990.

Wolf, J.P. (1985), Dynamic Soil-Structure Interaction, Prentice-Hall, Inc. Englewood, Cliffs, New Jersey.

LIST OF CSMIP DATA UTILIZATION REPORTS

California Department of Conservation
Division of Mines and Geology
Office of Strong Motion Studies
California Strong Motion Instrumentation Program (CSMIP)

The California Strong Motion Instrumentation Program (CSMIP) publishes data utilization reports as part of the Data Interpretation Project. These reports were prepared by investigators funded by CSMIP. Results obtained by the investigators were summarized in the papers included in the proceedings of the annual seminar. These reports and seminar proceedings are available from CSMIP at nominal cost. Requests for the reports, seminar proceedings and/or for additional information should be addressed to: Data Interpretation Project Manager, Office of Strong Motion Studies, Division of Mines and Geology, California Department of Conservation, 801 K Street, MS 13-35, Sacramento, California 95814-3531. Phone: (916)322-3105

CSMIP/92-01   "Evaluation of Soil-Structure Interaction in Buildings during Earthquakes," by G. Fenves and G. Serino, June 1992, 57 pp.

CSMIP/92-02   "Seismic Performance Investigation of the Hayward BART Elevated Section," by W. Tseng, M. Yang and J. Penzien, September 1992, 61 pp.

CSMIP/93-01   "Influence of Critical Moho Reflections on Strong Motion Attenuation in California," by P. Somerville, N. Smith and D. Dreger, December 1993, 84 pp.

CSMIP/93-02   "Investigation of the Response of Puddingstone Dam in the Whittier Narrows Earthquake of October 1, 1987," by J. Bray, R. Seed and R. Boulanger, December 1993, 60 pp.

CSMIP/93-03   "Investigation of the Response of Cogswell Dam in the Whittier Narrows Earthquake of October 1, 1987," by R. Boulanger, R. Seed and J. Bray, December 1993, 53 pp.

CSMIP/94-01   "Torsional Response Characteristics of Regular Buildings under Different Seismic Excitation Levels," by H. Sedarat, S. Gupta, and S. Werner, January 1994, 43 pp.

CSMIP/94-02   "Degradation of Plywood Roof Diaphragms under Multiple Earthquake Loading," by J. Bouwkamp, R. Hamburger and J. Gillengerten, February 1994, 32 pp.

CSMIP/94-03   "Analysis of the Recorded Response of Lexington Dam during Various Levels of Ground Shaking," by F. Makdisi, C. Chang, Z. Wang and C. Mok, March 1994, 60 pp.

CSMIP/94-04   "Correlation between Recorded Building Data and Non-Structural Damage during the Loma Prieta Earthquake of October 17, 1989," by S. Rihal, April 1994, 65 pp.

CSMIP/94-05   **"Simulation of the Recorded Response of Unreinforced Masonry (URM) Infill Buildings,"** by J. Kariotis, J. Guh, G. Hart and J. Hill, October 1994, 149 pp.

CSMIP/95-01   **"Seismic Response Study of the Hwy 101/Painter Street Overpass Near Eureka Using Strong-Motion Records,"** by R. Goel and A. Chopra, March 1995, 70 pp.

CSMIP/95-02   **"Evaluation of the Response of I-10/215 Interchange Bridge Near San Bernardino in the 1992 Landers and Big Bear Earthquakes,"** by G. Fenves and R. Desroches, March 1995, 132 pp.

CSMIP/95-03   **"Site Response Studies for Purpose of Revising NEHRP Seismic Provisions,"** by C.B. Crouse, March 1995, 68 pp.

CSMIP/96-01   **"An Investigation of UBC Serviceability Requirements from Building Responses Recorded During the 1989 Loma Prieta Earthquake,"** by C.-M. Uang and A. Maarouf, September 1996, 140 pp.

CSMIP/96-02   **"Evaluation of Displacement Amplification Factor for Seismic Design Provisions,"** by C.-M. Uang and A. Maarouf, September 1996, 167 pp.

CSMIP/00-01   **"Prediction of Ground Motions for Thrust Earthquakes,"** by P. Somerville and N. Abrahamson, February 2000, 56 pp.

CSMIP/00-02   **"Quantifying the Effect of Soil-Structure Interaction for Use in Building Design,"** by C. Poland, J. Soulages, J. Sun and L. Mejia, February 2000, 99 pp.

CSMIP/00-03   **"Seismic Performance and Design Considerations of Long Span Suspension Bridges,"** by W.D. Liu, A. Kartoum, K. Chang and R. Imbsen, February 2000, 132 pp.

SMIP89   "SMIP89 Seminar on Seismological and Engineering Implications on Recent Strong-motion Data," Preprints, Sacramento, California, May 9, 1989

SMIP90   "SMIP90 Seminar on Seismological and Engineering Implications on Recent Strong-motion Data," Preprints, Sacramento, California, June 8, 1990

SMIP91   "SMIP91 Seminar on Seismological and Engineering Implications on Recent Strong-motion Data," Preprints, Sacramento, California, May 30, 1991

SMIP92   "SMIP92 Seminar on Seismological and Engineering Implications on Recent Strong-motion Data," Proceedings, Sacramento, California, May 21, 1992

SMIP93   "SMIP93 Seminar on Seismological and Engineering Implications on Recent Strong-motion Data," Proceedings, Sacramento, California, May 20, 1993, 114 pp.

SMIP94   "SMIP94 Seminar on Seismological and Engineering Implications on Recent Strong-motion Data," Proceedings, Los Angeles, California, May 26, 1994, 120 pp.

SMIP95 "SMIP95 Seminar on Seismological and Engineering Implications on Recent Strong-motion Data," Proceedings, San Francisco, California, May 16, 1995, 105 pp

SMIP96 "SMIP96 Seminar on Seismological and Engineering Implications on Recent Strong-motion Data," Proceedings, Sacramento, California, May 14, 1996, 130 pp.

SMIP97 "SMIP97 Seminar on Utilization of Strong-Motion Data," Proceedings, Los Angeles, California, May 8, 1997, 127 pp.

SMIP98 "SMIP98 Seminar on Utilization of Strong-Motion Data," Proceedings, Oakland, California, September 15, 1998, 175 pp.

SMIP99 "SMIP99 Seminar on Utilization of Strong-Motion Data," Proceedings, Los Angeles, California, September 15, 1999, 154 pp.